DOKUZ EYLÜL UNIVERSITY
GRADUATE SCHOOL OF NATURAL AND APPLIED SCIENCES

MODELLING ELECTROMAGNETIC WAVES IN ANISOTROPIC MATERIALS

by
Barış ÇİÇEK

September, 2015
İZMİR

MODELLING ELECTROMAGNETIC WAVES IN ANISOTROPIC MATERIALS

A Thesis Submitted to the
Graduate School of Natural And Applied Sciences of Dokuz Eylül University
In Partial Fulfillment of the Requirements for the Degree of Doctor of Philosophy in Mathematics

by
Barış ÇİÇEK

September, 2015
İZMİR

Ph.D. THESIS EXAMINATION RESULT FORM

We have read the thesis entitled **"MODELLING ELECTROMAGNETIC WAVES IN ANISOTROPIC MATERIALS"** completed by **BARIŞ ÇİÇEK** under supervision of **PROF. DR. VALERY YAKHNO** and we certify that in our opinion it is fully adequate, in scope and in quality, as a thesis for the degree of Doctor of Philosophy.

Prof. Dr. Valery YAKHNO

Supervisor

Prof. Dr. Hamza POLAT

Thesis Committee Member

Asst. Prof. Dr. Melda DUMAN

Thesis Committee Member

Prof.Dr. Emine MISIRLI

Examining Committee Member

Assoc. Prof. Dr. İsmail YASLAN

Examining Committee Member

Prof.Dr. Ayşe OKUR
Director
Graduate School of Natural and Applied Sciences

ACKNOWLEDGEMENTS

First and foremost I would like to express my deepest gratitude to my supervisor Prof. Dr. Valery G. Yakhno for his continual presence, invaluable guidance, help and never ending patience throughout the course of this work.

I would like to thank Prof. Dr. Hamza POLAT, Asst. Prof. Dr. Melda DUMAN, Prof. Dr. Emine MISIRLI and Assoc. Prof. Dr. İsmail YASLAN for beeing members of my thesis committee. I would like to thank to all members of Dokuz Eylül University Department of Mathematics and to all members of İzmir Institute of Technology Department of Mathematics.

It is a pleasure to express my gratitude to my close friends who have always cared about my work, and increased my motivation which I have strongly needed. Especially, I would like to offer my sincerest thanks to my dear friend Barış ATEŞ who is as close as a brother to me.

I am also grateful to my family for their continual presence, understanding, endless supporting and confidence to me throughout my life.

Finally, I wish to express my special thanks to my wife, my love, Yeşim ÇİÇEK for her understanding and encouragement while this thesis was being written. I would also like to thank to the meaning of my life, my dear son Çınar ÇİÇEK for his endless love.

Barış ÇİÇEK

MODELLING ELECTROMAGNETIC WAVES IN ANISOTROPIC MATERIALS

ABSTRACT

The thesis deals with modelling electromagnetic waves in anisotropic media. In the first part of the thesis, a new method of approximate computation of the electric and magnetic matrix Green's functions in general gyrotropic media has been suggested and investigated. This method is based on the following. The Fourier images of the elements of the electric and magnetic matrix Green's functions with respect to space variables are computed exactly by some matrix transformations and symbolic computations in MATLAB. The element of the Green's functions for electric and magnetic fields are derived approximately by the regularized numerical computation of the inverse Fourier transform of their images obtained on the previous step. The regularization parameters are chosen by comparison the elements of regularized Green's functions for electric and magnetic fields with exact the Green's functions for electric and magnetic fields in the case of an isotropic medium. The computational experiments confirmed the robustness of the method.

In the second part of the thesis we suggested a new method of approximate computation of the fundamental solution of time-dependent Maxwell's equations for general anisotropic conductive materials. This method is based on the following. Applying the Fourier transformation with respect to the space variables, the initial value problem is reduced to the Volterra integral equations. The solution of the obtained integral equation is constructed by the method of successive approximations. Finally, the inverse Fourier transform is applied numerically to the fundamental solution for the time-dependent Maxwell's equations. The computational experiments confirmed the robustness of the method.

Keywords: Maxwell's equations, Green's functions, Anisotropic media, Gyrotropic media, initial value problem, integral equations, modeling, simulation, analytical method.

ELEKTROMANYETİK DALGALARIN ANİZOTROPİK ORTAMLARDA MODELLENMESİ

ÖZ

Bu tez eletromanyetik dalgaların anizotropik ortamlarda modellenmesi ile ilgilidir. Tezin ilk bölümünde, genel gyrotropic ortamdaki elektrik ve manyetik matris Green fonksiyonlarının yaklaşık olarak hesaplanması için yeni bir yöntem önerilmiş ve araştırılmıştır. Bu yöntem aşağıda belirtilenlere dayanmaktadır. Elektrik ve manyetik matris Green fonksiyonlarının elemanlarının uzay değişkenlerine göre Fourier görüntüleri bazı matris dönüşümleri ve MATLAB'da sembolik hesaplamalar ile tam olarak hesaplanmıştır. Elektrik ve manyetik alanlar için Green fonksiyonlarının elemanları, bir önceki adımda elde edilen görüntülerine ters Fourier dönüşümünün regülarize edilmiş sayısal hesaplanması ile yaklaşık olarak türetilmiştir. Regülarizasyon parametreleri, regülarize edilmiş elektrik ve manyetik alanların Green fonksiyonları ile tam elektrik ve manyetik alanların Green fonksiyonlarının izotropik ortamda kıyaslanması ile seçilir. Sayısal deneyimler bu yöntemin doğruluğunu göstermektedir.

Tezin ikinci bölümünde, zamana bağlı Maxwell denklemlerinin genel anizotropik iletken malzemelerdeki yaklaşık hesaplaması ile ilgili yeni bir yöntem önerilmiştir. Bu yöntem aşağıda belirtilenlere dayanmaktadır. Başlangıç değer problemi, uzay değişkenlerine göre Fourier dönüşümü uygulanarak Volterra integral denklemine indirgenmiştir. Elde edilmiş integral denkleminin çözümü ardışık yaklaşım yöntemiyle oluşturulmuştur. Son olarak zamana bağlı Maxwell denklemlerinin temel çözümünü bulmak için ters Fourier dönüşümü sayısal olarak uygulanmıştır. Sayısal deneyimler bu yöntemin doğruluğunu göstermektedir.

Anahtar Kelimeler : Maxwell denklemleri, Green fonksiyonu, anizotropik ortam, gyrotropic ortam, başlangıç değer problemi, integral denklemler, modelleme, simülasyon, analitik yöntem.

CONTENTS

Page

LIST OF FIGURES

LIST OF TABLES

CHAPTER ONE
INTRODUCTION

1.1 The Results of the Previous Research Related to the Thesis

In the 19th century, most basic laws in electromagnetic theory were established by a variety of talented scientists, including Gauss, Poisson, Ampère and Faraday. In that time, the equations existed in incomplete forms as a result of the work of these scientists. In 1873, James Clerk Maxwell added a displacement current term to these equations. It was important to prove that an electromagnetic field could exist as waves and these fundamental equations are named as Maxwell's equations. In 1888, Heinrich Hertz experimentally verified the wave nature of these equations and since then the importance of Maxwell's equations have been demonstrated in optics, microwaves, antennas, communications, radar and many sensing applications.

In vector notation and SI units, Maxwell's equations in differential representations (time-dependent domain) are (see, for example, Chew, 1995)

$$\begin{aligned} curl_x \mathbf{H}(x,t) &= \frac{1}{c}\frac{\partial \mathbf{D}(x,t)}{\partial t} + \frac{4\pi}{c}\mathbf{J}(x,t), && (1.1)\\ curl_x \mathbf{E}(x,t) &= -\frac{1}{c}\frac{\partial \mathbf{B}(x,t)}{\partial t}, && (1.2)\\ div_x(\mathbf{D}(x,t)) &= 4\pi\rho(x,t), && (1.3)\\ div_x(\mathbf{B}(x,t)) &= 0, && (1.4) \end{aligned}$$

where $x = (x_1, x_2, x_3) \in \mathbb{R}^3$ is a space variable, $t \in \mathbb{R}$ is a time variable, $\mathbf{E}$ and $\mathbf{H}$ denote the electric and magnetic fields, $\mathbf{E} = (E_1, E_2, E_3)$, $\mathbf{H} = (H_1, H_2, H_3)$, $E_k = E_k(x,t)$, $H_k = H_k(x,t)$, $k = 1,2,3$; $\mathbf{D}$, $\mathbf{B}$ are the displacement and magnetic induction, respectively; $\mathbf{J}(x,t)$ and $\rho(x,t)$ denote the densities of current and charge; $c > 0$ is the speed of light in vacuum.

Taking the divergence of (1.1) and using (1.3) we have

$$div_x \mathbf{J}(x,t) + \frac{\partial \rho(x,t)}{\partial t} = 0, \qquad (1.5)$$

which is known as conservation of charges.

It is also possible to represent Maxwell's equations in time-harmonic domain as (see, for example, Chew, 1995)

$$\begin{aligned} curl_x \mathbf{H}(x) &= -i\omega \mathbf{D}(x) + \mathbf{J}(x), && (1.6)\\ curl_x \mathbf{E}(x) &= i\omega \mathbf{B}(x), && (1.7)\\ div_x(\mathbf{D}(x)) &= \rho(x), && (1.8)\\ div_x(\mathbf{B}(x)) &= 0, && (1.9) \end{aligned}$$

where $x = (x_1, x_2, x_3) \in \mathbb{R}^3$ is a space variable, $\omega \in \mathbb{R}$ is a fixed parameter (frequency), $\mathbf{E}(x)$ and $\mathbf{H}(x)$ denote the electric and magnetic fields, $\mathbf{E}(x) = (E_1, E_2, E_3)$, $\mathbf{H}(x) = (H_1, H_2, H_3)$, $E_k = E_k(x)$, $H_k = H_k(x)$, $k = 1,2,3$; $\mathbf{D}(x)$, $\mathbf{B}(x)$ are the displacement and magnetic induction, respectively; $\mathbf{J}(x)$ and $\rho(x)$ denote the densities of current and charge.

If the electric and/or magnetic properties of a medium depend on the direction then the medium is called anisotropic and the constitutive relation for the electric and magnetic flux densities $\mathbf{D}$ and $\mathbf{B}$ have the following forms

$$\mathbf{D} = \varepsilon_0 \mathscr{E} \mathbf{E}, \qquad \mathbf{B} = \mu_0 \mathscr{M} \mathbf{H}, \tag{1.10}$$

where ε_0 and μ_0 are defined as the permittivity and permeability of free space; $\mathscr{E} = (\mathscr{E}_{ij})_{3\times 3}$ and $\mathscr{M} = (\mathscr{M}_{ij})_{3\times 3}$ are matrices of relative permittivity and permeability, respectively; $\mathbf{E}$ and $\mathbf{H}$ are the electric and magnetic fields, respectively.

Anisotropic media may be divided into two classes, depending on whether the natural modes of propagation are linearly polarized or circularly polarized waves. For the first class, the permittivity and permeability components are symmetric, that is $\mathscr{E}_{ik} = \mathscr{E}_{ki}$ and $\mathscr{M}_{ik} = \mathscr{M}_{ki}$ and for the second class, called 'gyrotropic anisotropic' or 'gyrotropic' media, the permittivity or permeability components are Hermitian, that is $\mathscr{E}_{ij} = \mathscr{E}^*_{ji}$ and $\mathscr{M}_{ij} = \mathscr{M}^*_{ji}$, where * is denoted as complex conjugate of the given component.

The fundamental solutions (Green's functions) technique can be considered as a useful tool for different methods in the presentation of acoustic, electromagnetic, elastic and other fields, in particular, for the method of moments and boundary element method (Kong, 1984; Chew, 1990; Tai, 1994; Lindell et al., 1994; Tewary, 1995, 2004; Rashed, 2004; Young et al., 2005; Yang & Tewary, 2008; Gu et al., 2009; Chen et al., 2009; Yakhno, 2011; Yakhno & Çerdik Yaslan, 2011; Yakhno & Ozdek, 2012, 2013). When the dyadic Green's functions can be constructed it leads to the significant simplification of modelling electromagnetic waves and allows engineers to overcome calculational difficulties (Tewary et al., 2002). The existence proofs for fundamental solutions (infinite-body Green's functions) in the spaces of generalized functions (tempered distributions) for any linear differential equations with constant coefficients were given by (Malgrange, 1955-56; Ehrenpreis, 1960; Hormander, 1963). The proofs were based on the Fourier transform meta-approach consisting of the application of the Fourier transform with respect to the space variables. As a result, the equations for the image of the fundamental solutions depending on the Fourier parameters were found. Finally, to get the fundamental solution it is necessary to apply the inverse Fourier transform to this image with respect to parameters of the Fourier transform. This inverse Fourier transform is defined in the space of tempered distribution only. Generally speaking, tempered distributions do not have values at fixed points and can not be presented in the graphic form (as graphs). Moreover, the inverse Fourier transform in the space of tempered distributions is presented in the form of the divergent integrals in the classical sense. Using the technique of generalized functions the inverse Fourier transform of the Fourier images has been calculated analytically in the space of the tempered distributions for some scalar partial differential equations with constant coefficients; see, for example, (Vladimirov, 1971)). Maxwell's equations in isotropic materials and the particular cases of anisotropic materials and media in (Ortner & Wagner, 2004; Wagner, 2011a). The methods for the derivation of the fundamental solutions and Green's functions for the Maxwell's equations in some anisotropic materials have been developed in (Malgrange, 1955-56; Ehrenpreis, 1960; Hormander, 1963; Pershan, 1967; Freiser, 1968; Chew, 1990; Barkleshli, 1993; Weiglhofer, 1993; Lindell & Weiglhofer, 1994; Tai, 1994; Weiglhofer, 1995; Lakhtakia & Weiglhofer, 1997; Tan, 2002; Ortner & Wagner, 2004; Burridge &

Qian, 2006; Lakhtakia & Mackay, 2006; Eroglu, 2010; Wagner, 2011a; V. Yakhno & T. Yakhno, 2012). We note that finding the fundamental solutions and Green's functions by methods of the above mentioned works have complicated mathematical forms, which are difficult to evaluate numerically for general anisotropic media. The approximate computation of fundamental solutions in general anisotropic materials of the first class (with symmetric permittivity and permeability components) by the Fourier transform approach was developed in the papers (Yakhno & Altunkaynak, 2010; V. Yakhno & T. Yakhno, 2012; Yakhno & Çerdik Yaslan, 2012; Yakhno et al., 2012; Yakhno & Ersoy, 2014, 2015).

For solving the initial value and initial boundary value problems of Maxwell's equations, boundary element method (BEM) is also used actively. BEM is related to the fundamental solutions (free space Green's functions) and the number of publications about applications of the BEM for solving applied problems indicates the growing importance of the BEM; see, for example, the works of (Beskos, 1987a,b, 1989; Hirose & Achenbach, 1989; Hirose & Kitahara, 1989, 1991; Wang et al., 1996; Beskos, 1997; Beskos & Manolis, 1997; Albuquerque et al., 2002; Tan et al., 2005; Takahashi et al., 2004). The BEM requires an integral presentation for a solution of the motion equations in an integral form. This integral presentation provides a solution in terms of its boundary values and traction by means of the fundamental solution (FS) (see review papers of (Beskos, 1987a, 1997) and their references). For this reason it is important to compute the FS values before application of BEM.

The methods for constructing Green's functions (fundamental solutions) of the Maxwell's equations in the second class (gyrotropic media) are given for the particular cases of anisotropic (or gyrotropic) media studied in (Barkleshli (1993); Eroglu & Lee, 2003, Prati, 2003; Eroglu & Lee, 2005, 2006a,b; Eroglu, 2010; Yakhno & Çiçek, 2014). The numerical computation of the Green's functions for the electric and magnetic fields of Maxwell's equations in general gyrotropic (and also electrically and magnetically gyrotropic) media is not known because these fundamental solutions are singular generalized functions and numerical methods are not developed in the space of these functions (tempered distributions).

There is also great interest in modelling electromagnetic waves in biological tissues (white and grey matter, outer skull and skin) and anisotropic earth materials (brine, water, oil and gas) using Maxwell's equations with an anisotropic conductive tensor; see, for example, (Wang & Fang, 2001; Weiss & Newman, 2002; Newman & Alumbaugh, 2002; Weiss & Newman, 2003; Sekino et al., 2003; Darvas et al., 2004; Commer et al., 2008). The electrical conductivity is an elegant experimental tool to probe the structural defects and internal purity of crystalline materials (see, for example, (Gowri & Shajan, 2006) and (Greena et al., 2010)). The wave propagation in these materials and media is described by the time-dependent Maxwell's equations containing the permittivity, permeability and conductivity tensors. The solutions of these equations are an important issue of the material science, geophysics, biology etc. Let us point out some methods solving these Maxwell's equations. A general solution for the time-dependent Maxwell's equations for an infinite isotropic medium with constant permittivity, permeability and conductivity has been studied in the paper (Moses & Prosser, 1990). In this paper the electric, magnetic vector fields and the current density have been expressed as sums of the longitudinal and transverse longitudinal component of magnetic field is shown to be zero, and longitudinal component of magnetic field is the gradient of the Coulomb potential. The transverse electromagnetic fields are solved in terms of the initial values of the transverse fields and the transverse part of the external current density. The method of the paper (Moses & Prosser, 1990) is based on the technique of the eigenfunctions of the curl operator. Using the expansion technique, the solution of the Maxwell's equations is constructed in a composite isotropic structure in the work (Oster & Turbe, 1993). Moreover, numerical experiments are given in (Oster & Turbe, 1993) for the optical medium presented a real interest. The integral presentation of the fundamental solution of the time-dependent Maxwell's equations in bi-axial, non-dispersive crystals has been studied in (Burridge & Qian, 2006) by the plane wave approach. In the paper (Burridge & Qian, 2006) the electric permittivity has been chosen as a diagonal matrix and crystals have been assumed to be non-conductive. The explicit formulas in the form of integrals over the Fresnel surface for the fundamental solution of the time-dependent Maxwell's equations of the crystal optics for cubic and hexagonal crystals were found by Herglotz-Petrovsky formulas in the papers (Wagner, 1999, 2004, 2005, 2006; Ortner & Wagner, 2008). The numerical procedure for the evaluating integrals over the Fresnel surface is discussed in (Burridge & Qian, 2006) for the bi-axial crystals. Using the Herglotz -Petrowsky formula technique the explicit formula for the singular part of the fundamental solutions of the time dependent equations of the crystals optics has been obtained for the crystal optics for the bi-axial crystals in (Wagner, 2011b). We note that the generalization of the methods of the works (Wagner, 1999, 2004, 2005; Burridge & Qian, 2006, Wagner, 2006; Ortner & Wagner, 2008; Wagner, 2011b) for the derivation and computation of the fundamental solution of the time-dependent Maxwell's equations in anisotropic materials is questionable. The computation of the fundamental solutions of the time-dependent Maxwell's equations in general anisotropic materials with zero conductivity has been made by the Fourier transform technique and matrix transformations in MATLAB in (Yakhno, 2005, Yakhno et al., 2006; V. Yakhno & T. Yakhno, 2007; Yakhno, 2008, 2010, 2011; Yakhno & Çerdik Yaslan, 2012). The methods of the works (Yakhno, 2005; Yakhno et al., 2006; V. Yakhno & T. Yakhno, 2007; Yakhno, 2008) have been generalized for the computation of the Green's functions of the time-dependent Maxwell's equations with the general anisotropic media, and in the works (Yakhno, 2010, 2011) for conductivity tensor in quasi-static approximations for the homogeneous anisotropic media. But the approximate solution of the time-dependent Maxwell's equations in general anisotropic conductive materials is not studied because of its complexness.

1.2 The Goal of the Thesis

The main goal of the thesis is to work out methods for the approximate computation of magnetic and electric matrix Green's functions in general gyrotropic media and the fundamental solutions of the time-dependent Maxwell's equations in general anisotropic conductive media.

1.3 Methods of the Thesis

The methods of the generalized functions and partial differential equations of hyperbolic and elliptic types as well as the theory and application of the mathematical and functional analysis, theory of integral equations and computational methods and computational tools are actively applied and used in the thesis.

1.4 The Descriptions of Historical Background of the Main Problems and Results of the Thesis

Media with the gyrotropic behavior arise from the application of a finite magnetic field to plasma, ferrite, and some dielectric crystals. Michael Faraday in 1845 (Faraday, 1933) was the first who discovered such kind gyrotropic behavior medium in a piece of glass between the poles of magnet. The study of electromagnetic wave propagation in gyrotropic media is an important issue of the recent electromagnetic theory (Eroglu & Lee, 2003; Lee & Rhee, 2005; Eroglu, 2010). The electromagnetic wave propagation in gyrotropic media are an active research topic because the gyrotropic behavior arises in new microwave devices such as circulators, isolators, resonators, and optical devices such as modulators, switches, phase shifters and so on (see (Eroglu & Lee, 2003, 2006a)). Moreover, the study of electromagnetic wave propagation in gyrotropic media can be used in development of new devices for ionospheric applications (Eroglu & Lee, 2006a). The electromagnetic fields observed in magnetically biased plasma or ferrite can be modeled as electromagnetic waves in gyrotropic media (Eroglu & Lee, 2006a).

Many problems of remote sensing, monolithic integrated circuits and optics, geophysical probing, microstrip circuits and antennas, submarine communication, opto-electronics etc. are connected with electromagnetic fields in gyro-electric media (Eroglu & Lee, 2003; Prati, 2003; Eroglu & Lee, 2006a; Eroglu, 2010).

The methods for constructing Green's functions and fundamental solutions for the electric and magnetic fields of Maxwell's equations in the second class (gyrotropic media) are given for the particular cases of gyrotropic media in (Barkleshli, 1993; Eroglu & Lee, 2003; Prati, 2003; Eroglu & Lee, 2006a; Eroglu, 2010; Yakhno & Çiçek, 2014). The numerical computation of the fundamental solutions of Maxwell's equations in general gyrotropic media is not known because these fundamental solutions are singular generalized functions and numerical methods are not developed in the space of these functions (tempered distributions). (Ortner & Wagner, 2004; Wagner, 2011a) have applied the Fourier meta-approach and found the explicit formulae of the Green's functions for the systems of elasticity and Maxwell's equations for some particular cases of anisotropy only by the Fourier transform meta-approach. These formulae can be used for the computer implementation. The approximate computation of the time-dependent three-dimensional Green's functions (fundamental solutions) in general anisotropic materials by the Fourier transform meta-approach was suggested in the papers (Yakhno, 2008; Yakhno, 2011). Using the Lorentz reciprocity relation and the multiple scattering approach the dyadic Green's functions for gyro-electric media are found in (Barkleshli, 1993). The dyadic Green's functions for an electrically gyrotropic medium with particular form of $\bar{\bar{\varepsilon}}$ have been derived by matrix method with dyadic decomposition in (Eroglu & Lee, 2003, 2006a,b). The time-harmonic Green's dyadics have been constructed in closed form for a particular case of homogeneous gyrotropic materials by Fourier transform approach in (Olyslager, 1997).

The classical example of the gyro-magnetic medium is a ferrite (Tsutaoka, 2003). The ferrites were invented in 1930 by Kato and Takei (Okamoto, 2006) and then they have become commercially available. The ferrites have various important applications as phase shifters, isolators and circulators (Eroglu, 2010). Ferrite materials are applied in such modern electromagnetic devices as inductors, converters and electromagnetic wave absorbers (Tsutaoka, 2003).

The first problem of the thesis consists of the approximate computation of the frequency dependent electric and magnetic Green's functions in the gyrotropic materials.

Let us introduce constitutive relations and structure of our problem. The matrices of relative permittivity and permeability have the following form for a general gyrotropic medium (see, for example, ((Eroglu, 2010))):

$$\mathscr{E} = \bar{\bar{\epsilon}} + i\bar{\bar{g}}, \qquad \mathscr{M} = \bar{\bar{\mu}} + i\bar{\bar{h}}, \qquad i^2 = -1, \tag{1.11}$$

$$\bar{\bar{\epsilon}} = \begin{pmatrix} \epsilon_{11} & \epsilon_{12} & \epsilon_{13} \\ \epsilon_{12} & \epsilon_{22} & \epsilon_{23} \\ \epsilon_{13} & \epsilon_{23} & \epsilon_{33} \end{pmatrix}, \bar{\bar{g}} = \begin{pmatrix} 0 & g_3 & -g_2 \\ -g_3 & 0 & g_1 \\ g_2 & -g_1 & 0 \end{pmatrix},$$
$$\bar{\bar{\mu}} = \begin{pmatrix} \mu_{11} & \mu_{12} & \mu_{13} \\ \mu_{12} & \mu_{22} & \mu_{23} \\ \mu_{13} & \mu_{23} & \mu_{33} \end{pmatrix}, \bar{\bar{h}} = \begin{pmatrix} 0 & h_3 & -h_2 \\ -h_3 & 0 & h_1 \\ h_2 & -h_1 & 0 \end{pmatrix}. \tag{1.12}$$

Let $\mathscr{E}$ and $\mathscr{M}$ be matrices of the form (1.11). The Green's functions for the electric and magnetic fields of Maxwell's equations are matrix functions

$$\mathbb{E}(x) = \begin{pmatrix} E_1^1(x) & E_1^2(x) & E_1^3(x) \\ E_2^1(x) & E_2^2(x) & E_2^3(x) \\ E_3^1(x) & E_3^2(x) & E_3^3(x) \end{pmatrix}, \mathbb{H}(x) = \begin{pmatrix} H_1^1(x) & H_1^2(x) & H_1^3(x) \\ H_2^1(x) & H_2^2(x) & H_2^3(x) \\ H_3^1(x) & H_3^2(x) & H_3^3(x) \end{pmatrix}, \tag{1.13}$$

whose columns $\mathbf{E}^k(x) = (E_1^k(x), E_2^k(x), E_3^k(x))^T$ and $\mathbf{H}^k(x) = (H_1^k(x), H_2^k(x), H_3^k(x))^T$ (the superscript “T" means “transpose") satisfy equations

$$curl_x \mathbf{E}^k(x) = i\omega\mu_0 \mathscr{M} \mathbf{H}^k(x), \tag{1.14}$$
$$curl_x \mathbf{H}^k(x) = -i\omega\varepsilon_0 \mathscr{E} \mathbf{E}^k(x) + \mathbf{e}^k \delta(x), \tag{1.15}$$

where $x = (x_1, x_2, x_3) \in \mathbb{R}^3$ is the $3D$ space variable; ω is a fixed parameter (frequency); $\mathbf{e}^1 = (1,0,0)^T$, $\mathbf{e}^2 = (0,1,0)^T$, $\mathbf{e}^3 = (0,0,1)^T$ are basis vectors of $\mathbb{R}^3$; i is the imaginary unit $i^2 = -1$; $\delta(x) = \delta(x_1)\delta(x_2)\delta(x_3)$, where $\delta(x_j)$ is the Dirac delta function concentrated at $x_j = 0$ for $j = 1,2,3$; $curl_x$ is the differential operator defined by

$$curl_x \mathbf{E}(x) = \left(\frac{\partial E_3}{\partial x_2} - \frac{\partial E_2}{\partial x_3}, \frac{\partial E_1}{\partial x_3} - \frac{\partial E_3}{\partial x_1}, \frac{\partial E_2}{\partial x_1} - \frac{\partial E_1}{\partial x_2} \right)$$

for a vector function $\mathbf{E}(x) = (E_1(x), E_2(x), E_3(x))$.

We suppose that matrices $\bar{\bar{\epsilon}}$, $\bar{\bar{g}}$, $\bar{\bar{\mu}}$, $\bar{\bar{h}}$ of the form (1.12) such that 6×6 symmetric matrices B and K defined by

$$B = \begin{pmatrix} \bar{\bar{\epsilon}} & -\bar{\bar{g}} \\ \bar{\bar{g}} & \bar{\bar{\epsilon}} \end{pmatrix}, \quad K = \begin{pmatrix} \bar{\bar{\mu}} & -\bar{\bar{h}} \\ \bar{\bar{h}} & \bar{\bar{\mu}} \end{pmatrix} \tag{1.16}$$

are positive definite.

Remark 1.4.1. Positive definiteness of B and K is the natural condition for a wide class of gyrotropic media. This is due to the facts that matrices $\bar{\bar{\epsilon}}$ and $\bar{\bar{\mu}}$ are always positive definite, and the elements of matrix $\bar{\bar{g}}$ are essentially smaller then elements of $\bar{\bar{\epsilon}}$, and the elements of matrix $\bar{\bar{h}}$ are essentially smaller then elements of $\bar{\bar{\mu}}$; see, for example, (Freiser, 1968; Pershan, 1967). Moreover for the positive definite matrices B and K, the matrices $\mathscr{E} = \bar{\bar{\epsilon}} + i\bar{\bar{g}}$ and $\mathscr{M} = \bar{\bar{\mu}} + i\bar{\bar{h}}$ are invertible, i.e. the inverse matrix $\mathscr{E}^{-1}$ and $\mathscr{M}^{-1}$ exist.

Multiplying (1.14) by $\mathscr{M}^{-1}$ from the left side and then applying the operator $curl_x$, we find

$$curl_x\left(\mathscr{M}^{-1} curl_x \mathbf{E}^k(x)\right) = i\omega\mu_0\, curl_x \mathbf{H}^k(x). \tag{1.17}$$

The following equation follows from (1.15), (1.17)

$$-\left(\frac{\omega}{c}\right)^2 \mathscr{E}\,\mathbf{E}^k(x) + curl_x(\mathscr{M}^{-1} curl_x \mathbf{E}^k(x)) = i\omega\mu_0 \mathbf{e}^k \delta(x). \tag{1.18}$$

Similarly, multiplying (1.15) by $\mathscr{E}^{-1}$ from the left side and then applying the operator $curl_x$, we find

$$curl_x\left(\mathscr{E}^{-1} curl_x \mathbf{H}^k(x)\right) = -i\omega\varepsilon_0\, curl_x \mathbf{E}^k(x) + curl_x\left(\mathbf{e}^k\delta(x)\right). \tag{1.19}$$

It follows from (1.14) and (1.19) that

$$-\left(\frac{\omega}{c}\right)^2 \mathscr{M}\,\mathbf{H}^k(x) + curl_x(\mathscr{E}^{-1} curl_x \mathbf{H}^k(x)) = curl_x\left(\mathscr{E}^{-1}\mathbf{e}^k\delta(x)\right). \tag{1.20}$$

Remark 1.4.2. Equations (1.18) and (1.20) can be written in the form (1.14), (1.15). This means that (1.18), (1.20) are equivalent to (1.14), (1.15). Moreover we can say that the Green's functions for the electric field is the matrix $\mathbb{E}(x)$ of the form (1.13) whose columns satisfy (1.18) and the Green's functions for the magnetic field is the matrix $\mathbb{H}(x)$ of the form (1.13) whose columns satisfy (1.20).

In chapter 2, we constructed a new method for the approximate computation of the Green's functions for the electric and magnetic fields of the time-harmonic Maxwell's equations in the general gyrotropic media. This method is based on the Fourier transform meta-approach where the Fourier image of the Green's functions for the electric and magnetic fields are computed exactly by some matrix transformations and symbolic computations in MATLAB and the inverse Fourier transform is computed in a regularized (approximate) form. The parameters of the regularization have been chosen by the comparison of the regularized Green's functions for the electric and magnetic fields with the Green's functions for the electric and magnetic fields obtained by the explicit formula for the isotropic case. The approximate computation of the inverse Fourier transform has been implemented by MATLAB tools. The computational experiments are presented in this chapter and confirms the robustness of this method. Using our method, we approximately compute the Green's functions for the electric and magnetic fields of the time-harmonic Maxwell's equations in the general electrically gyrotropic media in Chapter 3 and magnetically gyrotropic media in Chapter 4.

The second problem of the thesis is the approximate computation of the fundamental solutions of the electric field for general anisotropic conductive materials.

The time-dependent Maxwell's equations given as (1.1)-(1.4) with conservation law of charges (1.5) and the constitutive relations for anisotropic conductive materials given by

$$\mathbf{D} = \mathscr{E}\mathbf{E}, \quad \mathbf{B} = \mathscr{M}\mathbf{H}, \quad \mathbf{J} = \sigma\mathbf{E} + \mathbf{j}, \tag{1.21}$$

where $\mathscr{E} = (\mathscr{E}_{km})_{3\times 3}$ is the relative dielectric permittivity matrix (which is assume to be symmetric positive definite with constant elements); $\mathscr{M} = (\mathscr{M}_{km})_{3\times 3}$ is the relative magnetic permeability matrix (which is assume to be symmetric positive definite with constant elements), $k, m = 1, 2, 3$; σ is the conductivity matrix with constant elements;

$\mathbf{j} = (j_1, j_2, j_3)$ is the density of the electric current, $j_k = j_k(x,t)$, $k = 1,2,3$; $\sigma\mathbf{E}$ is the density of the eddy current.

Inserting (1.21) into (1.2) and using (1.1) we obtain 3×3 system of equations for the electric field $\mathbf{E}$; see, for example, (Courant & Hilbert, 1962), (p. 603)

$$\mathscr{E}\frac{\partial^2\mathbf{E}}{\partial t^2} + 4\pi\sigma\frac{\partial\mathbf{E}}{\partial t} + c^2 curl_x\left(\mathscr{M}^{-1}curl_x\mathbf{E}\right) = -4\pi\frac{\partial\mathbf{j}}{\partial t}. \tag{1.22}$$

The fundamental solution of the electric field for general anisotropic conductive materials is defined as a 3×3 matrix $\mathbb{E}$ whose columns $\mathbf{E}^m(x,t) = (E_1^m(x,t), E_2^m(x,t), E_3^m(x,t))^T$ are equal to zero for $t \le 0$ and satisfy (1.22) for $\mathbf{j}(x,t) = \mathbf{e}^m\delta(x_1)\delta(x_2)\delta(x_3)\delta(t)$, where $\mathbf{e}^1 = (1,0,0)^T$, $\mathbf{e}^2 = (0,1,0)^T$, $\mathbf{e}^3 = (0,0,1)^T$ are basis vector in $\mathbb{R}^3$; $\delta(t)$ is the Dirac delta function of the variable t concentrated at $t = 0$.

The system (1.22) is a hyperbolic system with constant coefficients. Using the meta-approach of (Hormander, 1963), (Section 3.8, p. 94) and (Schwartz, 1966) (p. 140) the existence of the fundamental solutions of the electric fields for general anisotropic media can be obtained in the space of distributions with finite supports if the time t runs the bounded interval $[0,T]$ (see, also a brief review of (Wagner, 2011b), (p. 2666-2668)). The fact that, the fundamental solutions are generalized functions (distributions) with compact supports for a fixed time variable, physically means that perturbation from the pulse point of force is propagated in a bounded domain anisotropic conductive media for a fixed time and therefore there is a quiet in all points outside of this bounded domain. Using the Paley-Wiener theorem (see, for example, (Simon & Reed, 1997)) we obtain that the Fourier transform of the fundamental solution with respect to space variables is an analytic function depending on Fourier parameters. Here the expression of the Fourier transform of the fundamental solutions presented in terms of the Fourier parameters does not contain singularities. We also note that to apply directly the meta-approach of (Hormander, 1963) (Section 3.8, p. 94) and (Schwartz, 1966) (p. 140) for computation of the fundamental solutions for general anisotropic conductive materials is questionable because of complexity of the technique over solutions of the hyperbolic equation (1.14) which is generalized function (distributions) having the nontrivial singular part; see, for example, (Wagner, 2011b)).

In Chapter 5, we suggest a new method of approximate computation of the fundamental solution of Maxwell's equations for the general anisotropic conductive materials. The method consists of the following. The equations for the fundamental solution are written in the form of the Fourier transformation with respect to the space variables. The obtained equations are reduced to a vector integral equation of the Volterra type. The solution of the obtained integral equation is corrected by the successive approximations in the form of the uniformly convergent infinite functional series. Finally, the inverse Fourier transform is applied to constructed series with respect to the Fourier parameters. The computation of the fundamental solutions of electric fields in general anisotropic conductive materials have been made by replacement of infinite series by a sum with finite terms and implemented numerically in MATLAB, the inverse Fourier transform by the integration over a bounded domain. The robustness of our method approved by the computational experiments.

CHAPTER TWO
THE APPROXIMATE COMPUTATION OF TIME HARMONIC MAXWELL'S EQUATIONS IN GENERAL GYROTROPIC MEDIA

This chapter deals with the frequency dependent Maxwell's equation in gyrotropic media and their applications. We suggest a method of an approximate (regularized) computation of the Green's functions for the electric and magnetic fields of the Maxwell's equations in the general gyrotropic media. This method is based on the Fourier transform meta-approach where the Fourier image of the Green's functions for the electric and magnetic fields are computed exactly by some matrix transformations and symbolic computations in MATLAB and the inverse Fourier transform is computed in a regularized (approximate) form. The parameters of the regularization have been chosen by the comparison of the regularized Green's functions for the electric and magnetic fields with the Green's functions for the electric and magnetic fields obtained by the explicit formula for the isotropic case. The approximate computation of the inverse Fourier transform has been implemented by MATLAB tools. The computational experiments are presented in this chapter.

2.1 Approximate Computation of the Green's Functions of the Electric Field

The construction of formulas for the approximate computation of the Green's functions for the electric and magnetic fields of the electric field for the Maxwell's equations is the main topic of this section. Equation (1.18) is used to obtain these formulas.

Let us consider the Fourier transform with respect to space variables $x = (x_1, x_2, x_3)$. The operator of this transform is denoted as $\mathcal{F}_x$ and defined by the following formula

$$\mathcal{F}_x[E(x)](\nu) = \int_{-\infty}^{\infty}\int_{-\infty}^{\infty}\int_{-\infty}^{\infty} E(x)e^{i\nu\cdot x}dx_1dx_2dx_3, \tag{2.1}$$

for the scalar integrable function $E(x)$, where $\nu = (\nu_1, \nu_2, \nu_3)$ is a $3D$ parameter of the Fourier transform; $\nu \cdot x = \nu_1 x_1 + \nu_2 x_2 + \nu_3 x_3$. The definition of the Fourier transform and its operator for any generalized function (tempered distribution) is given, for example, in (Vladimirov, 1979). The image of the Fourier transform of elements $E_j^k(x)$ of the Green's functions $\mathbb{E}(x)$ is denoted by $\widetilde{E}_j^k(\nu)$, i.e. $\widetilde{E}_j^k(\nu) = \mathcal{F}_x[E_j^k(x)](\nu)$, $j,k = 1,2,3$. Moreover we use the notation $\widetilde{\mathbf{E}}^k(\nu) = (\widetilde{E}_1^k(\nu), \widetilde{E}_2^k(\nu), \widetilde{E}_3^k(\nu))$ for the Fourier image of k-th column of $\mathbb{E}(x)$.

The constitutive relations for general gyrotropic media as (1.10) with (1.11)-(1.13), applying the operator of the Fourier transform $\mathcal{F}_x$, given as (2.1), to (1.18) and using the following equality (see, Yakhno, 2008)

$$\mathcal{F}_x[curl_x(\mathscr{M}^{-1} curl_x \mathbf{E}^k(x))] = S(\nu)\mathscr{M}^{-1} S(\nu)\widetilde{\mathbf{E}}^k(\nu),$$

we find

$$-\left(\frac{\omega}{c}\right)^2 \mathscr{E}\,\widetilde{\mathbf{E}}^k(\nu) + S(\nu)\mathscr{M}^{-1} S(\nu)\widetilde{\mathbf{E}}^k(\nu) = i\omega\mu_0\mathbf{e}^k, \tag{2.2}$$

where

$$S(\nu) = \begin{pmatrix} 0 & -\nu_3 & \nu_2 \\ \nu_3 & 0 & -\nu_1 \\ -\nu_2 & \nu_1 & 0 \end{pmatrix}. \tag{2.3}$$

Let us denote the real part of j component of $\widetilde{\mathbf{E}}^k(\nu)$ as $V_j^k(\nu)$ and the imaginary part of j component of $\widetilde{\mathbf{E}}^k(\nu)$ as $V_{j+3}^k(\nu)$, i.e. $V_j^k(\nu) = Re(\widetilde{E}_j^k(\nu))$ and $V_{j+3}^k(\nu) = Im(\widetilde{E}_j^k(\nu))$, $j = 1,2,3$. Then (2.2) can be written as a vector equation

$$-\left(\frac{\omega}{c}\right)^2 B\mathbf{V}^k(\nu) + C(\nu)\mathbf{V}^k(\nu) = \mathbf{F}^k, \tag{2.4}$$

where the matrix B is defined by (1.16) and $\mathbf{F}^1 = \omega\mu_0(0,0,0,1,0,0)^T$,
$\mathbf{F}^2 = \omega\mu_0(0,0,0,0,1,0)^T$, $\mathbf{F}^3 = \omega\mu_0(0,0,0,0,0,1)^T$.

Since B is positive definite and $C(\nu)$ is symmetric then it is possible to diagonalize simultaneously both matrices B and $C(\nu)$ (see, for example, Goldberg, 1992). Applying computational technique from (Yakhno, 2008) we can compute an orthogonal matrix $T(\nu)$ and diagonal matrix $D(\nu) = diag(d_1(\nu), d_2(\nu), \ldots, d_6(\nu))$, such that

$$\begin{aligned} T^T(\nu)C(\nu)T(\nu) &= D(\nu), \\ T^T(\nu)BT(\nu) &= I, \end{aligned}$$

where I is identity matrix and the superscript “T" means “transpose".

MATLAB code of this computation is given in Appendix A1.1.

Equation (2.4) is written in terms of a new unknown vector function $\mathbf{Y}^k(\nu)$ which is defined by

$$\mathbf{V}^k(\nu) = T(\nu)\mathbf{Y}^k(\nu). \tag{2.5}$$

After substitution (3.7) into (2.4) we find

$$-\left(\frac{\omega}{c}\right)^2 BT(\nu)\mathbf{Y}^k(\nu) + C(\nu)T(\nu)\mathbf{Y}^k(\nu) = \mathbf{F}^k. \tag{2.6}$$

Multiplying the equation (2.6) from the left side by $T^T(\nu)$, we find

$$-\left(\frac{\omega}{c}\right)^2 \mathbf{Y}^k(\nu) + D(\nu)\mathbf{Y}^k(\nu) = T^T(\nu)\mathbf{F}^k,$$

or in the component form

$$-\left(\frac{\omega}{c}\right)^2 Y_l^k(\nu) + d_l(\nu)Y_l^k(\nu) = (T^T(\nu)\mathbf{F}^k)_l, l = 1,2,...,6. \tag{2.7}$$

For $(\frac{w}{c})^2 - d_l(\nu) \neq 0$, the solution of (2.7) can be written as

$$Y_l^k(\nu) = \frac{(T^T(\nu)\mathbf{F}^k)_l}{-(\omega/c)^2 + d_l(\nu)}, \tag{2.8}$$

where $l = 1,2,...,6$. Let $\mathbf{Y}^k(\nu) = (Y_1^k(\nu), Y_2^k(\nu), \ldots, Y_6^k(\nu))$, then a solution $\mathbf{V}^k(\nu) = (V_1^k(\nu), V_2^k(\nu), \ldots, V_6^k(\nu))$ of (2.4) is determined by

$$\mathbf{V}^k(\nu) = T(\nu)\mathbf{Y}^k(\nu),$$

and components of solutions $\widetilde{\mathbf{E}}^k(\nu) = (E_1^k(\nu), E_2^k(\nu), E_3^k(\nu))$ of (2.2) for $k = 1,2,3$ are found by formulae

$$\widetilde{E}_j^k(\nu) = V_j^k(\nu) + iV_{j+3}^k(\nu), j = 1,2,3; k = 1,2,3. \tag{2.9}$$

Finally, applying the inverse Fourier transform to (2.9), we find columns of the electric matrix Green’s functions as vector functions whose components are tempered distributions, i.e.

$$\mathbf{E}^k(x) = \mathcal{F}_\nu^{-1}[\widetilde{\mathbf{E}}^k(\nu)](x), \tag{2.10}$$

where $\mathcal{F}_\nu^{-1}$ is the operator of the inverse Fourier transform in the space of distribution $S'(\mathbb{R}^3)$ (the definition of $\mathcal{F}_\nu^{-1}$ in the space $S'(\mathbb{R}^3)$ can be found, for example, in Vladimirov, 1979).

Usually the classical functions are defined by a point-wise manner and we can draw their graphs. Unfortunately, this point-wise definition and its graphical presentation is not adequate to singular tempered distributions (Vladimirov, 1979). They are very often replaced by regularized functions which are classical and have graphic presentations. This regularization has a parameter of the regularization and the singular generalized function is a limit in sense of the generalized functions space, when the parameter of the regularization tends to $+\infty$. Applying this approach the right hand side of (2.10) can be regularized by

$$\frac{1}{(2\pi)^3}\int_{-A}^{A}\int_{-A}^{A}\int_{-A}^{A}\widetilde{\mathbf{E}}^k(\nu)\,e^{-i\nu\cdot x}d\nu_1 d\nu_2 d\nu_3\,, \tag{2.11}$$

where A is the parameter of regularization.

For the numerical computation we take $A = N\Delta$ and approximate the integral (2.11) by the integral sum

$$\frac{1}{(2\pi)^3}\sum_{n=-N}^{N}\sum_{m=-N}^{N}\sum_{l=-N}^{N}\widetilde{\mathbf{E}}^k(n\Delta, m\Delta, l\Delta)\,e^{-i\Delta(nx_1+mx_2+lx_3)}(\Delta\nu)^3\,. \tag{2.12}$$

The parameters N and Δ are determined by the procedure described in Section 2.3.1.

2.2 Approximate Computation of the Green's Functions of the Magnetic Field

Let k be one of numbers 1, 2, 3. Applying the Fourier transform with respect to x to the equation (1.20) and using equalities

$$\begin{aligned}\mathcal{F}_x[\,curl_x(\mathscr{E}^{-1}\,curl_x\mathbf{H}^k(x))] &= S(\nu)\mathscr{E}^{-1}S(\nu)\widetilde{\mathbf{H}}^k(\nu)\,,\\ \mathcal{F}_x[\,curl_x(\mathscr{E}^{-1}\mathbf{e}^k)] &= S(\nu)\mathscr{E}^{-1}\mathbf{e}^k\,,\end{aligned}$$

we find

$$-\left(\frac{\omega}{c}\right)^2\mathscr{M}\widetilde{\mathbf{H}}^k(\nu) + S(\nu)\mathscr{E}^{-1}S(\nu)\widetilde{\mathbf{H}}^k(\nu) = S(\nu)\mathscr{E}^{-1}\mathbf{e}^k\,, \tag{2.13}$$

where $\mathscr{E}$ and $\mathscr{M}$ are defined by (1.11) and (1.12); $S(\nu)$ is given by (2.3); $\widetilde{\mathbf{H}}^k(\nu) = (\widetilde{H}_1^k(\nu), \widetilde{H}_2^k(\nu), \widetilde{H}_3^k(\nu))$, $\widetilde{H}_n^k(\nu) = \mathcal{F}_x[H_n^k(x)](\nu)$, $n = 1,2,3$.

We denote the real and imaginary parts of $\widetilde{H}_n^k(\nu)$ as $X_n^k(\nu)$ and $X_{n+3}^k(\nu)$, i.e. $\widetilde{H}_n^k(\nu) = X_n^k(\nu) + iX_{n+3}^k(\nu)$, $n = 1,2,3$. Moreover the real and imaginary parts of $S(\nu)\mathscr{E}^{-1}\mathbf{e}^k$ and $S(\nu)\mathscr{E}^{-1}S(\nu)$ are denoted as $(G_1^k(\nu), G_2^k(\nu), G_3^k(\nu))^T$, $(G_4^k(\nu), G_5^k(\nu), G_6^k(\nu))^T$ and $R_r(\nu)$, $R_i(\nu)$, respectively. This means that

$$\begin{aligned} S(\nu)\mathscr{E}^{-1}\mathbf{e}^k &= (G_1^k(\nu), G_2^k(\nu), G_3^k(\nu))^T + i(G_4^k(\nu), G_5^k(\nu), G_6^k(\nu))^T, \\ S(\nu)\mathscr{E}^{-1}S(\nu) &= R_r(\nu) + iR_i(\nu). \end{aligned}$$

We introduce vector functions $\mathbf{X}^k(\nu)$, $\mathbf{G}^k(\nu)$ and 6×6 matrix $P(\nu)$ by

$$\mathbf{X}^k(\nu) = (X_1^k(\nu), X_2^k(\nu), \ldots, X_6^k(\nu)),\ \mathbf{G}^k(\nu) = (G_1^k(\nu), G_2^k(\nu), \ldots, G_6^k(\nu)),$$

$$P(\nu) = \begin{pmatrix} R_r(\nu) & -R_i(\nu) \\ R_i(\nu) & R_r(\nu) \end{pmatrix}. \tag{2.14}$$

Using these notations the equation (2.13) can be written in the form

$$-\left(\frac{\omega}{c}\right)^2 K\mathbf{X}^k(\nu) + P(\nu)\mathbf{X}^k(\nu) = \mathbf{G}^k(\nu), \tag{2.15}$$

where K is 6×6 matrix defined by (1.16). We note that the matrix K is symmetric and positive definite (see Remark 1.4).

Moreover applying symbolic computation in MATLAB we can compute matrices $R_r(\nu)$, $R_i(\nu)$ in the exact form. They are the following

$$R_i(\nu) = \frac{1}{\xi_4}\begin{pmatrix} 0 & -a_{12} & a_{13} \\ a_{12} & 0 & -a_{23} \\ -a_{13} & a_{23} & 0 \end{pmatrix}, \quad R_r(\nu) = \frac{1}{\xi_4}\begin{pmatrix} b_{11} & b_{12} & b_{13} \\ b_{12} & b_{22} & b_{23} \\ b_{13} & b_{23} & b_{33} \end{pmatrix}, \tag{2.16}$$

where

$$\begin{aligned} &a_{12} = \nu_2\nu_3\xi_1 + \nu_3^2\xi_2 + \nu_1\nu_3\xi_3,\ a_{13} = \nu_2^2\xi_1 + \nu_2\nu_3\xi_2 + \nu_1\nu_2\xi_3, \\ &a_{23} = \nu_1\nu_3\xi_2 + \nu_1^2\xi_3 + \nu_1\nu_2\xi_1, \\ &b_{11} = -\nu_2^2\xi_5 + 2\nu_2\nu_3\xi_6 - \nu_3^2\xi_7,\ b_{12} = \nu_1\nu_2\xi_5 - \nu_1\nu_3\xi_6 - \nu_2\nu_3\xi_8 + \nu_3^2\xi_9, \\ &b_{13} = \nu_1\nu_3\xi_7 - \nu_1\nu_2\xi_6 - \nu_2^2\xi_8 - \nu_2\nu_3\xi_9,\ b_{22} = -\nu_1^2\xi_5 + 2\nu_1\nu_3\xi_8 - \nu_3^2\xi_{10}, \\ &b_{23} = \nu_2\nu_3\xi_{10} - \nu_1\nu_2\xi_8 - \nu_1^2\xi_6 + \nu_1\nu_3\xi_9,\ b_{33} = -\nu_1^2\xi_7 + 2\nu_1\nu_2\xi_8 - \nu_2^2\xi_{10}, \end{aligned}$$

$$\xi_1 = \epsilon_{12}g_1 + \epsilon_{22}g_2 + \epsilon_{23}g_3\,,\ \xi_2 = \epsilon_{13}g_1 + \epsilon_{23}g_2 + \epsilon_{33}g_3\,,$$

$$\xi_3 = \epsilon_{11}g_1 + \epsilon_{12}g_2 + \epsilon_{13}g_3\,,\ xi_4 = \epsilon_{33}\epsilon_{12}^2 - 2\epsilon_{12}\epsilon_{13}\epsilon_{23} + 2\epsilon_{12}g_1g_2 + \epsilon_{22}\epsilon_{13}^2$$

$$+2\epsilon_{13}g_1g_3 + \epsilon_{11}\epsilon_{23}^2 + 2\epsilon_{23}g_2g_3 + \epsilon_{11}g_1^2 + \epsilon_{22}g_2^2 + \epsilon_{33}g_3^2 - \epsilon_{11}\epsilon_{22}\epsilon_{33}\,,$$

$$\xi_5 = \epsilon_{12}^2 + g_3^2 - \epsilon_{11}\epsilon_{22}\,,\ \xi_6 = g_2g_3 - \epsilon_{12}\epsilon_{13} + \epsilon_{11}\epsilon_{23}\,,\ \xi_7 = \epsilon_{13}^2 + g_3^2 - \epsilon_{11}\epsilon_{33}\,,$$

$$\xi_8 = g_1g_3 - \epsilon_{12}\epsilon_{23} + \epsilon_{13}\epsilon_{22}\,,\ \xi_9 = g_1g_2 - \epsilon_{13}\epsilon_{23} + \epsilon_{12}\epsilon_{33}\,,$$

$$\xi_{10} = \epsilon_{23}^2 + g_1^2 - \epsilon_{22}\epsilon_{33}\,.$$

It follows from (2.14) and (2.16) that the matrix $P(\nu)$ is symmetric. Since K is positive definite and $P(\nu)$ is symmetric we can make the reasonings which are similar to Section 2.2 (see also Goldberg, 1992) to diagonalize simultaneously both matrices K and $P(\nu)$. Therefore using the computational technique from (Kong, 1984) we can compute symbolically in MATLAB an orthogonal matrix $Q(\nu)$ and diagonal matrix $M(\nu) = diag(\,m_n(\nu)\,, n = 1,2,3,4,5,6\,)$ such that

$$\begin{aligned} Q^T(\nu)KQ(\nu) &= I\,, \\ Q^T(\nu)P(\nu)Q(\nu) &= M(\nu)\,. \end{aligned}$$

MATLAB code of computation of $Q(\nu)$ and $M(\nu)$ is given in Appendix A1.2.

Equation (2.15) is written in terms of vector function $\mathbf{Z}^k(\nu) = Q^T(\nu)\mathbf{X}^k(\nu)$ as follows

$$-\left(\frac{\omega}{c}\right)^2 KQ(\nu)\mathbf{Z}^k(\nu) + P(\nu)Q(\nu)\mathbf{Z}^k(\nu) = \mathbf{G}^k(\nu)\,. \tag{2.17}$$

Multiplying the equation (2.17) by $Q^T(\nu)$ from the left side we find

$$-\left(\frac{\omega}{c}\right)^2 \mathbf{Z}^k(\nu) + M(\nu)\mathbf{Z}^k(\nu) = Q^{-1}(\nu)\mathbf{G}^k\,. \tag{2.18}$$

For $(\omega/c)^2 - m_n(\nu) \neq 0$ the solution of (2.18) can be written in a component form as follows

$$Z_n^k(\nu) = \frac{(Q^{-1}(\nu)\mathbf{G}^k)_n}{-(\omega/c)^2 + m_n(\nu)}\,, \tag{2.19}$$

where $n = 1,2,...,6$. A solution $\mathbf{X}^k(\nu) = (X_1^k(\nu), X_2^k(\nu), \ldots, X_6^k(\nu))$ of (2.15) is determined by (2.19) and formulae

$$\mathbf{Z}^k(\nu) = (Z_1^k(\nu), Z_2^k(\nu), \ldots, Z_6^k(\nu)),\ \mathbf{X}^k(\nu) = Q(\nu)\mathbf{Z}^k(\nu).$$

The components of a solution $\mathbf{H}^k(\nu) = (H_1^k(\nu), H_2^k(\nu), H_3^k(\nu))$ of (2.13) is found by

$$\widetilde{H}_n^k = X_n^k(\nu) + iX_{n+3}^k(\nu)\,,\, j = 1,2,3\,; n = 1,2,3\,. \tag{2.20}$$

Applying the inverse Fourier operator $\mathcal{F}_\nu^{-1}$ to $\mathbf{H}^k(\nu)$ we find the $k-$column of the matrix fundamental solution of the magnetic field $\mathbf{H}^k(x)$ as a vector function whose components are tempered distributions, i.e.

$$\mathbf{H}^k(x) = \mathcal{F}_\nu^{-1}[\widetilde{\mathbf{H}}^k(\nu)](x)\,. \tag{2.21}$$

The right hand side of (2.21) can be regularized by

$$\frac{1}{(2\pi)^3}\int_{-A}^{A}\int_{-A}^{A}\int_{-A}^{A}\widetilde{\mathbf{H}}^k(\nu)\,e^{-i\nu\cdot x}d\nu_1 d\nu_2 d\nu_3\,, \tag{2.22}$$

where A is the parameter of regularization.

For the numerical computation we take $A = N\Delta$ and approximate the integral (2.22) by the integral sum

$$\frac{1}{(2\pi)^3}\sum_{n=-N}^{N}\sum_{m=-N}^{N}\sum_{l=-N}^{N}\widetilde{\mathbf{H}}^k(\Delta n, \Delta m, \Delta l)\,e^{-i\Delta(nx_1+mx_2+lx_3)}(\Delta\nu)^3\,. \tag{2.23}$$

The parameters N and Δ are determined by the procedure described in Section 2.3.1.

2.3 Computational Experiments

The images of the Fourier transform of the elements of the Green's functions solutions of electric and magnetic fields in general gyrotropic media are found exactly by symbolic computations in MATLAB. The code of these symbolic computations is given in Appendix A1.1 and Appendix A1.2. We note that the inverse Fourier transform of elements of fundamental solutions and their images are defined as transformations in the space of the tempered distributions. Moreover the symbolic (analytic) computation of the inverse Fourier transform of the Fourier images of the Green's functions of electric and magnetic fields can be done in isotropic media only. Unfortunately symbolic and numerical computations of the inverse Fourier transform are not developed in the space of the tempered distributions. For this reason we suggest to compute the Green's functions for the electric and magnetic fields in the regularized (approximate) form. In our approach we use formulae (2.12), (2.23) and select the parameter of regularization N and Δ using the comparison of the Green's functions for the electric and magnetic fields in an isotropic medium which can be found in exact and regularized forms. Because of the type of the Green's functions (type of singularities) for isotropic media and fundamental solutions of the electric and magnetic fields for gyrotropic media are similar, we apply the same parameters of regularization which are found for the isotropic medium for the computation of approximate fundamental solutions.

2.3.1 Determining Parameters for the Approximate Computation of the Inverse Fourier Transform (Using Isotropic Maxwell's Equations)

Equations (1.14)-(1.15) for columns of the electric and magnetic matrix Green's functions in isotropic homogeneous medium (free space) have the form

$$curl_x \mathbf{E}^k(x) = i\omega\mu_0 \mathbf{H}^k(x), \tag{2.24}$$

$$curl_x \mathbf{H}^k(x) = -i\omega\varepsilon_0 \mathbf{E}^k(x) + \mathbf{e}^k \delta(x). \tag{2.25}$$

Let $\mathbf{E}^k(x)$, $\mathbf{H}^k(x)$ satisfy (2.24), (2.25). The condition $div_x \mathbf{H}^k(x) = 0$ follows from (2.24). Applying $curl_x$ operator to (2.25) and using $div_x \mathbf{H}^k(x) = 0$ we find that $\mathbf{H}^k(x)$ satisfies

$$\Delta \mathbf{H}^k(x) + \left(\frac{w}{c}\right)^2 \mathbf{H}^k(x) = -curl_x(\mathbf{e}^k \delta(x)). \tag{2.26}$$

The vector function $\mathbf{H}^k(x)$ defined by

$$\mathbf{H}^k(x) = \frac{1}{4\pi} curl_x \left(\frac{\mathbf{e}^k \exp(i\omega|x|/c)}{|x|} \right), \; |x| = \sqrt{x_1^2 + x_2^2 + x_3^2}, \tag{2.27}$$

is a solution of (2.26) (see, Vladimirov, 1971) and therefore this vector function is the $k-column$ of the magnetic matrix Green's functions in free space. From the other hand we compute approximately $\mathbf{H}^k(x)$ in MATLAB by the method described in Section 2.2.

Namely, applying the symbolic computation by the code of Appendix A1.2 we find the Fourier image of $\mathbf{H}^k(x)$ in the exact form. Then using the integral sum (2.22), we compute $H^k|_{(N,\Delta)}(x)$, for $\Delta = 0.1, 0.5, 0.8, 1.0$, $N = 20, 30, 40, 50, 60, 80$ and so on, numerically. Further, we compare the computed values of $H^k|_{(N,\Delta)}(x)$ with values of the function $H^k(x)$ obtained by (2.27). We have observed that the difference between the values of $H^k|_{(N,\Delta)}(x)$ and $H^k(x)$ corresponding to $\Delta = 1$ and $N = 30, 40, 50, 60, 80, 100$ becomes small and increment of the approximation for the parameter N is not essential, according to the case $\Delta = 1$, $N = 40$. For this reason we choose $\Delta = 1$, $N = 40$ as the suitable parameters for the calculation of the inverse Fourier transform by (2.23).

We have presented $1D$ graphs of the functions $H_3^1(x)$ and $H_3^1|_{(N,\Delta)}(x)$ for the different values of N and Δ in Figure 2.1 and Figure 2.2.

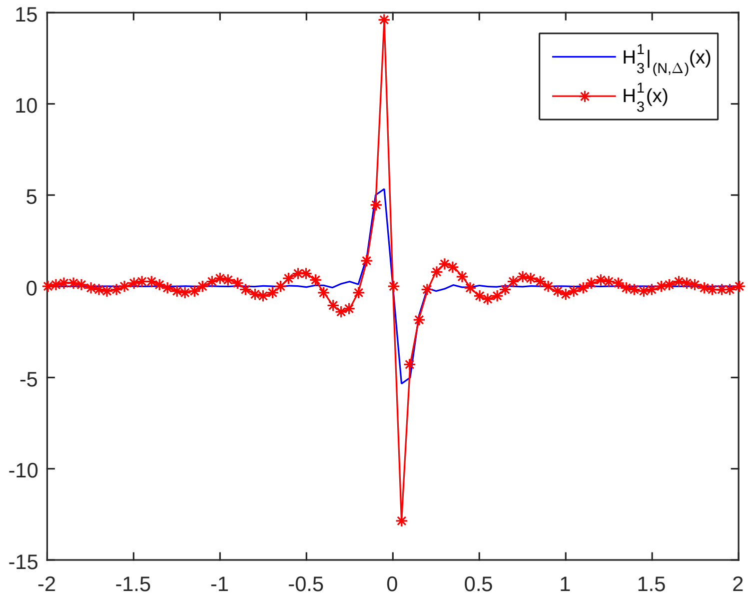

Figure 2.1 $1D$ plot of $H_3^1(x)$ and $H_3^1|_{(N,\Delta)}(x)$ for $N = 40$, $\Delta = 0.5$

2.3.2 The Approximate Computation of the Electric and Magnetic Green's Functions in General Gyrotropic Media

For computational experiments, we take $\omega = 3Ghz$ and $\omega = 6Ghz$ (microwave region) and consider three media characterized by the permittivity $\varepsilon_0\mathscr{E}$ and permeability

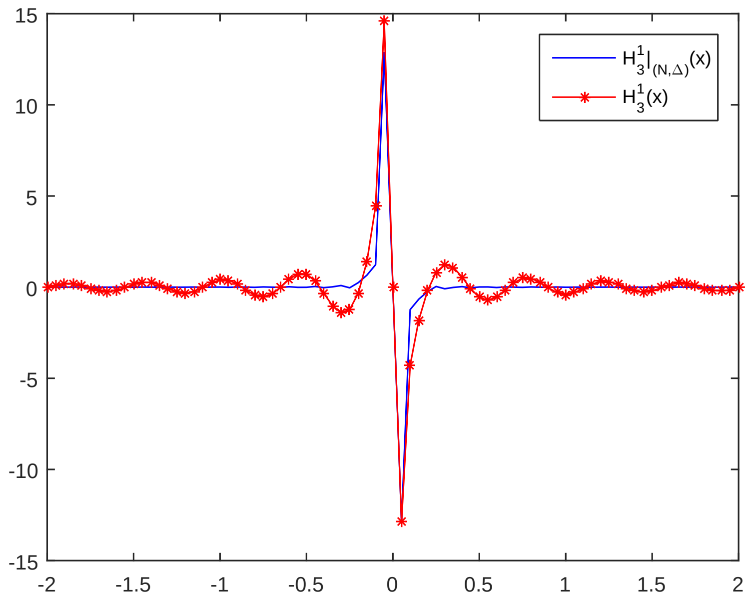

Figure 2.2 $1D$ plot of $H_3^1(x)$ and $H_3^1|_{(N,\Delta)}(x)$ for $N = 40$, $\Delta = 1.0$

$\mu_0\mathscr{M}$ (ε_0, μ_0 are the permittivity and permeability of free space and $\mathscr{E}$, $\mathscr{M}$ are relative permittivity and permeability).

Case 1: The first medium is electrically and magnetically anisotropic without magneto-optic activity. The electric and magnetic susceptibilities $\bar{\bar{g}}$ and $\bar{\bar{h}}$ are vanished in this medium. This medium is characterized by $\varepsilon_0\mathscr{E}$ and $\mu_0\mathscr{M}$ where

$$\mathscr{E} = \begin{pmatrix} 13.4 & -0.3 & -2.1 \\ -0.3 & 0.7 & 1.9 \\ -2.1 & 1.9 & 6.4 \end{pmatrix}, \mathscr{M} = \begin{pmatrix} 4.3 & -2.1 & -0.2 \\ -2.1 & 3.5 & 1.4 \\ -0.2 & 1.4 & 2.9 \end{pmatrix}.$$

Moreover we consider two media with magneto-optic activities. The electric and magnetic susceptibilities $\bar{\bar{g}}$ and $\bar{\bar{h}}$ are different from zero and different from each other. They are the following

Case 2: $\bar{\bar{g}} = \bar{\bar{g}}_0$, $\bar{\bar{h}} = \bar{\bar{h}}_0$; **Case 3:** $\bar{\bar{g}} = 2\bar{\bar{g}}_0$, $\bar{\bar{h}} = 2\bar{\bar{h}}_0$, where $\bar{\bar{g}}_0$ and $\bar{\bar{h}}_0$ are given by

$$\bar{\bar{g}}_0 = \begin{pmatrix} 0 & i0.5 & -i0.4 \\ -i0.5 & 0 & i0.2 \\ i0.4 & -i0.2 & 0 \end{pmatrix}, \bar{\bar{h}}_0 = \begin{pmatrix} 0 & i0.1 & -i0.3 \\ -i0.1 & 0 & i0.4 \\ i0.3 & -i0.4 & 0 \end{pmatrix}.$$

The relative permittivities and permeabilities for both cases are given by

Case 2:

$$\mathscr{E} = \begin{pmatrix} 13.4 & -0.3+i0.5 & -2.1-i0.4 \\ -0.3-i0.5 & 0.7 & 1.7+i0.2 \\ -2.1+i0.4 & 1.7-i0.2 & 6.4 \end{pmatrix},$$

$$\mathscr{M} = \begin{pmatrix} 4.3 & -2.1+i0.1 & -0.2-i0.3 \\ -2.1-i0.1 & 3.5 & 1.4+i0.4 \\ -0.2+i0.3 & 1.4-i0.4 & 2.9 \end{pmatrix}.$$

Case 3:

$$\mathscr{E} = \begin{pmatrix} 13.4 & -0.3+i1.0 & -2.1-i0.8 \\ -0.3-i1.0 & 0.7 & 1.7+i0.4 \\ -2.1+i0.8 & 1.7-i0.4 & 6.4 \end{pmatrix},$$

$$\mathscr{M} = \begin{pmatrix} 4.3 & -2.1+i0.2 & -0.2-i0.6 \\ -2.1-i0.2 & 3.5 & 1.4+i0.8 \\ -0.2+i0.6 & 1.4-i0.8 & 2.9 \end{pmatrix}.$$

Applying codes of Appendix A1.1 and Appendix A1.2 for the symbolic computations in MATLAB, we have found the Fourier images of all columns of the Green's functions of the electric and magnetic fields in the exact forms. After that, applying the method described in Sections 2.1 and 2.2, we have computed approximately all columns of the Green's functions for these fields. In this computations, we have taken the parameters of the regularization as: $N = 40$, $\Delta = 1$.

The results of computations are presented in Figure 2.3-Figure 2.9. Figure 2.3, Figure 2.5-Figure 2.7 show the dependence of elements E_2^1, E_3^1, H_3^1 of the Green's functions of the electric and magnetic fields from the magneto-optic activities for $x_1 = x_2 = z$, $x_3 = 0$, $\omega = 3Ghz$; Figure 2.4, Figure 2.8 demonstrate the effect of frequency on the Green's functions.

Figure 2.3(a), (b) present the $1D$ plots of $Im(E_2^1(z,z,0))$, $Re(E_2^1(z,z,0))$ for $x_1 = x_2 = z$, $x_3 = 0$, $\omega = 3Ghz$ for Cases 1-3, respectively. Figure 2.8(a), (b) present the $1D$ plots of $Re(H_3^1(z,z,0))$, $Im(H_3^1(z,z,0))$ for $x_1 = x_2 = z$, $x_3 = 0$, $\omega = 3Ghz$ for Cases 1-3, respectively.

The behavior of the real and imaginary parts of the computed components of the Green's functions is presented in Figure 2.5-Figure 2.7. The result of the simulation $Im(E_2^1(x_1, x_2, 0))$ for $\omega = 3Ghz$, Case 1, is presented in Figure 2.5. The $3D$ plot of $Im(E_2^1(x_1, x_2, 0))$ is shown in Figure 2.5(b). Here the horizontal axes are x_1 and x_2, respectively. The vertical axis is the magnitude of $Im(E_2^1 x_1, x_2, 0))$. Figure 2.5(a) is a screen shot of $2D$ level plot of the same surface $Im(E_2^1(x_1, x_2, 0))$, i.e. a view of the surface $z = Im(E_2^1(x_1, x_2, 0))$ presented in Figure 2.5(b) from the top of z-axis. Figure 2.6(a) presents $2D$ graph of $Im(E_2^1(x_1, x_2, 0))$. Figure 2.6(b) presents the $3D$ graph of $Im(E_2^1(x_1, x_2, 0))$ for $\omega = 3Ghz$, Case 3. Figure 2.7(a) presents $2D$ graph of $Re(E_3^1(x_1, x_2, 0))$. Figure 2.7(b) presents the $3D$ graph of $Re(E_3^1(x_1, x_2, 0))$ for $\omega = 3Ghz$, Case 3.

Figure 2.4, Figure 2.9 demonstrates the results of the computation of real and imaginary parts of $E_3^1(x)$, $H_1^1(x)$ for Case 2 for $\omega = 3Ghz, 6Ghz$, respectively.

Figure 2.4(a), (b) present the $1D$ plots of $Re(E_3^1(z,z,0))$, $Im(E_3^1(z,z,0))$ for $x_1 = x_2 = z$, $x_3 = 0$, for $\omega = 3Ghz$ and $\omega = 6Ghz$ respectively. Figure 2.9(a), (b) present the $1D$ graphs of $Re(H_1^1(x_1, x_2, 0))$ and $Im(H_1^1(x_1, x_2, 0))$, respectively for $\omega = 3Ghz, 6Ghz$. These graphs show the influence of frequency ω on the components of the Green's functions.

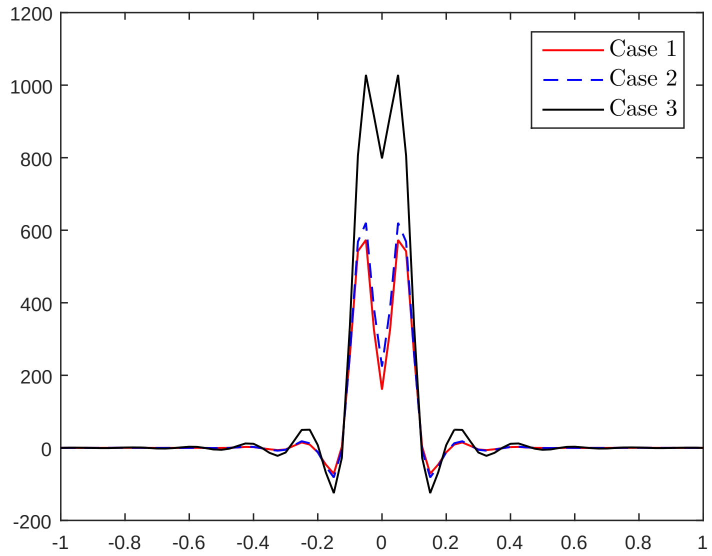

(a)

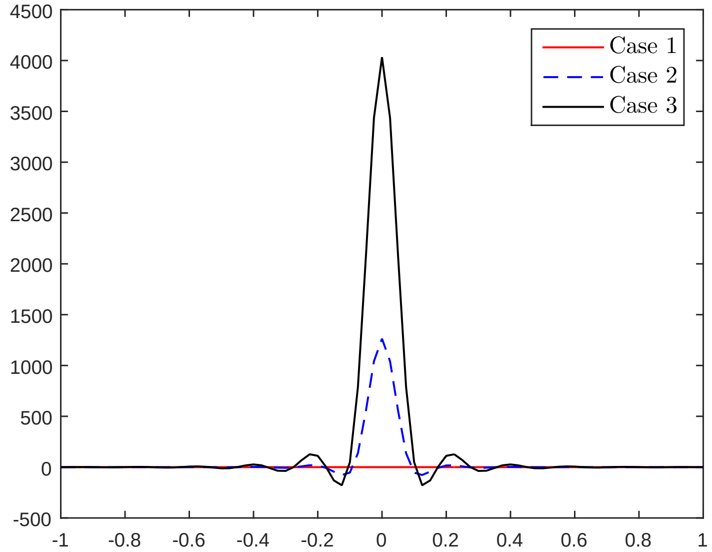

(b)

Figure 2.3 $\omega = 3Ghz$, Case 1-3, (a) $1D$ plot of $Im(E_2^1(z,z,0))$; (b) $1D$ plot of $Re(E_2^1(z,z,0))$.

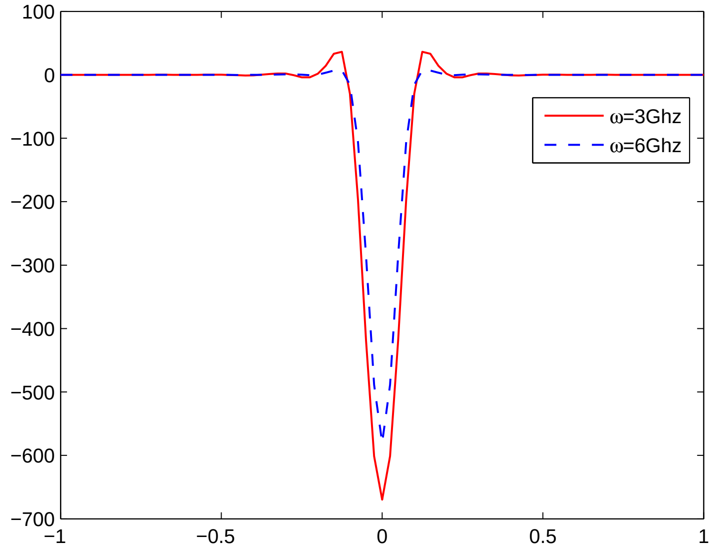

(a)

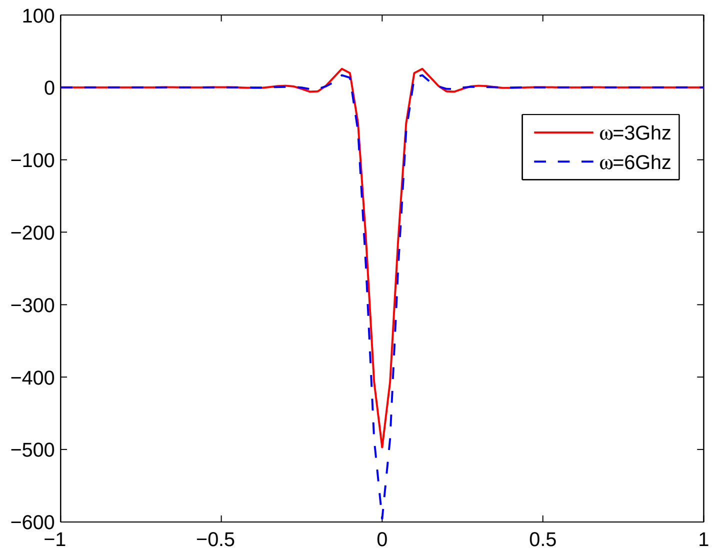

(b)

Figure 2.4 $\omega = 3Ghz, 6Ghz$, Case 2, (a) $1D$ plot of $Im(E_3^1(z,z,0))$; (b) $1D$ plot of $Re(E_3^1(z,z,0))$.

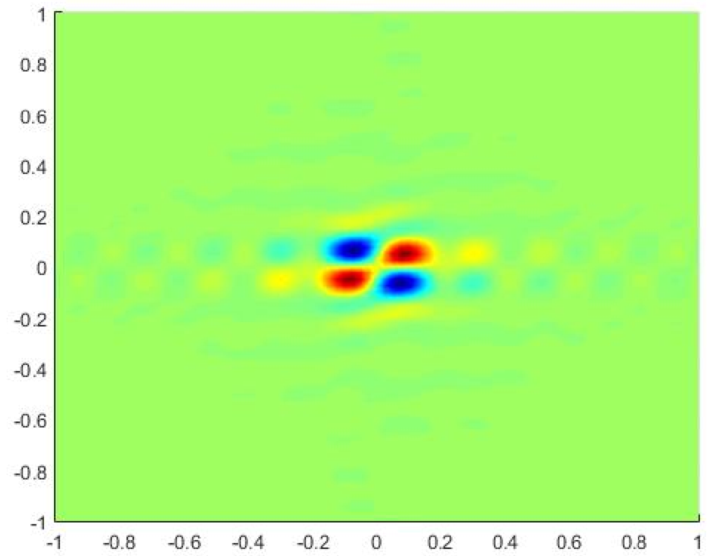

(a)

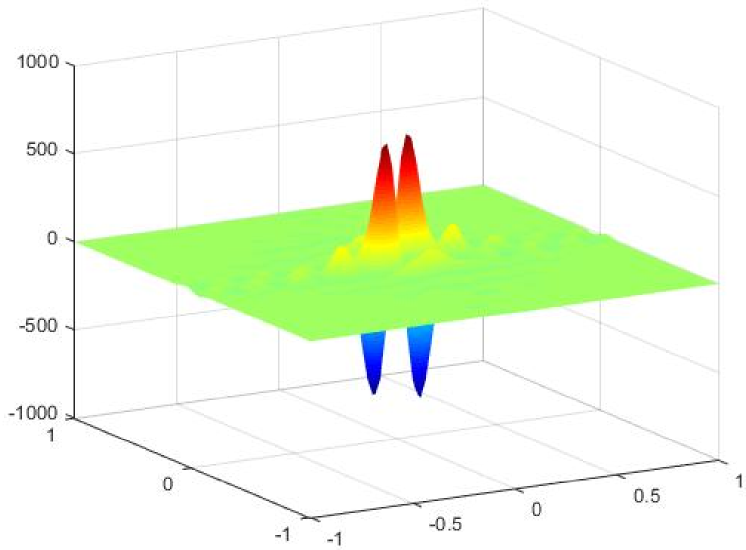

(b)

Figure 2.5 $\omega = 3Ghz$, Case 1, (a) $2D$ plot of $Im(E_2^1(x_1, x_2, 0))$; (b) $3D$ plot of $Im(E_2^1(x_1, x_2, 0))$.

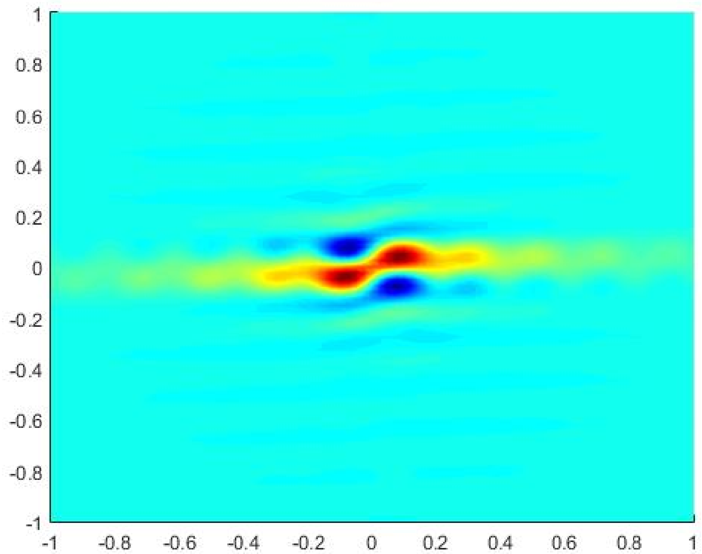

(a)

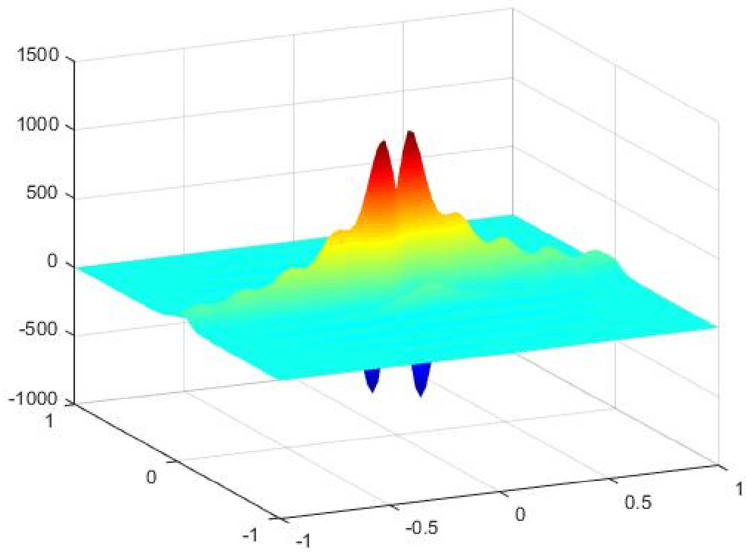

(b)

Figure 2.6 $\omega = 3Ghz$, Case 3, (a) $2D$ plot of $Im(E_2^1(x_1, x_2, 0))$; (b) $3D$ plot of $Im(E_2^1(x_1, x_2, 0))$.

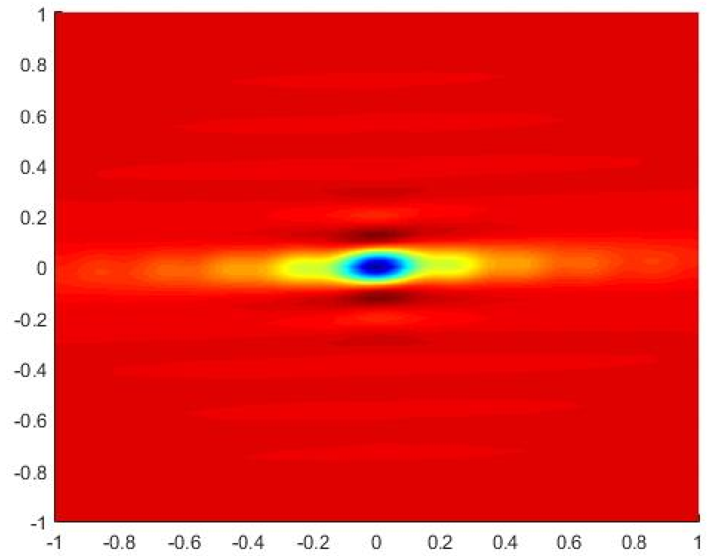

(a)

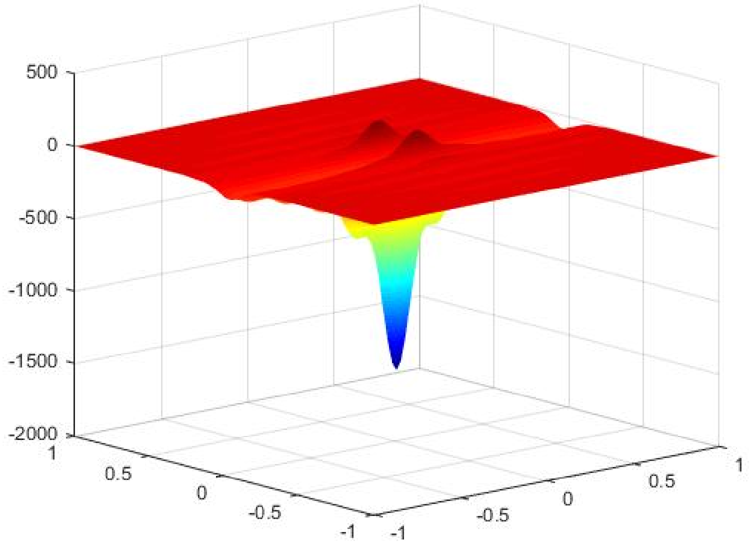

(b)

Figure 2.7 $\omega = 3Ghz$, Case 3, (a) $2D$ plot of $Re(E_3^1(x_1, x_2, 0))$; (b) $3D$ plot of $Re(E_3^1(x_1, x_2, 0))$.

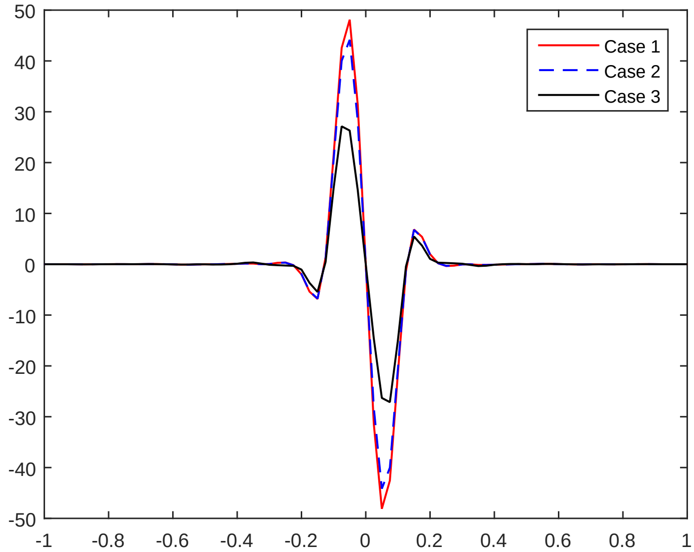

(a)

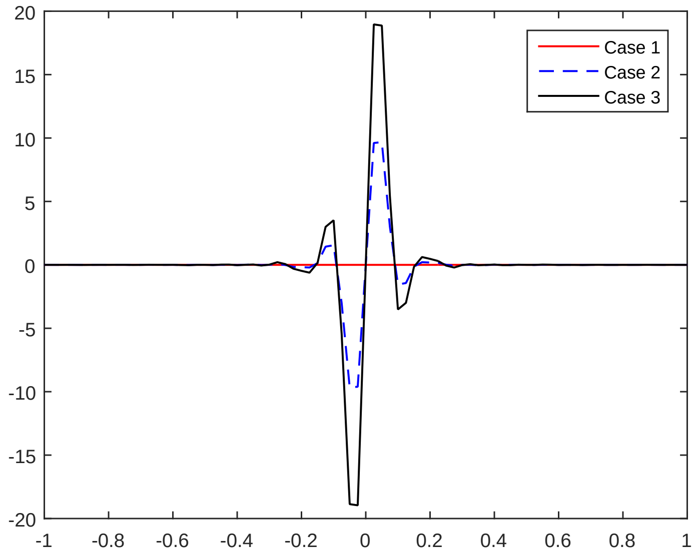

(b)

Figure 2.8 $\omega = 3Ghz$, Case 1-3, (a) $1D$ plot of $Im(H_3^1(z,z,0))$; (b) $1D$ plot of $Re(H_3^1(z,z,0))$.

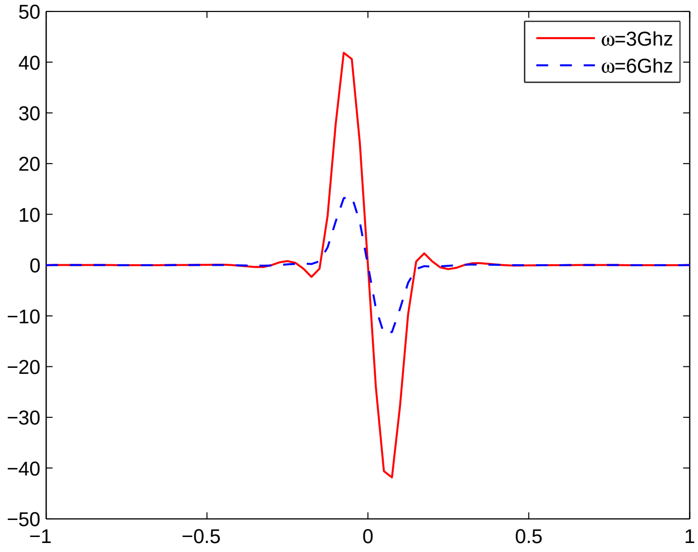

(a)

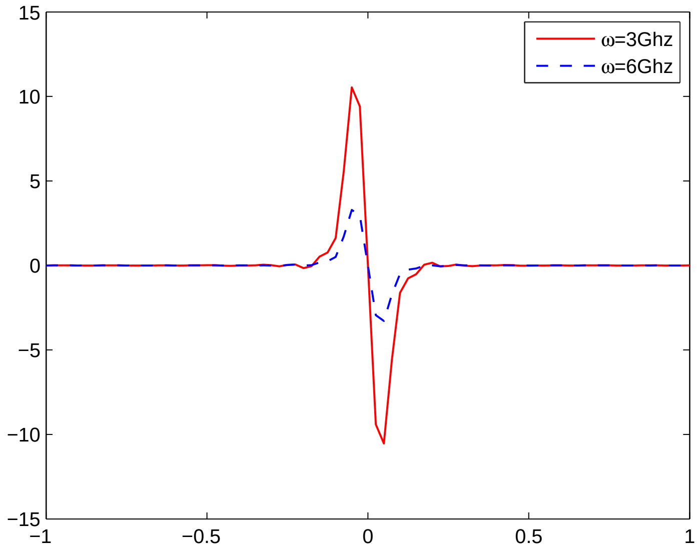

(b)

Figure 2.9 $\omega = 3Ghz, 6Ghz$, Case 2, (a) $1D$ plot of $Im(H_1^1(z,z,0))$; (b) $1D$ plot of $Re(H_1^1(z,z,0))$.

2.4 Summary of the Chapter Two

The new method of the approximate computation of the Green's functions for the electric and magnetic fields in general gyrotropic media has been developed. This method has two steps. On the first step the Fourier images of the elements of the electric and magnetic matrix Green's functions with respect to space variables are computed exactly by symbolic transformations in MATLAB. Finally, the elements of the electric and magnetic matrix Green's functions are derived approximately by the regularized numerical computation of the inverse Fourier transform of their images obtained on the previous step. The parameters of the regularization are chosen by comparison the elements of regularized Green's functions for the electric and magnetic fields with exact Green's functions for the electric and magnetic fields in the case of an isotropic medium, which can be found explicitly.

The robustness of the method for the approximate computation of the Green's functions has been tested by the comparison with exact formulae for the Green's functions of magnetic fields in isotropic homogeneous media. A dependence of values of the electric and magnetic matrix Green's functions from the different level of electric and magnetic susceptibility and frequency has been determined.

CHAPTER THREE
COMPUTING THE ELECTRIC AND MAGNETIC MATRIX GREEN'S FUNCTIONS IN GENERAL ELECTRICALLY GYROTROPIC MEDIA

A method for an approximate computation of the electric and magnetic Green's functions for the time-harmonic Maxwell's equations in the general electrically gyrotropic materials is proposed in this chapter. This method is based on the Fourier transform meta-approach: the equations for electric and magnetic fields are written in terms of images of the Fourier transform with respect to space variables and as a result of it the linear algebraic systems for finding Fourier images of the columns of the Green's functions for the electric and magnetic fields are obtained. The explicit formulas for the solutions of the obtained systems have been found. Finally, elements of the Green's functions for the electric and magnetic fields are determined by the inverse Fourier transform in the space of tempered distributions. The approximate computation of the inverse Fourier transform has been implemented by MATLAB tools. The computational experiments confirm the robustness of the method.

3.1 Electric and Magnetic Green's Functions in General Gyro-electric Media

For gyro-electric materials, $\mathscr{M} = I$ in (1.10) and the columns of electric and magnetic matrix Green's functions (1.13) satisfies

$$-\left(\frac{\omega}{c}\right)^2 \mathscr{E}\mathbf{E}^{\mathbf{k}}(x,\omega) + curl_x(curl_x\mathbf{E}^{\mathbf{k}}(x,\omega)) = i\omega\mu_0\mathbf{e}^{\mathbf{k}}\delta(x). \tag{3.1}$$

$$-\left(\frac{\omega}{c}\right)^2 \mathbf{H}^{\mathbf{k}}(x,\omega) + curl_x(\mathscr{E}^{-1}curl_x\mathbf{H}^{\mathbf{k}}(x,\omega)) = curl_x(\mathscr{E}^{-1}\mathbf{e}^{\mathbf{k}}\delta(x)). \tag{3.2}$$

Here $x = (x_1, x_2, x_3) \in \mathbb{R}^3$ is the $3D$ space variable; ω is a fixed parameter (frequency); $\varepsilon_0 = 8.854 \times 10^{-12} F/m$, $\mu_0 = 1.257 \times 10^{-6} N/A^2$ are positive constants (dielectric permittivity and magnetic permeability) of vacuum, respectively; $\mathbf{e}^1 = (1,0,0)^T$, $\mathbf{e}^2 = (0,1,0)^T$, $\mathbf{e}^3 = (0,0,1)^T$ are basis vectors of $\mathbb{R}^3$; i is the imaginary unit $i^2 = -1$; $\delta(x) = \delta(x_1)\delta(x_2)\delta(x_3)$, $\delta(x_j)$ is the Dirac delta function concentrated at $x_j = 0$ for $j = 1,2,3$.

3.1.1 Computing the Electric Green's Function

Let $\widetilde{\mathbf{E}}^{\mathbf{k}}(\nu) = (\widetilde{E}_1^k, \widetilde{E}_2^k, \widetilde{E}_3^k)$, where $\widetilde{E}_j^k = \mathcal{F}_x[E_j^k(x)](\nu)$, $j,k = 1,2,3$. Applying the operator of the Fourier transform $\mathcal{F}_x$ given in (2.1) to (3.1) and using equality (see, Yakhno, 2008)

$$\mathcal{F}_x[curl_x(curl_x \mathbf{E}^{\mathbf{k}}(x))] = A(\nu)\widetilde{\mathbf{E}}^{\mathbf{k}}(\nu),$$

we find

$$-\left(\frac{\omega}{c}\right)^2 \mathcal{E}\widetilde{\mathbf{E}}^{\mathbf{k}}(\nu) + A(\nu)\widetilde{\mathbf{E}}^{\mathbf{k}}(\nu) = i\omega\mu_0 \mathbf{e}^{\mathbf{k}}, \tag{3.3}$$

where

$$A(\nu) = \begin{pmatrix} \nu_2^2 + \nu_3^2 & -\nu_1\nu_2 & -\nu_1\nu_3 \\ -\nu_1\nu_2 & \nu_1^2 + \nu_3^2 & -\nu_2\nu_3 \\ -\nu_1\nu_3 & -\nu_2\nu_3 & \nu_1^2 + \nu_2^2 \end{pmatrix}. \tag{3.4}$$

The matrix $\mathcal{E}$ is defined by (1.11) with $\mathcal{M} = I$. And from (1.16), the matrix B is symmetric and from Remark (1.4.1) it is positive definite and $C(\nu)$ is symmetric 6×6 matrices defined by

$$C(\nu) = \begin{pmatrix} A(\nu) & 0 \\ 0 & A(\nu) \end{pmatrix}. \tag{3.5}$$

Moreover under assumption of positive definiteness of B the matrix $\mathcal{E}$ is invertible, i.e. the inverse matrix $\mathcal{E}^{-1}$ exists.

Let us denote V_j^k as the real part of j component of $\widetilde{\mathbf{E}}^{\mathbf{k}}(\nu)$ and V_{j+3}^k as the imaginary part of j component of $\widetilde{\mathbf{E}}^{\mathbf{k}}(\nu)$, i.e. $V_j^k = Re(\widetilde{E}_j^k(\nu))$ and $V_{j+3}^k = Im(\widetilde{E}_j^k(\nu))$, $j = 1,2,3$. Then equality (3.3) can be written as a vector equation

$$-\left(\frac{\omega}{c}\right)^2 B\mathbf{V}^{\mathbf{k}}(\nu) + C(\nu)\mathbf{V}^{\mathbf{k}}(\nu) = \mathbf{F}^{\mathbf{k}}, \tag{3.6}$$

where $\mathbf{F}^{\mathbf{1}} = \omega\mu_0(0,0,0,1,0,0)^T$, $\mathbf{F}^{\mathbf{2}} = \omega\mu_0(0,0,0,0,1,0)^T$, $\mathbf{F}^{\mathbf{3}} = \omega\mu_0(0,0,0,0,0,1)^T$.

Applying technique and computational tools of (Yakhno, 2011), it is possible to compute a non-singular matrix $T(\nu)$ and diagonal matrix $D(\nu) = diag(d_1(\nu), d_2(\nu),$

$\ldots, d_6(\nu))$, such that

$$\begin{aligned} T^T(\nu)C(\nu)T(\nu) &= D(\nu), \\ T^T(\nu)BT(\nu) &= I. \end{aligned}$$

(MATLAB code of this computation is given in Appendix A2.1).

Below the equation (3.6) is written in terms of a new unknown vector function $\mathbf{Y^k}$ which is defined by

$$\mathbf{V^k}(\nu) = T(\nu)\mathbf{Y^k}(\nu). \tag{3.7}$$

Substituting (3.7) into (3.6) we find

$$-\left(\frac{\omega}{c}\right)^2 BT(\nu)\mathbf{Y^k}(\nu) + C(\nu)T(\nu)\mathbf{Y^k}(\nu) = \mathbf{F^k}. \tag{3.8}$$

Multiplying the equation (3.8) by $T^T(\nu)$, we find

$$-\left(\frac{\omega}{c}\right)^2 I\mathbf{Y^k}(\nu) + D(\nu)\mathbf{Y^k}(\nu) = T^T(\nu)\mathbf{F^k},$$

or in a component form

$$-\left(\frac{\omega}{c}\right)^2 Y_l^k(\nu) + d_l(\nu)Y_l^k(\nu) = (T^T(\nu)\mathbf{F^k})_l\,, l = 1,2,...,6. \tag{3.9}$$

For $(\frac{w}{c})^2 - d_l(\nu) \neq 0$, the solution of (3.9) can be written as

$$Y_l^k(\nu) = \frac{(T^T\mathbf{F^k})_l}{-(\omega/c)^2 + d_l(\nu)}, \tag{3.10}$$

where $l = 1,2,...,6$, $c = 1/\sqrt{\varepsilon_0\mu_0}$. As a result, the solution of (3.6) is determined by

$$\mathbf{V^k}(\nu) = T(\nu)\mathbf{Y^k},$$

and the solution $\widetilde{\mathbf{E}}^{\mathbf{k}}(\nu,\omega)$ is found by

$$\widetilde{E}_j^k = V_j^k(\nu) + iV_{j+3}^k(\nu), j = 1,2,3; k = 1,2,3. \tag{3.11}$$

Finally, applying the inverse Fourier transform to (3.11), we find the k-column of the electric Green's function as a tempered distribution, i.e.

$$\mathbf{E^k}(x) = \mathcal{F}_\nu^{-1}[\widetilde{\mathbf{E}}^{\mathbf{k}}(\nu)](x), \tag{3.12}$$

where $\mathcal{F}_\nu^{-1}$ is the operator of the inverse Fourier transform in the space of distribution $S'(\mathbb{R}^3)$ (Vladimirov, 1979).

Usually the classical functions are defined by a point-wise manner and we can draw their graphs. Unfortunately, this point-wise definition and its graphical presentation is not adequate to singular tempered distributions (Vladimirov, 1979). They are very often replaced by regularized functions which are classical and have graphic presentations. This regularization has a parameter of the regularization and the singular generalized function is a limit in sense of the generalized functions space, when the parameter of the regularization tends to $+\infty$. The right hand side of (3.12) can be regularized by

$$\frac{1}{(2\pi)^3}\int_{-A}^{A}\int_{-A}^{A}\int_{-A}^{A}\widetilde{\mathbf{E}}^{\mathbf{k}}(\nu)\,e^{-i\nu\cdot x}d\nu_1 d\nu_2 d\nu_3\,, \tag{3.13}$$

where A is the parameter of regularization.

We take $A = N\Delta$ and approximate the integral (3.13) by the integral sum

$$\frac{1}{(2\pi)^3}\sum_{n=-N}^{N}\sum_{m=-N}^{N}\sum_{l=-N}^{N}\widetilde{\mathbf{E}}^{\mathbf{k}}(n\Delta, m\Delta, l\Delta)\,e^{-i\Delta(nx_1+mx_2+lx_3)}(\Delta\nu)^3\,, \tag{3.14}$$

for the numerical computation. The parameters N and Δ are determined by the procedure described in Section 3.2.2.

3.1.2 Computing the Magnetic Green's Function

Applying the Fourier transform with respect to x to the equation (3.2) and using equalities

$$\begin{aligned}\mathcal{F}_x[curl_x(\mathscr{E}^{-1}curl_x\mathbf{H}^{\mathbf{k}}(x))] &= S(\nu)\mathscr{E}^{-1}S(\nu)\widetilde{\mathbf{H}}^{\mathbf{k}}(\nu),\\ \mathcal{F}_x[curl_x(\mathscr{E}^{-1}\mathbf{e}^{\mathbf{k}})] &= S(\nu)\mathscr{E}^{-1}\mathbf{e}^{\mathbf{k}},\end{aligned}$$

we find

$$-\left(\frac{\omega}{c}\right)^2\widetilde{\mathbf{H}}^{\mathbf{k}}(\nu)+S(\nu)\mathscr{E}^{-1}S(\nu)\widetilde{\mathbf{H}}^{\mathbf{k}}(\nu) = S(\nu)\mathscr{E}^{-1}\mathbf{e}^{\mathbf{k}}\,, \tag{3.15}$$

where $\widetilde{\mathbf{H}}^{\mathbf{k}}(\nu) = (\widetilde{H}_1^k, \widetilde{H}_2^k, \widetilde{H}_3^k)$, $\widetilde{H}_n^k(\nu) = \mathcal{F}_x[H_n^k(x)](\nu)$, $n = 1,2,3$; and $S(\nu)$ is given in (2.3).

Let $X_n^k(\nu)$, $G_n^k(\nu)$, $R_r(\nu)$ be the real parts of $\widetilde{H}_n^k(\nu)$, $(S(\nu)\mathscr{E}^{-1}\mathbf{e}^{\mathbf{k}})$, $(S(\nu)\mathscr{E}^{-1}S(\nu))$ and $X_{n+3}^k(\nu)$, $G_{n+3}^k(\nu)$, $R_i(\nu)$ be the imaginary parts of $\widetilde{H}_n^k(\nu)$, $(S(\nu)\mathscr{E}^{-1}\mathbf{e}^{\mathbf{k}})$, $(D(\nu)\mathscr{E}^{-1}D(\nu))$, respectively.

Denoting $\mathbf{X}^{\mathbf{k}}(\nu) = (X_1^k(\nu), X_2^k(\nu), \ldots, X_6^k(\nu))$ and $\mathbf{G}^{\mathbf{k}}(\nu) = (G_1^k(\nu), G_2^k(\nu), \ldots, G_6^k(\nu))$ the equation (3.15) can be written in the form

$$-\left(\frac{\omega}{c}\right)^2 \mathbf{X}^{\mathbf{k}}(\nu) + P(\nu)\mathbf{X}^{\mathbf{k}}(\nu) = \mathbf{G}^{\mathbf{k}}(\nu), \tag{3.16}$$

where $P(\nu)$ is a 6×6 symmetric matrix defined by

$$P(\nu) = \begin{pmatrix} R_r(\nu) & -R_i(\nu) \\ R_i(\nu) & R_r(\nu) \end{pmatrix}. \tag{3.17}$$

We note that $(S(\nu)\mathscr{E}^{-1}S(\nu)) = R_r(\nu) + iR_i(\nu)$, where

$$R_i(\nu) = \frac{1}{\xi_4}\begin{pmatrix} 0 & -a_{12} & a_{13} \\ a_{12} & 0 & -a_{23} \\ -a_{13} & a_{23} & 0 \end{pmatrix}, \quad R_r(\nu) = \frac{1}{\xi_4}\begin{pmatrix} b_{11} & b_{12} & b_{13} \\ b_{12} & b_{22} & b_{23} \\ b_{13} & b_{23} & b_{33} \end{pmatrix},$$

$$\begin{aligned}
&a_{12} = \nu_2\nu_3\xi_1 + \nu_3^2\xi_2 + \nu_1\nu_3\xi_3\,,\ a_{13} = \nu_2^2\xi_1 + \nu_2\nu_3\xi_2 + \nu_1\nu_2\xi_3\,,\\
&a_{23} = \nu_1\nu_3\xi_2 + \nu_1^2\xi_3 + \nu_1\nu_2\xi_1\,,\\
&b_{11} = -\nu_2^2\xi_5 + 2\nu_2\nu_3\xi_6 - \nu_3^2\xi_7\,,\ b_{12} = \nu_1\nu_2\xi_5 - \nu_1\nu_3\xi_6 - \nu_2\nu_3\xi_8 + \nu_3^2\xi_9\,,\\
&b_{13} = \nu_1\nu_3\xi_7 - \nu_1\nu_2\xi_6 - \nu_2^2\xi_8 - \nu_2\nu_3\xi_9\,,\ b_{22} = -\nu_1^2\xi_5 + 2\nu_1\nu_3\xi_8 - \nu_3^2\xi_{10}\,,\\
&b_{23} = \nu_2\nu_3\xi_{10} - \nu_1\nu_2\xi_8 - \nu_1^2\xi_6 + \nu_1\nu_3\xi_9\,,\ b_{33} = -\nu_1^2\xi_7 + 2\nu_1\nu_2\xi_8 - \nu_2^2\xi_{10}\,,
\end{aligned}$$

$$\xi_1 = \epsilon_{12}g_1 + \epsilon_{22}g_2 + \epsilon_{23}g_3\,,\ \xi_2 = \epsilon_{13}g_1 + \epsilon_{23}g_2 + \epsilon_{33}g_3\,,$$
$$\xi_3 = \epsilon_{11}g_1 + \epsilon_{12}g_2 + \epsilon_{13}g_3\,,$$
$$\xi_4 = \epsilon_{33}\epsilon_{12}^2 - 2\epsilon_{12}\epsilon_{13}\epsilon_{23} + 2\epsilon_{12}g_1g_2 + \epsilon_{22}\epsilon_{13}^2 + 2\epsilon_{13}g_1g_3 + \epsilon_{11}\epsilon_{23}^2 + 2\epsilon_{23}g_2g_3$$
$$+\epsilon_{11}g_1^2 + \epsilon_{22}g_2^2 + \epsilon_{33}g_3^2 - \epsilon_{11}\epsilon_{22}\epsilon_{33}\,,$$
$$\xi_5 = \epsilon_{12}^2 + g_3^2 - \epsilon_{11}\epsilon_{22}\,,\ \xi_6 = g_2g_3 - \epsilon_{12}\epsilon_{13} + \epsilon_{11}\epsilon_{23}\,,\ \xi_7 = \epsilon_{13}^2 + g_3^2 - \epsilon_{11}\epsilon_{33}\,,$$
$$\xi_8 = g_1g_3 - \epsilon_{12}\epsilon_{23} + \epsilon_{13}\epsilon_{22}\,,\ \xi_9 = g_1g_2 - \epsilon_{13}\epsilon_{23} + \epsilon_{12}\epsilon_{33}\,,$$
$$\xi_{10} = \epsilon_{23}^2 + g_1^2 - \epsilon_{22}\epsilon_{33}\,. \tag{3.18}$$

Using the symbolic matrix transformation in MATLAB and the technique from (Yakhno, 2011) we can compute an invertible matrix $Q(\nu)$ and $M(\nu)$ such that

$$\begin{aligned} Q^{-1}(\nu)Q(\nu) &= I\,, \\ Q^{-1}(\nu)P(\nu)Q(\nu) &= M(\nu)\,, \end{aligned}$$

where $M(\nu) = diag(m_n(\nu), n = 1,2,3,4,5,6)$. (MATLAB code of computation of $Q(\nu)$ and $M(\nu)$ is given in Appendix A2.2)

Let $\mathbf{Z^k}(\nu) = Q^{-1}(\nu)\mathbf{X^k}(\nu)$, then

$$\mathbf{X^k}(\nu) = Q(\nu)\mathbf{Z^k}(\nu)\,. \tag{3.19}$$

Using (4.5) the equation (3.16) can be written in the form

$$-\left(\frac{\omega}{c}\right)^2 Q(\nu)\mathbf{Z^k}(\nu) + P(\nu)Q(\nu)\mathbf{Z^k}(\nu) = \mathbf{G^k}\,. \tag{3.20}$$

Multiplying the equation (3.20) by $Q^{-1}(\nu)$, we find

$$-\left(\frac{\omega}{c}\right)^2 \mathbf{Z^k}(\nu) + M(\nu)\mathbf{Z^k} = Q^{-1}(\nu)\mathbf{G^k}\,. \tag{3.21}$$

For $(\omega/c)^2 - m_n(\nu) \neq 0$ the solution of (3.21) can be written in a component form as follows

$$Z_n^k(\nu) = \frac{(Q^{-1}(\nu)\mathbf{G^k})_n}{-(\omega/c)^2 + m_n(\nu)}\,, \tag{3.22}$$

where $n = 1,2,...,6$. As a result the solution of (3.16) is determined by

$$\mathbf{X^k}(\nu) = Q(\nu)\mathbf{Z^k},$$

and the solution of (3.15) is found by

$$\widetilde{H}_n^k = X_n^k(\nu) + iX_{n+3}^k(\nu)\,,\; j = 1,2,3\,; n = 1,2,3\,. \tag{3.23}$$

Applying the inverse Fourier transform to (3.23), we find the $k-$column of the magnetic Green's function as a tempered distribution, i.e.

$$\mathbf{H^k}(x) = \mathcal{F}_\nu^{-1}[\widetilde{\mathbf{H}}^\mathbf{k}(\nu)](x)\,. \tag{3.24}$$

The right hand side of (3.24) can be regularized by

$$\frac{1}{(2\pi)^3}\int_{-A}^{A}\int_{-A}^{A}\int_{-A}^{A}\widetilde{\mathbf{H}}^\mathbf{k}(\nu)\,e^{-i\nu\cdot x}d\nu_1 d\nu_2 d\nu_3\,, \tag{3.25}$$

where A is the parameter of regularization.
We take $A = N\Delta$ and approximate the integral (3.25) by the integral sum

$$\frac{1}{(2\pi)^3}\sum_{n=-N}^{N}\sum_{m=-N}^{N}\sum_{l=-N}^{N}\widetilde{\mathbf{H}}^\mathbf{k}(\Delta n, \Delta m, \Delta l)\,e^{-i\Delta(nx_1+mx_2+lx_3)}(\Delta\nu)^3\,. \tag{3.26}$$

for the numerical computation. The parameters N and Δ are determined by the procedure described in Section 3.2.2.

3.2 Computational Experiments

The images of the Fourier transform of the elements of the Green's functions of electric and magnetic fields in general electrically gyrotropic media can be found exactly by symbolic computations in MATLAB by using the method which is explained in Chapter 2. But in this chapter, we will demonstrate another approach. It is possible to find explicit formulas for the Fourier images of the electric and magnetic Green's functions and we can compare with our results which are computed by our method. This idea is given in section 3.2.1. In this chapter, we also demonstrated a second way for determining parameters for the approximate computation of the Fourier transform in the space of generalized functions in section 3.2.2. For this case, we used fundamental solution of Helmholtz equation and we obtained the same parameters which is given in Chapter 2, Section 2.3.1. This computation supports correctness of our approximate computation of the Fourier transform in the space of generalized functions. The computational experiments for general electricaly gyrotropic media are given in section 3.2.3.

3.2.1 Computational Accuracy of the Fourier Transform of the Electric Green's Function

The Fourier transform of the electric and magnetic Green's functions can be found by exact formulas for the case of isotropic homogeneous materials. We use these formulas to compute the exact values of the Fourier transform of Green's functions and then to compare them with values computed by our method.

The components of $\widetilde{\mathbf{E}}^{\mathbf{k}}(\nu) = (\widetilde{\mathbf{E}}^{\mathbf{k}}_{\mathbf{1}}(\nu), \widetilde{\mathbf{E}}^{\mathbf{k}}_{\mathbf{2}}(\nu), \widetilde{\mathbf{E}}^{\mathbf{k}}_{\mathbf{3}}(\nu))$, $\widetilde{\mathbf{H}}^{\mathbf{k}}(\nu) = (\widetilde{\mathbf{H}}^{\mathbf{k}}_{\mathbf{1}}(\nu), \widetilde{\mathbf{H}}^{\mathbf{k}}_{\mathbf{2}}(\nu), \widetilde{\mathbf{H}}^{\mathbf{k}}_{\mathbf{3}}(\nu))$ satisfying equations (3.3) and (3.15) respectively for $k = 1$ in the case of the isotropic homogeneous medium with permittivity ε_0 and permeability μ_0 are given by formulas

$$\widetilde{E}^1_1(\nu) = \frac{\frac{1}{i\omega\varepsilon_0}(-\nu_1^2) - i\omega\mu_0}{(\frac{\omega}{c})^2 - |\nu|^2}\,,\ \widetilde{E}^1_2(\nu) = \frac{-\frac{1}{i\omega\varepsilon_0}\nu_1\nu_2}{(\frac{\omega}{c})^2 - |\nu|^2}\,,\ \widetilde{E}^1_3(\nu) = \frac{-\frac{1}{i\omega\varepsilon_0}\nu_1\nu_3}{(\frac{\omega}{c})^2 - |\nu|^2}\,, \tag{3.27}$$

$$\widetilde{H}^1_1(\nu) = 0\,,\ \widetilde{H}^1_2(\nu) = \frac{\nu_3}{(\frac{\omega}{c})^2 - |\nu|^2}\,,\ \widetilde{H}^1_3(\nu) = \frac{-\nu_2}{(\frac{\omega}{c})^2 - |\nu|^2}\,. \tag{3.28}$$

The functions $\widetilde{E}^1_j(\nu)$, $\widetilde{H}^1_j(\nu)$ defined by the explicit formulas (3.27), (3.28) will be denoted as $\widetilde{E}^e_j(\nu)$, $\widetilde{H}^e_j(\nu)$. The functions $\widetilde{E}^1_j(\nu)$, $\widetilde{H}^1_j(\nu)$ computed by our method for the isotropic medium will be denoted as $\widetilde{E}^m_j(\nu)$, $\widetilde{H}^m_j(\nu)$. The results of computations of their values for $\omega = 1/\sqrt{\mu_0\varepsilon_0}$ and $\nu_1 = r\cos\phi\sin\theta$, $\nu_2 = r\sin\phi\sin\theta$, $\nu_3 = r\cos\theta$ for fixed $\theta = \pi/4$, $\phi = \pi/4$ and for fixed parameter r are presented in Table 3.1 and Table 3.2.

These computational experiments have shown that values of $\widetilde{E}^1_j$, $\widetilde{H}^1_j$ found by our method and by explicit formulas are almost the same (the accuracy is around 10^{-6}).

Table 3.1 The comparison for **imaginary part** of $\widetilde{E}$ for isotropic case.

r	$\widetilde{E}_1^m$	$\lvert\widetilde{E}_1^m - \widetilde{E}_1^e\rvert$	$\widetilde{E}_2^m$	$\lvert\widetilde{E}_2^m - \widetilde{E}_2^e\rvert$	$\widetilde{E}_3^m$	$\lvert\widetilde{E}_3^m - \widetilde{E}_3^e\rvert$
10^{-4}	$-0.37678x10^3$	0	$0.94197x10^{-6}$	$0.18990x10^{-13}$	$0.13321x10^{-5}$	$0.44490x10^{-13}$
10^{-3}	$-0.37678x10^3$	0	$0.94197x10^{-6}$	$0.15462x10^{-14}$	$0.13321x10^{-3}$	$0.21486x10^{-13}$
10^{-2}	$-0.37681x10^3$	$0.56843x10^{-13}$	$0.94206x10^{-2}$	$0.53030x10^{-14}$	$0.13322x10^{-1}$	$0.44632x10^{-13}$
10^{-1}	$-0.37964x10^3$	$0.56843x10^{-13}$	$0.56843x10^{-1}$	$0.81046x10^{-14}$	$0.13456x10^{-1}$	$0.11324x10^{-13}$
0	$-0.37678x10^3$	0	0	0	0	0
10^1	$-0.91342x10^2$	$0.13073x10^{-11}$	$-0.95148x10^2$	$0.12931x10^{-11}$	$-1.34560x10^2$	$0.18474x10^{-11}$
10^2	$-0.94168x10^2$	$0.17135x10^{-9}$	$-0.94206x10^2$	$0.17136x10^{-9}$	$-1.33228x10^2$	$0.24232x10^{-9}$
10^3	$-0.94196x10^2$	$0.10965x10^{-7}$	$-0.94197x10^2$	$0.10965x10^{-7}$	$-1.33215x10^2$	$0.15508x10^{-7}$
10^4	$-0.94197x10^2$	$0.70182x10^{-6}$	$-0.94197x10^2$	$0.70182x10^{-6}$	$-1.33214x10^2$	$0.99252x10^{-6}$

Table 3.2 The comparison for **real** part of $\widetilde{H}$ for isotropic case.

r	$\widetilde{H}_1^m$	$\lvert\widetilde{H}_1^m - \widetilde{H}_1^e\rvert$	$\widetilde{H}_2^m$	$\lvert\widetilde{H}_2^m - \widetilde{H}_2^e\rvert$	$\widetilde{H}_3^m$	$\lvert\widetilde{H}_3^m - \widetilde{H}_3^e\rvert$
10^{-4}	$-0.13552x10^{-21}$	$0.13552x10^{-21}$	$-0.70710x10^{-6}$	$0.14142x10^{-14}$	$0.49999x10^{-6}$	$0.99999x10^{-14}$
10^{-3}	$-0.81315x10^{-21}$	$0.81315x10^{-21}$	$-0.70710x10^{-5}$	$0.14142x10^{-10}$	$0.49999x10^{-5}$	$0.99999x10^{-11}$
10^{-2}	$0.86736x10^{-20}$	$0.86736x10^{-20}$	$-0.70703x10^{-5}$	$0.14142x10^{-7}$	$0.49999x10^{-5}$	$0.10000x10^{-7}$
10^{-1}	$0.17347x10^{-18}$	$0.17347x10^{-18}$	$0.70010x10^{-4}$	$0.14143x10^{-5}$	$0.49505x10^{-4}$	$0.10001x10^{-5}$
0	0	0	0	0	0	0
10^{1}	$-0.15196x10^{-16}$	$0.15196x10^{-16}$	$0.70010x10^{-4}$	$0.14143x10^{-5}$	$0.49505x10^{-4}$	$0.10001x10^{-5}$
10^{2}	$-0.71032x10^{-16}$	$0.71032x10^{-16}$	$-0.70703x10^{-5}$	$0.14142x10^{-7}$	$0.49995x10^{-5}$	$0.10000x10^{-7}$
10^{3}	$-0.28421x10^{-15}$	$0.28421x10^{-15}$	$-0.70710x10^{-6}$	$0.14141x10^{-10}$	$0.49999x10^{-5}$	$0.10000x10^{-10}$
10^{4}	$0.45474x10^{-14}$	$0.45474x10^{-14}$	$-0.707106x10^{-6}$	$0.186896x10^{-13}$	$0.50000x10^{-6}$	$0.35689x10^{-14}$

3.2.2 Determining Parameters for the Approximate Computation of the Fourier Transform in the Space of Generalized Functions (Using Helmholtz Eqn.)

The fundamental solution of the Helmholtz equation as well as the image of the Fourier transform with respect to a space variable are given by explicit formulas. We apply these explicit formulas to determine the parameters which we use for the numerical computation of the inverse Fourier transform for finding the electric and magnetic Green's functions in gyro-electric media.

Let us consider the fundamental solution

$$U(x) = -\frac{e^{i\omega|x|/c}}{4\pi|x|}, \quad x = (x_1, x_2, x_3), \tag{3.29}$$

of the Helmholtz equation

$$\omega^2 U(x) + c^2 \Delta U = \delta(x). \tag{3.30}$$

Applying the Fourier transform (the Fourier transform of generalized functions Vladimirov, 1979) to equation (3.30), we find

$$\omega^2 \widetilde{U}(\nu) - c^2|\nu|^2 \widetilde{U}(\nu) = 1,$$

where $\nu = (\nu_1, \nu_2, \nu_3) \in \mathbb{R}^3$ is the parameter of the Fourier transform, $|\nu|^2 = \nu_1^2 + \nu_2^2 + \nu_3^2$.

For $c^2|\nu|^2 - \omega^2 \neq 0$ we have

$$\tilde{U}(\nu) = \frac{1}{\omega^2 - c^2|\nu|^2}. \tag{3.31}$$

The fundamental solution $U(x)$, defined by (3.29), can be found by application of the inverse Fourier transform (as the inverse Fourier transform of generalized functions Vladimirov, 1979) to $\tilde{U}(\nu)$ determined by (3.31).

For the approximate computation $U_{N,\Delta}(x)$ of the function $U(x)$ we apply the approximation of the inverse Fourier transform by

$$\frac{1}{(2\pi)^3} \sum_{n=-N}^{N} \sum_{m=-N}^{N} \sum_{l=-N}^{N} \frac{1}{\omega^2 - c^2\Delta^2(n^2 + m^2 + l^2)} e^{-i\Delta(nx_1 + mx_2 + lx_3)} (\Delta\nu)^3. \tag{3.32}$$

The parameters N and Δ have been chosen using the empirical observation and natural logic. Namely, using the formula (3.32) we compute values $U_{N,\Delta}(x)$ for $\Delta = 0.1, 0.5, 0.8, 1.0$, $N = 20, 30, 40, 50, 60, 80$ and so on numerically in MATLAB. We compare the computed values of $U_{N,\Delta}(x)$ with values of the function $U(x)$, defined by (3.29). We have observed that the difference between the values of $U_{N,\Delta}(x)$ and $U(x)$ corresponding to $\Delta = 1$ and $N = 30, 40, 50, 60, 80, 100$ becomes small and increment of the approximation for the parameter N is not essential, according to the case $\Delta = 1$, $N = 40$. For this reason we choose $\Delta = 1$, $N = 40$ as the suitable parameters for the calculation of the inverse Fourier transform by (3.32).

We have presented $1D$ graphs of the functions $U(x)$ and $U_{N,\Delta}(x)$ for the different values of N and Δ in Figure 3.1 and Figure 3.2.

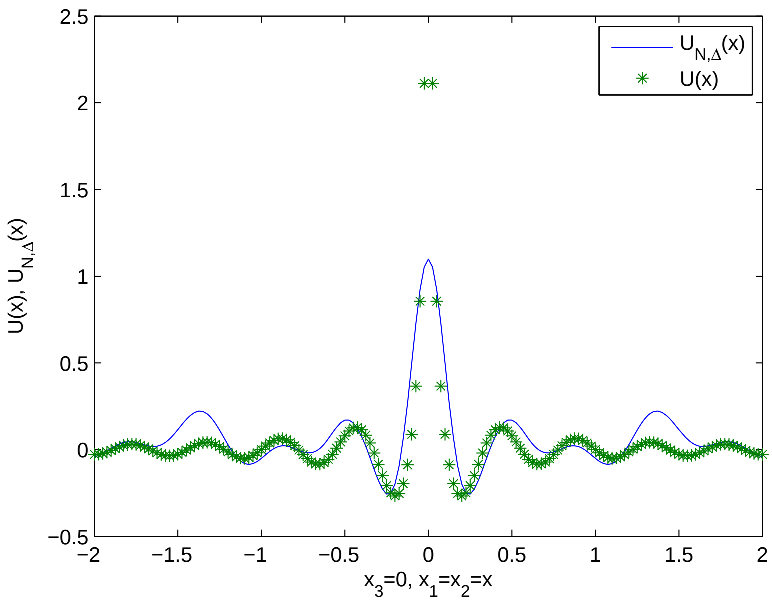

Figure 3.1 $1D$ plot of $U(x)$ and $U_{N,\Delta}(x)$ for $N = 40$, $\Delta = 0.5$

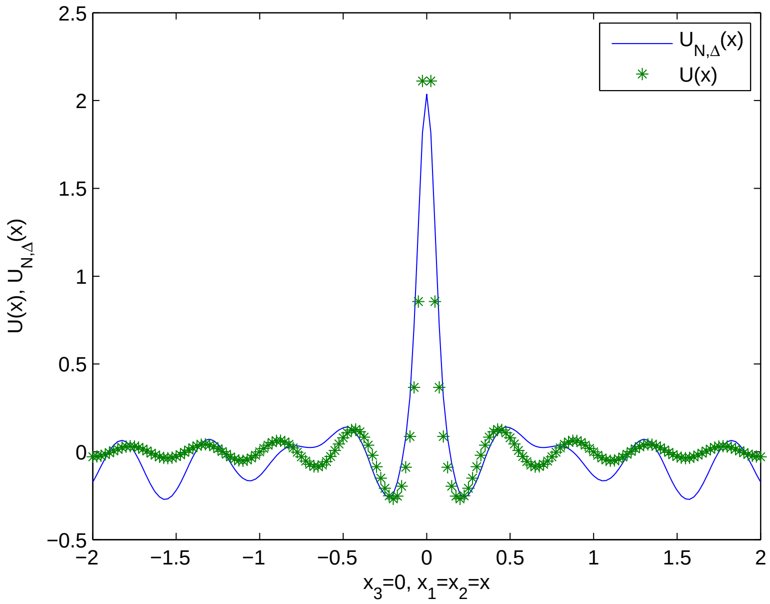

Figure 3.2 $1D$ plot of $U(x)$ and $U_{N,\Delta}(x)$ for $N = 40$, $\Delta = 1.0$

3.2.3 The Approximate Computation of the Electric and Magnetic Green's Functions in General Gyro-electric Media

In this section we consider the approximate computation of electric and magnetic Green's functions for general gyro-electric media characterizing by

$$\mathscr{E} = \begin{pmatrix} 30.7929 & -12.7337 + i0.5\kappa & -14.3432 - i0.4\kappa \\ -12.7337 - i0.5\kappa & 5.51479 & 5.86982 + i0.2\kappa \\ -14.3432 + i0.4\kappa & 5.86982 - i0.2\kappa & 6.74556 \end{pmatrix} \tag{3.33}$$

where $\kappa = 10^{-1}$ and 10^{-2}.

Applying the method of Section 3.1.1 we have computed $T(\nu)$, $T^T(\nu)$, $D(\nu)$ and then using the formula (3.14) we have derived solutions $\mathbf{E^1}(x)$, $\mathbf{E^2}(x)$, $\mathbf{E^3}(x)$ of (3.3) numerically and applying the method of Section 3.1.2 we have computed $Q(\nu)$, $Q^{-1}(\nu)$, $M(\nu)$ and then using the formula (3.26) we have derived solutions $\mathbf{H^1}(x)$, $\mathbf{H^2}(x)$, $\mathbf{H^3}(x)$ of (3.15) numerically.

Results of the computation of real and imaginary parts of $E^1_1(x)$, $E^1_2(x)$ and $H^1_1(x)$, $H^1_2(x)$ for $\kappa = 10^{-1}, 10^{-2}$ are presented in Figure 3.3, Figure 3.5-Figure 3.6 and

Figure 3.4, Figure 3.7-Figure 3.8, respectively.

In Figure 3.3(a), the $1D$ plots of $Im(E_2^1(x, x, 0))$ for $x_1 = x_2 = x$, $x_3 = 0$, $\omega = 2c$ for $\kappa = 10^{-1}$ and $\kappa = 10^{-2}$ is given. Figure 3.3(b) presents the zoomed part of the graph of Figure 3.3(a) in the indicated rectangle. Figure 3.4(a), (b) present the $1D$ graphs of $Im(H_1^1(x_1, x_2, 0))$ and $Re(H_1^1(x_1, x_2, 0))$, respectively for $\kappa = 10^{-1}, 10^{-2}$. These graphs show the influence of κ on the components of the electric and magnetic Green's functions.

The behaviour of real and imaginary parts of the computed components of the electric and magnetic Green's functions is presented in Figure 3.3, Figure 3.5 and Figure 3.6. The result of the simulation $Im(E_1^1(x_1, x_2, 0))$ for $\omega = 2c$, $\kappa = 10^{-1}$ is presented in Figure 3.5. The $3D$ plot of $Im(E_1^1(x_1, x_2, 0))$ is shown in Figure 3.5(b). Here the horizontal axes are x_1 and x_2, respectively. The vertical axis is the magnitude of $Im(E_1^1(x_1, x_2, 0))$. Figure 3.5(a) is a screen shot of $2D$ level plot of the same surface $Im(E_1^1(x_1, x_2, 0))$, i.e. a view of the surface $z = Im(E_1^1(x_1, x_2, 0))$ presented in Figure 3.5(b) from the top of z-axis. Figure 3.6(a), (b) illustrate the $2D$ level plots of $Re(E_1^1(x_1, x_2, 0))$ and $Re(E_2^1(x_1, x_2, 0))$, respectively.

The result of simulation $Im(H_1^1(x_1, x_2, 0))$ and $Re(H_1^1(x_1, x_2, 0))$ are presented in Figure 3.7. Figure 3.7(a), (b) are the $2D$ plots of $Im(H_1^1(x_1, x_2, 0))$ and $Re(H_1^1(x_1, x_2, 0))$ respectively. The illustration of $Im(H_2^1(x_1, x_2, 0))$ and $Re(H_2^1(x_1, x_2, 0))$ is given in Fig.Figure 3.8.

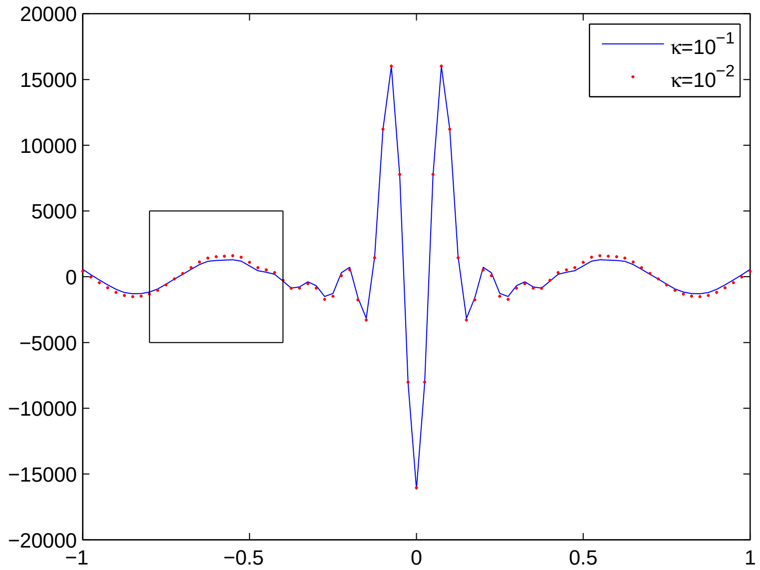

(a)

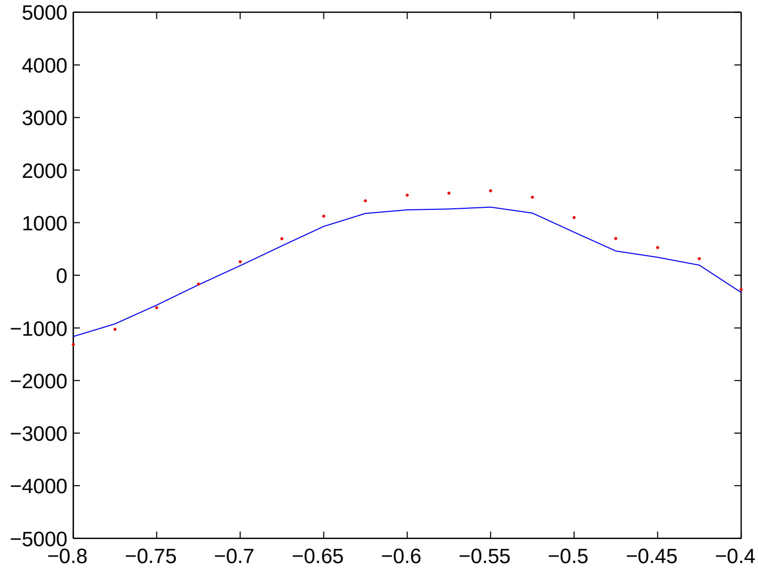

(b)

Figure 3.3 $\omega = 2c$, $\kappa = 10^{-1}, 10^{-2}$, (a) $1D$ plot of $Im(E_2^1(x,x,0))$; (b) $1D$ plot of $Im(E_2^1(x,x,0))$ in rectangular region

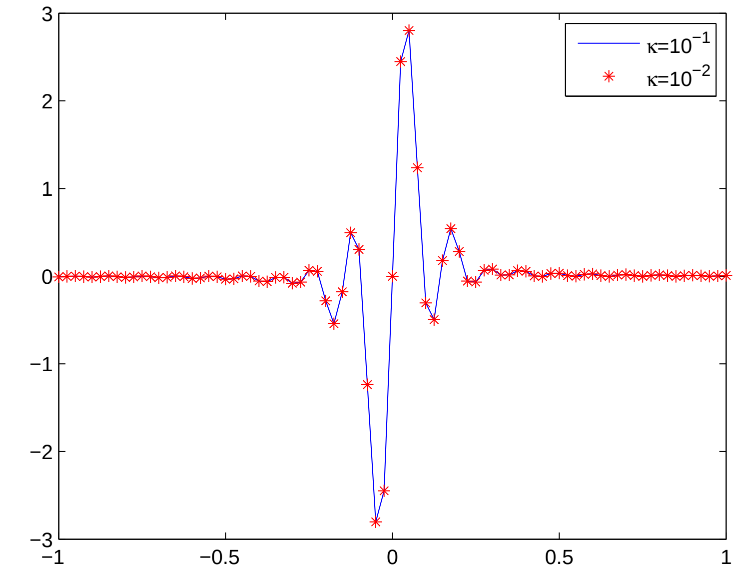

(a)

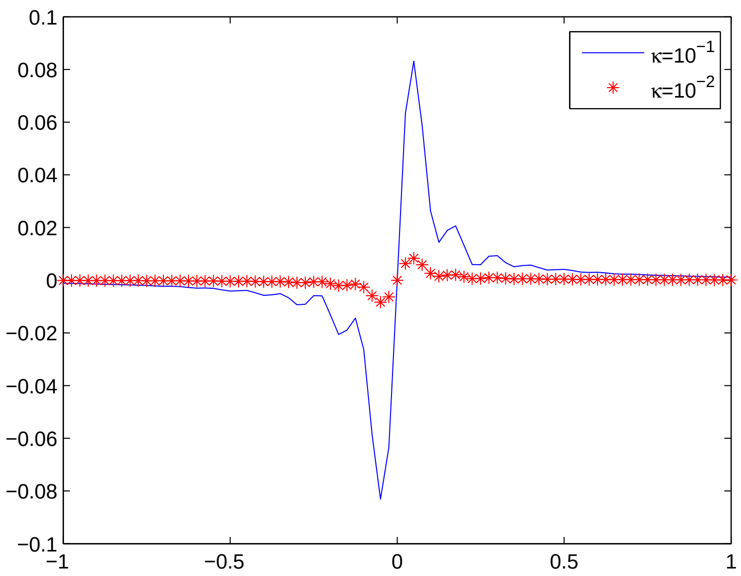

(b)

Figure 3.4 $\omega = 2c$, $\kappa = 10^{-1}, 10^{-2}$, (a) $2D$ plot of $Im(H_1^1(x,x,0))$; (b) $2D$ plot of $Re(H_1^1(x,x,0))$

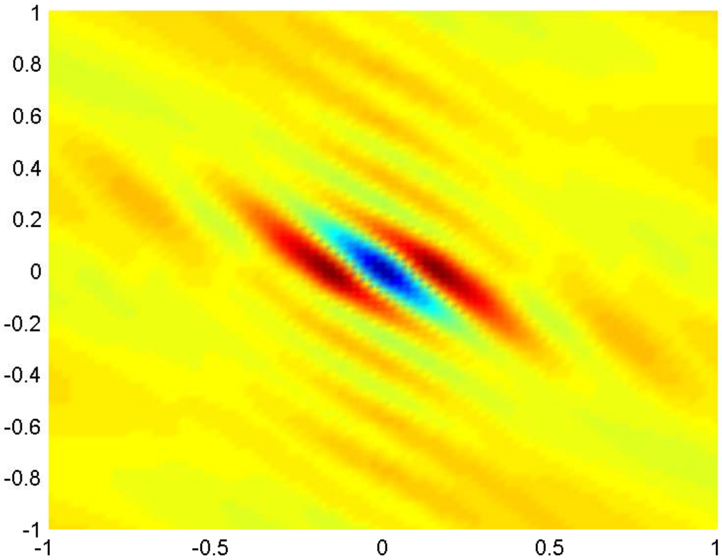

(a)

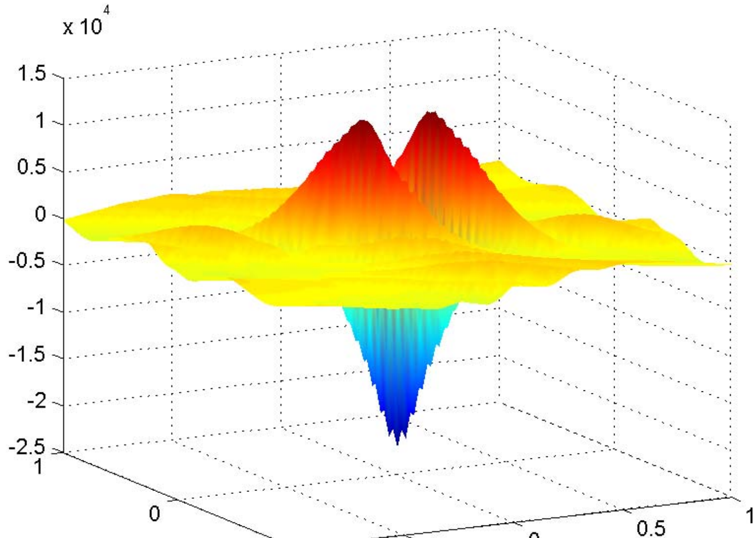

(b)

Figure 3.5 $\omega = 2c$, $\kappa = 10^{-1}$, (a) $2D$ plot of $Im(E_1^1(x_1, x_2, 0))$; (b) $3D$ plot of $Im(E_1^1(x_1, x_2, 0))$

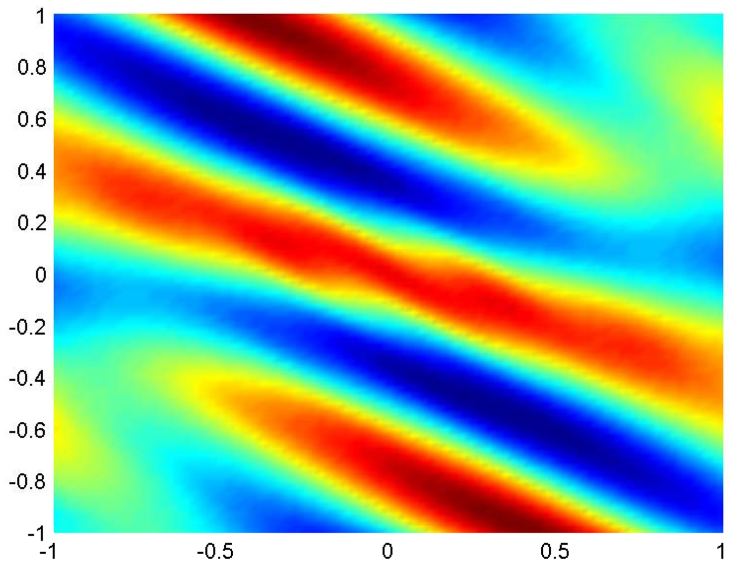

(a)

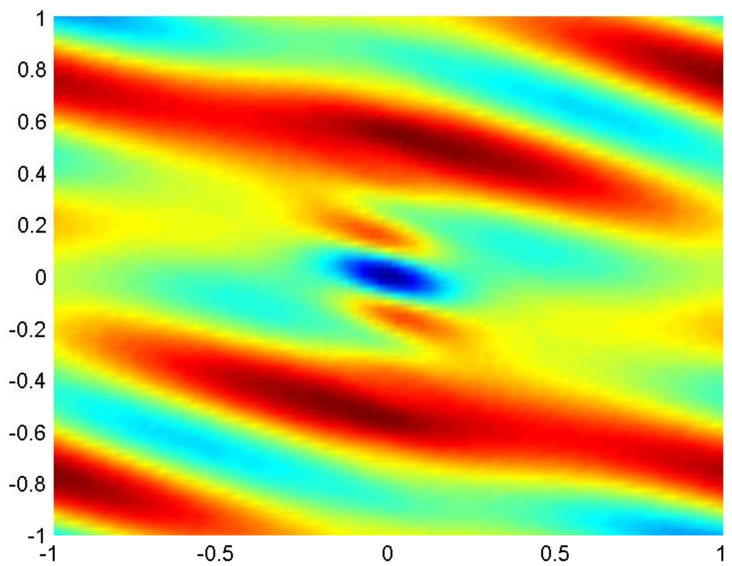

(b)

Figure 3.6 $\omega = 2c$, $\kappa = 10^{-1}$, (a) $2D$ plot of $Re(E_1^1(x_1, x_2, 0))$; (b) $2D$ plot of $Re(E_2^1(x_1, x_2, 0))$

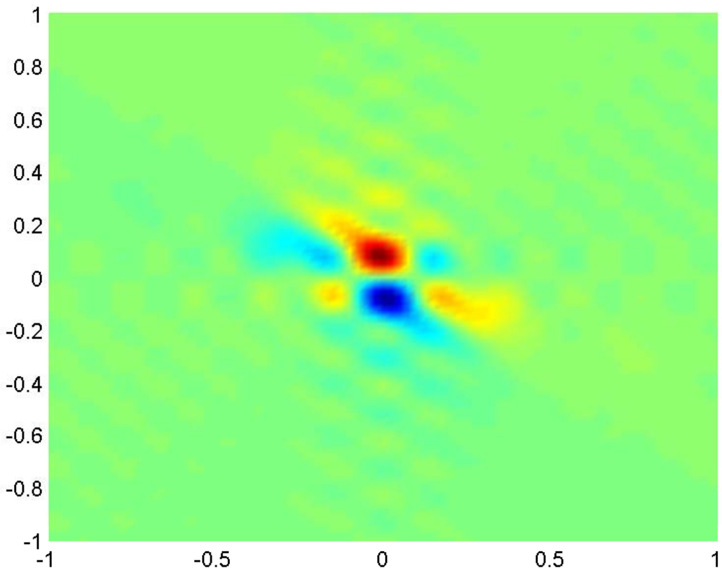

(a)

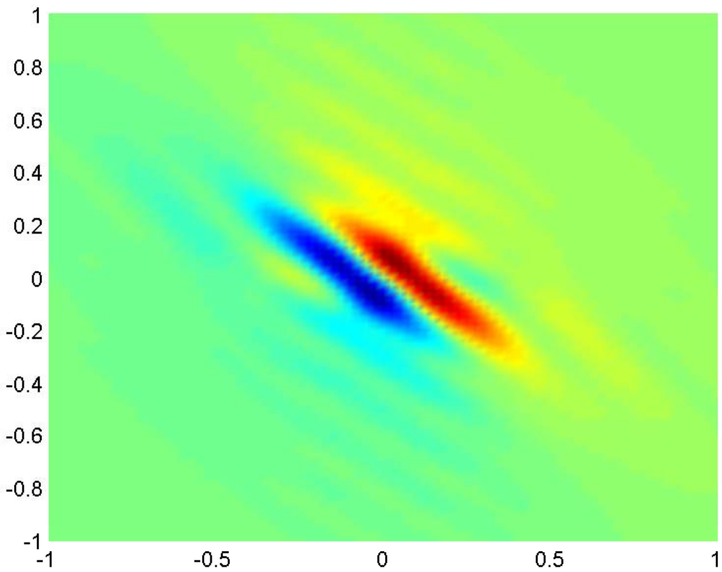

(b)

Figure 3.7 $\omega = 2c$, $\kappa = 10^{-1}$, (a) $2D$ plot of $Im(H_1^1(x_1, x_2, 0))$; (b) $2D$ plot of $Re(H_1^1(x_1, x_2, 0))$

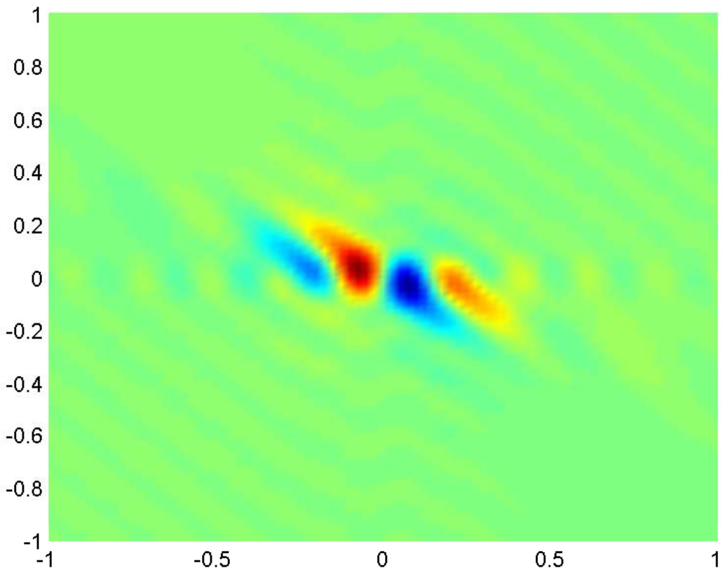

(a)

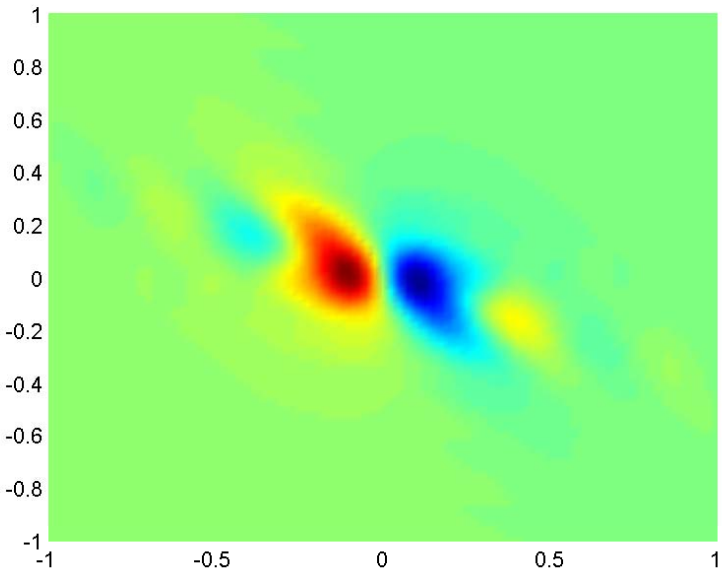

(b)

Figure 3.8 $\omega = 2c$, $\kappa = 10^{-1}$, (a) $2D$ plot of $Im(H_2^1(x_1, x_2, 0))$; (b) $2D$ plot of $Re(H_2^1(x_1, x_2, 0))$

3.3 Summary of the Chapter Three

The method for the approximate computation of the electric and magnetic Green's functions for the time-harmonic Maxwell's equations in general gyro-electric materials has been developed in this chapter. The method is based on the Fourier transform meta-approach. The Fourier transform with respect to the $3D$ space variable has been applied to partial differential equations for electric and magnetic Green's functions. The images of the Fourier transform of Green's functions for the electric and magnetic fields were found from the obtained equations by the matrix transformations in MATLAB. The inverse Fourier transform of these images has been done numerically in the regularized (approximate) form in MATLAB. The parameters of this regularization have been chosen using the explicit formulae of the Green's function and its Fourier image for the Helmholtz equation. Two types of the computational experiments were presented in this chapter. The first one demonstrates the high level of computational accuracy for the Fourier images and the inverse Fourier transform. The second one has been done for computing the electric and magnetic Green's functions in a general gyro-electric material. These computational experiments confirm the robustness of the method.

CHAPTER FOUR
COMPUTING THE ELECTRIC AND MAGNETIC MATRIX GREEN'S FUNCTIONS IN GENERAL MAGNETICALLY GYROTROPIC MEDIA

A new method for the approximate computation of the frequency-dependent electric and magnetic Green's functions of Maxwell's equations in general magnetically gyrotropic media is suggested. The method is based on the Fourier transform with respect to space variables, matrix transformations and numerical computation of the inverse Fourier transform. The numerical computation of the magnetic and electric Green's functions for the electric and magnetic fields have been implemented in MATLAB. Two types of the computational experiments have been done. The first one is related to the error analysis of the method, and second one is the computation of the elements of magnetic and electric Green's matrices in a general gyro-magnetic medium. The computational experiments confirm the robustness of the method.

4.1 Electric and Magnetic Green's Functions in General Gyro-magnetic Media

For gyro-magnetic materials, $\mathscr{E} = I$ in (1.10) and the columns of electric and magnetic matrix Green's functions (1.13) satisfies

$$-\left(\frac{\omega}{c}\right)^2 \mathscr{M}\mathbf{H}^{\mathbf{k}}(x) + \nabla\times(\nabla\times\mathbf{H}^{\mathbf{k}}(x)) = \nabla\times(\mathbf{e}^{\mathbf{k}}\delta(x)), \tag{4.1}$$

$$-\left(\frac{\omega}{c}\right)^2 \mathbf{E}^{\mathbf{k}}(x) + \nabla\times(\mathscr{M}^{-1}\nabla\times\mathbf{E}^{\mathbf{k}}(x)) = i\omega\mu_0\mathbf{e}^{\mathbf{k}}\delta(x). \tag{4.2}$$

Here $x = (x_1, x_2, x_3) \in \mathbb{R}^3$ is the $3D$ space variable; ω is a fixed parameter (frequency); $\varepsilon_0 = 8.854\times10^{-12}F/m$, $\mu_0 = 1.257\times10^{-6}N/A^2$ and $c = 1/\sqrt{\varepsilon_0\mu_0}$ are positive constants (dielectric permittivity, magnetic permeability and speed of light) in vacuum, respectively; $\mathbf{e}^1 = (1,0,0)^T$, $\mathbf{e}^2 = (0,1,0)^T$, $\mathbf{e}^3 = (0,0,1)^T$ are basis vectors of $\mathbb{R}^3$; i is the imaginary unit $i^2 = -1$; $\delta(x) = \delta(x_1)\delta(x_2)\delta(x_3)$, $\delta(x_j)$ is the Dirac delta function concentrated at $x_j = 0$ for $j = 1,2,3$. We also assume that the inverse of the matrix $\mathscr{M}$ exists (explained in Remark 1.4).

4.1.1 Computing the Magnetic Green's Function

Let $\widetilde{\mathbf{H}}^{\mathbf{k}}(\nu) = (\widetilde{H}_1^k, \widetilde{H}_2^k, \widetilde{H}_3^k)$, where $\widetilde{H}_j^k = \mathcal{F}_x[H_j^k(x)](\nu)$, $j,k = 1,2,3$. Applying the operator of the Fourier transform $\mathcal{F}_x$ given in (2.1) to (4.1) and using the equality

$$\mathcal{F}_x[\nabla\times(\nabla\times\mathbf{H}^{\mathbf{k}}(x))] = A(\nu)\widetilde{\mathbf{H}}^{\mathbf{k}}(\nu),$$

we find

$$-\left(\frac{\omega}{c}\right)^2 \mathscr{M}\widetilde{\mathbf{H}}^{\mathbf{k}}(\nu) + A(\nu)\widetilde{\mathbf{H}}^{\mathbf{k}}(\nu) = S(\nu)\mathbf{e}^{\mathbf{k}}, \tag{4.3}$$

where $A(\nu)$ and $S(\nu)$ are given in (3.4) and (2.3) respectively.

The matrix $\mathscr{M}$ is defined by (1.11) with $\mathscr{E} = I$. From (1.16), the matrix K is symmetric and from Remark (1.4.1) it is positive definite and $C(\nu)$ is symmetric 6×6 matrices given in (3.5).

Let us denote W_j^k as the real part of j component of $\widetilde{\mathbf{H}}^{\mathbf{k}}(\nu)$ and W_{j+3}^k as the imaginary part of j component of $\widetilde{\mathbf{H}}^{\mathbf{k}}(\nu)$, i.e. $W_j^k = Re(\widetilde{H}_j^k(\nu))$ and $W_{j+3}^k = Im(\widetilde{H}_j^k(\nu))$, $j = 1,2,3$. Then equality (4.3) can be written as a vector equation

$$-\left(\frac{\omega}{c}\right)^2 K\mathbf{W}^{\mathbf{k}}(\nu) + C(\nu)\mathbf{W}^{\mathbf{k}}(\nu) = \mathbf{L}^{\mathbf{k}}, \tag{4.4}$$

where $\mathbf{L}^{\mathbf{1}} = (0,\nu_3,-\nu_2,0,0,0)^T$, $\mathbf{L}^{\mathbf{2}} = (-\nu_3,0,\nu_1,0,0,0)^T$, $\mathbf{L}^{\mathbf{3}} = (\nu_2,-\nu_1,0,0,0,0)^T$.

Applying technique and computational tools of (Yakhno, 2008), it is possible to compute a non-singular matrix $T(\nu)$ and diagonal matrix $D(\nu) = diag(d_1(\nu), d_2(\nu), \ldots, d_6(\nu))$, such that

$$\begin{aligned} T^T(\nu)C(\nu)T(\nu) &= D(\nu), \\ T^T(\nu)KT(\nu) &= I. \end{aligned}$$

MATLAB code of this computation is given in Appendix A3.1.

Below the equation (4.4) is written in terms of a new unknown vector function $\mathbf{Y}^{\mathbf{k}}$ which is defined by

$$\mathbf{W}^{\mathbf{k}}(\nu) = T\mathbf{Y}^{\mathbf{k}}(\nu). \tag{4.5}$$

Substituting (4.5) into (4.4) we find

$$-\left(\frac{\omega}{c}\right)^2 KT\mathbf{Y}^{\mathbf{k}}(\nu) + C(\nu)T\mathbf{Y}^{\mathbf{k}}(\nu) = \mathbf{L}^{\mathbf{k}}. \tag{4.6}$$

Multiplying the equation (4.6) by T^T, we get

$$-\left(\frac{\omega}{c}\right)^2 I\mathbf{Y}^{\mathbf{k}}(\nu) + D(\nu)\mathbf{Y}^{\mathbf{k}}(\nu) = T^T(\nu)\mathbf{L}^{\mathbf{k}},$$

or in a component form

$$-\left(\frac{\omega}{c}\right)^2 Y_l^k(\nu) + d_l(\nu)Y_l^k(\nu) = (T^T(\nu)\mathbf{L}^{\mathbf{k}})_l, l = 1,2,...,6. \tag{4.7}$$

For $(\frac{w}{c})^2 - d_l(\nu) \neq 0$, the solution of (4.7) can be written as

$$Y_l^k(\nu) = \frac{(T^T\mathbf{L}^{\mathbf{k}})_l}{-(\omega/c)^2 + d_l(\nu)}, \tag{4.8}$$

where $l = 1,2,...,6$, $c = 1/\sqrt{\varepsilon_0\mu_0}$. As a result, the solution of (4.4) is determined by

$$\mathbf{W}^{\mathbf{k}}(\nu) = T(\nu)\mathbf{Y}^{\mathbf{k}},$$

and the solution $\widetilde{\mathbf{H}}^{\mathbf{k}}(\nu,\omega)$ is found by

$$\widetilde{H}_j^k = W_j^k(\nu) + iW_{j+3}^k(\nu), j = 1,2,3; k = 1,2,3. \tag{4.9}$$

Finally, applying the inverse Fourier transform to (4.9), we find that the electric Green's function as a tempered distribution has the following form, i.e.

$$\mathbf{H}_{\mathbf{j}}^{\mathbf{k}}(x) = \mathcal{F}_\nu^{-1}[\widetilde{\mathbf{H}}_{\mathbf{j}}^{\mathbf{k}}(\nu)](x), \tag{4.10}$$

where $\mathcal{F}_\nu^{-1}$ is the operator of the inverse Fourier transform in the space of distribution $S'(\mathbb{R}^3)$ (Vladimirov, 1979).

Usually the classical functions are defined by a point-wise manner and we can draw their graphs. Unfortunately, this point-wise definition and its graphical presentation is not adequate to singular tempered distributions (Vladimirov, 1979). They are very often replaced by regularized functions which are classical and have graphic presentations. Such regularization has a parameter of the regularization and the singular generalized function is a limit in terms of the generalized functions space, when the parameter of the regularization tends to $+\infty$. The right hand side of (4.10) can be regularized by

$$\frac{1}{(2\pi)^3}\int_{-A}^{A}\int_{-A}^{A}\int_{-A}^{A}\widetilde{\mathbf{H}}_{\mathbf{j}}^{\mathbf{k}}(\nu)\,e^{-i\nu\cdot x}d\nu_1 d\nu_2 d\nu_3\,, \tag{4.11}$$

where A is the parameter of regularization.

We take $A = N\Delta$ and approximate the integral (4.11) by the integral sum

$$\frac{1}{(2\pi)^3}\sum_{n=-N}^{N}\sum_{m=-N}^{N}\sum_{l=-N}^{N}\widetilde{\mathbf{H}}_{\mathbf{j}}^{\mathbf{k}}(n\Delta,m\Delta,l\Delta)\,e^{-i\Delta(nx_1+mx_2+lx_3)}(\Delta\nu)^3\,, \tag{4.12}$$

for the numerical computation. The parameters N and Δ are determined by the procedure described in Chapter 2, Section 2.3.1.

4.1.2 Computing the Electric Green's Function

Applying the Fourier transform with respect to x to the equation (4.2) and using equalities

$$\mathcal{F}_x[\nabla\times(\mathcal{M}^{-1}\nabla\times\mathbf{E}^{\mathbf{k}}(x))] \;=\; S(\nu)\mathcal{M}^{-1}S(\nu)\widetilde{\mathbf{E}}^{\mathbf{k}}(\nu)\,,$$

we find

$$-\left(\frac{\omega}{c}\right)^2\widetilde{\mathbf{E}}^{\mathbf{k}}(\nu)+S(\nu)\mathcal{M}^{-1}S(\nu)\widetilde{\mathbf{E}}^{\mathbf{k}}(\nu) = i\omega\mu_0\mathbf{e}^{\mathbf{k}}\,, \tag{4.13}$$

where $\widetilde{\mathbf{E}}^{\mathbf{k}}(\nu) = (\widetilde{E}_1^k,\widetilde{E}_2^k,\widetilde{E}_3^k)$, $\widetilde{E}_n^k(\nu) = \mathcal{F}_x[E_n^k(x)](\nu)$, $n = 1,2,3$; and $S(\nu)$ is given as (2.3).

Let $Z_n^k(\nu)$, $N_n^k(\nu)$, $R_r(\nu)$ be the real parts of $\widetilde{E}_n^k(\nu)$, $i\omega\mu_0\mathbf{e}^{\mathbf{k}}$, $(S(\nu)\mathcal{M}^{-1}S(\nu))$ and $Z_{n+3}^k(\nu)$, $N_{n+3}^k(\nu)$, $R_i(\nu)$ be the imaginary parts of $\widetilde{E}_n^k(\nu)$, $i\omega\mu_0\mathbf{e}^{\mathbf{k}}$, $(S(\nu)\mathcal{M}^{-1}S(\nu))$, respectively.

Denoting $\mathbf{Z}^{\mathbf{k}}(\nu) = (Z_1^k(\nu),Z_2^k(\nu),\ldots,Z_6^k(\nu))$ and $\mathbf{N}^{\mathbf{k}}(\nu) = (N_1^k(\nu),N_2^k(\nu),\ldots,N_6^k(\nu))$ the equation (4.13) can be written in the form

$$-\left(\frac{\omega}{c}\right)^2\mathbf{Z}^{\mathbf{k}}(\nu)+P(\nu)\mathbf{Z}^{\mathbf{k}}(\nu) = \mathbf{N}^{\mathbf{k}}(\nu)\,, \tag{4.14}$$

where $P(\nu)$ is a 6×6 symmetric matrix defined by

$$P(\nu) = \begin{pmatrix} R_r(\nu) & -R_i(\nu) \\ R_i(\nu) & R_r(\nu) \end{pmatrix}. \tag{4.15}$$

We note that $(S(\nu)\mathscr{M}^{-1}S(\nu)) = R_r(\nu) + iR_i(\nu)$, where

$$S_i(\nu) = \frac{1}{\xi_4}\begin{pmatrix} 0 & -l_{12} & l_{13} \\ l_{12} & 0 & -l_{23} \\ -l_{13} & l_{23} & 0 \end{pmatrix}, \quad S_r(\nu) = \frac{1}{\xi_4}\begin{pmatrix} m_{11} & m_{12} & m_{13} \\ m_{12} & m_{22} & m_{23} \\ m_{13} & m_{23} & m_{33} \end{pmatrix},$$

$$\begin{aligned}
&l_{12} = \nu_2\nu_3\eta_1 + \nu_3^2\eta_2 + \nu_1\nu_3\eta_3\,,\ l_{13} = \nu_2^2\eta_1 + \nu_2\nu_3\eta_2 + \nu_1\nu_2\eta_3\,,\\
&l_{23} = \nu_1\nu_3\eta_2 + \nu_1^2\eta_3 + \nu_1\nu_2\eta_1\,,\\
&m_{11} = -\nu_2^2\eta_5 + 2\nu_2\nu_3\eta_6 - \nu_3^2\eta_7\,,\ m_{12} = \nu_1\nu_2\eta_5 - \nu_1\nu_3\eta_6 - \nu_2\nu_3\eta_8 + \nu_3^2\eta_9\,,\\
&m_{13} = \nu_1\nu_3\eta_7 - \nu_1\nu_2\eta_6 - \nu_2^2\eta_8 - \nu_2\nu_3\eta_9\,,\ m_{22} = -\nu_1^2\eta_5 + 2\nu_1\nu_3\eta_8 - \nu_3^2\eta_{10}\,,\\
&m_{23} = \nu_2\nu_3\eta_{10} - \nu_1\nu_2\eta_8 - \nu_1^2\eta_6 + \nu_1\nu_3\eta_9\,,\ m_{33} = -\nu_1^2\eta_7 + 2\nu_1\nu_2\eta_8 - \nu_2^2\eta_{10}\,,
\end{aligned}$$

where

$$\begin{aligned}
&\eta_1 = \mu_{12}h_1 + \mu_{22}h_2 + \mu_{23}h_3\,,\ \eta_2 = \mu_{13}h_1 + \mu_{23}h_2 + \mu_{33}h_3\,,\\
&\eta_3 = \mu_{11}h_1 + \mu_{12}h_2 + \mu_{13}h_3\,,\\
&\eta_4 = \mu_{33}{\mu_{12}}^2 - 2\mu_{12}\mu_{13}\mu_{23} + 2\mu_{12}h_1h_2 + \mu_{22}{\mu_{13}}^2 + 2\mu_{13}h_1h_3 + \mu_{11}{\mu_{23}}^2\\
&+2\mu_{23}h_2h_3 + \mu_{11}h_1^2 + \mu_{22}h_2^2 + \mu_{33}h_3^2 - \mu_{11}\mu_{22}\mu_{33}\,,\\
&\eta_5 = {\mu_{12}}^2 + h_3^2 - \mu_{11}\mu_{22}\,,\ \eta_6 = h_2h_3 - \mu_{12}\mu_{13} + \mu_{11}\mu_{23}\,,\\
&\eta_7 = {\mu_{13}}^2 + h_3^2 - \mu_{11}\mu_{33}\,,\ \eta_8 = h_1h_3 - \mu_{12}\mu_{23} + \mu_{13}\mu_{22}\,,\\
&\eta_9 = h_1h_2 - \mu_{13}\mu_{23} + \mu_{12}\mu_{33}\,,\ \eta_{10} = {\mu_{23}}^2 + h_1^2 - \mu_{22}\mu_{33}\,.
\end{aligned}$$

Using the standard technique, from (Yakhno, 2011) we can compute an invertible matrix $Q(\nu)$ and $M(\nu)$ such that

$$\begin{aligned}
Q^{-1}(\nu)Q(\nu) &= I,\\
Q^{-1}(\nu)P(\nu)Q(\nu) &= M(\nu),
\end{aligned}$$

where $M(\nu) = diag(m_n(\nu), n = 1,2,3,4,5,6)$. MATLAB code of computation of $Q(\nu)$ and $M(\nu)$ is given in Appendix A3.2.

Let $\mathbf{U^k}(\nu) = Q^{-1}(\nu)\mathbf{Z^k}(\nu)$, then

$$\mathbf{Z^k}(\nu) = Q(\nu)\mathbf{U^k}(\nu)\,. \tag{4.16}$$

Using (4.5) the equation (4.14) can be written in the form

$$-\left(\frac{\omega}{c}\right)^2 Q(\nu)\mathbf{Z^k}(\nu) + P(\nu)Q(\nu)\mathbf{Z^k}(\nu) = \mathbf{N^k}\,. \tag{4.17}$$

Multiplying the equation (4.17) by Q^{-1}, we find

$$-\left(\frac{\omega}{c}\right)^2 \mathbf{U^k}(\nu) + M(\nu)\mathbf{U^k} = Q^{-1}(\nu)\mathbf{N^k}\,. \tag{4.18}$$

For $(\omega/c)^2 - m_n(\nu) \neq 0$ the solution of (4.18) can be written in a component form as follows

$$U_n^k(\nu) = \frac{(Q^{-1}(\nu)\mathbf{N^k})_n}{-(\omega/c)^2 + m_n(\nu)}\,, \tag{4.19}$$

where $n = 1, 2, ..., 6$. As a result the solution of (4.14) is determined by

$$\mathbf{Z^k}(\nu) = Q(\nu)\mathbf{U^k}\,,$$

and the solution of (4.13) is found by

$$\widetilde{E}_n^k = Z_n^k(\nu) + iZ_{n+3}^k(\nu)\,, j = 1, 2, 3\,; n = 1, 2, 3\,. \tag{4.20}$$

Applying the inverse Fourier transform to (4.20), we find the electric Green's function as a tempered distribution, i.e.

$$\mathbf{E_j^k}(x) = \mathcal{F}_\nu^{-1}[\widetilde{\mathbf{E}}\mathbf{{}_j^k}(\nu)](x)\,. \tag{4.21}$$

The right hand side of (4.21) can be regularized by

$$\frac{1}{(2\pi)^3}\int_{-A}^{A}\int_{-A}^{A}\int_{-A}^{A} \widetilde{\mathbf{E}}\mathbf{{}_j^k}(\nu)\, e^{-i\nu\cdot x} d\nu_1 d\nu_2 d\nu_3\,, \tag{4.22}$$

where A is the parameter of regularization.

We take $A = N\Delta$ and approximate the integral (4.22) by the integral sum

$$\frac{1}{(2\pi)^3}\sum_{n=-N}^{N}\sum_{m=-N}^{N}\sum_{l=-N}^{N} \widetilde{\mathbf{E}}\mathbf{{}_j^k}(\Delta n, \Delta m, \Delta l)\, e^{-i\Delta(nx_1+mx_2+lx_3)}(\Delta\nu)^3\,, \tag{4.23}$$

for the numerical computation. The parameters N and Δ are determined by the procedure described in Section 2.3.1.

4.2 Computational Experiments

The electric and magnetic matrix Green's functions are computed symbolically by MATLAB. The code of these computations are given in Appendix A3.1 and Appendix A3.2. The inverse Fourier transformation is computed numerically by using the idea given in Chapter 2, Section 2.3.1.

4.2.1 The Approximate Computation of the Electric and Magnetic Green's Functions in Gyro-magnetic Media

In this section we consider the approximate computation of electric and magnetic Green's functions for gyro-magnetic media characterizing by

$$\mathscr{M} = \begin{pmatrix} 31.5 & -13.1 & -14.1 \\ -13.1 & 5.5 & 5.8 \\ -14.1 & 5.8 & 6.7 \end{pmatrix} + i \begin{pmatrix} 0 & 0.5\gamma & -0.4\gamma \\ -0.5\gamma & 0 & 0.2\gamma \\ 0.4\gamma & -0.2\gamma & 0 \end{pmatrix}.$$

In our computations we choose two different parameters. The first part of computation is related to different γ values such as $\gamma = 10^{-1}$ and $\gamma = 10^{-2}$ for fixed frequency $\omega = 2c$. We add the parameter γ to demonstrate how small changes on γ affect the solution of the electric and magnetic field vectors. The second part is related to different frequency such as $\omega = 2c$ and $\omega = 5c$ for fixed $\gamma = 10^{-1}$. We add the parameter ω to demonstrate the characteristics of the solution of the electric and magnetic field vectors for different frequencies, i.e. $\omega = 2c, 5c$.

Applying the method of Section 4.1.1 we have computed $T(\nu)$, $T^T(\nu)$, $D(\nu)$ and then using the formula (4.12) we have derived solutions $\mathbf{H^1}(x)$, $\mathbf{H^2}(x)$, $\mathbf{H^3}(x)$ of (4.3) numerically and applying the method of Section 4.1.2 we have computed $Q(\nu)$, $Q^{-1}(\nu)$, $M(\nu)$ and then using the formula (4.23) we have derived solutions $\mathbf{E^1}(x)$, $\mathbf{E^2}(x)$, $\mathbf{E^3}(x)$ of (4.13) numerically.

For the first part of computational experiments, we fixed frequency $\omega = 2c$ and results of the computation of real and imaginary parts of $E_1^1(x)$, $E_2^1(x)$, $E_3^1(x)$ and

$H_1^1(x)$, $H_3^1(x)$ for $\gamma = 10^{-1}, 10^{-2}$ are presented in Figure 4.1, Figure 4.3-Figure 4.5 and Figure 4.2, Figure 4.6-Figure 4.8, respectively.

In Figure 4.1(a), (b) present the $1D$ plots of $Re(E_2^1(z,z,0))$, $Re(E_3^1(z,z,0))$ for $x_1 = x_2 = z$, $x_3 = 0$, $\omega = 2c$ for $\gamma = 10^{-1}$ and $\gamma = 10^{-2}$ respectively. Figure 4.2(a), (b) present the $1D$ graphs of $Im(H_3^1(x_1,x_2,0))$ and $Re(H_3^1(x_1,x_2,0))$, respectively for $\gamma = 10^{-1}, 10^{-2}$. These graphs show the influence of γ on the components of the electric and magnetic Green's functions.

The behavior of the real and imaginary parts of the computed components of the electric and magnetic Green's functions is presented in Figure 4.1, Figure 4.3 and Figure 4.4. The result of the simulation $Im(E_1^1(x_1,x_2,0))$ for $\omega = 2c$, $\gamma = 10^{-1}$ is presented in Figure 4.3. The $3D$ plot of $Im(E_1^1(x_1,x_2,0))$ is shown in Figure 4.3(b). Figure 4.3(a) is a screen shot of $2D$ level plot of the same surface $Im(E_1^1(x_1,x_2,0))$, i.e. a view of the surface $z = Im(E_1^1(x_1,x_2,0))$ presented in Figure 4.3(b) from the top of z-axis. Figure 4.4(a) presents $2D$ graph of $Im(E_2^1(x_1,x_2,0))$. Figure 4.4(b) presents the $3D$ graph of $Im(E_2^1(x_1,x_2,0))$ for $\omega = 2c$, $\gamma = 10^{-1}$. Figure 4.5(a), (b) presents $2D$ graph of $Im(E_3^1(x_1,x_2,0))$ and $Re(E_3^1(x_1,x_2,0))$ for $\omega = 2c$, $\gamma = 10^{-1}$ respectively.

The result of simulation $Im(H_1^1(x_1,x_2,0))$ is presented in Figure 4.6. Figure 4.6(a), (b) are the $2D$ and $3D$ plots of $Im(H_1^1(x_1,x_2,0))$ respectively. Figure 4.7(a), (b) are the $2D$ and $3D$ plots of $Im(H_3^1(x_1,x_2,0))$ respectively. The $2D$ illustration of $Re(H_1^1(x_1,x_2,0))$, $Re(H_3^1(x_1,x_2,0))$ is given in Figure 4.8(a), (b).

For the second part of computational experiments, we fixed γ as $\gamma = 10^{-1}$ and results of the computation of real and imaginary parts of $E_2^1(x)$, $E_3^1(x)$ and $H_3^1(x)$ for $\omega = 2c, 5c$ are presented in Figure 4.9 and Figure 4.10, respectively. Figure 4.9(a), (b) present the $1D$ plots of $Re(E_2^1(z,z,0))$, $Re(E_3^1(z,z,0))$ for $x_1 = x_2 = z$, $x_3 = 0$, $\gamma = 10^{-1}$ for $\omega = 2c$ and $\omega = 5c$ respectively. Figure 4.10(a), (b) present the $1D$ graphs of $Im(H_3^1(x_1,x_2,0))$ and $Re(H_3^1(x_1,x_2,0))$, respectively for $\omega = 2c, 5c$. These graphs show the influence of ω on the components of the electric and magnetic Green's functions.

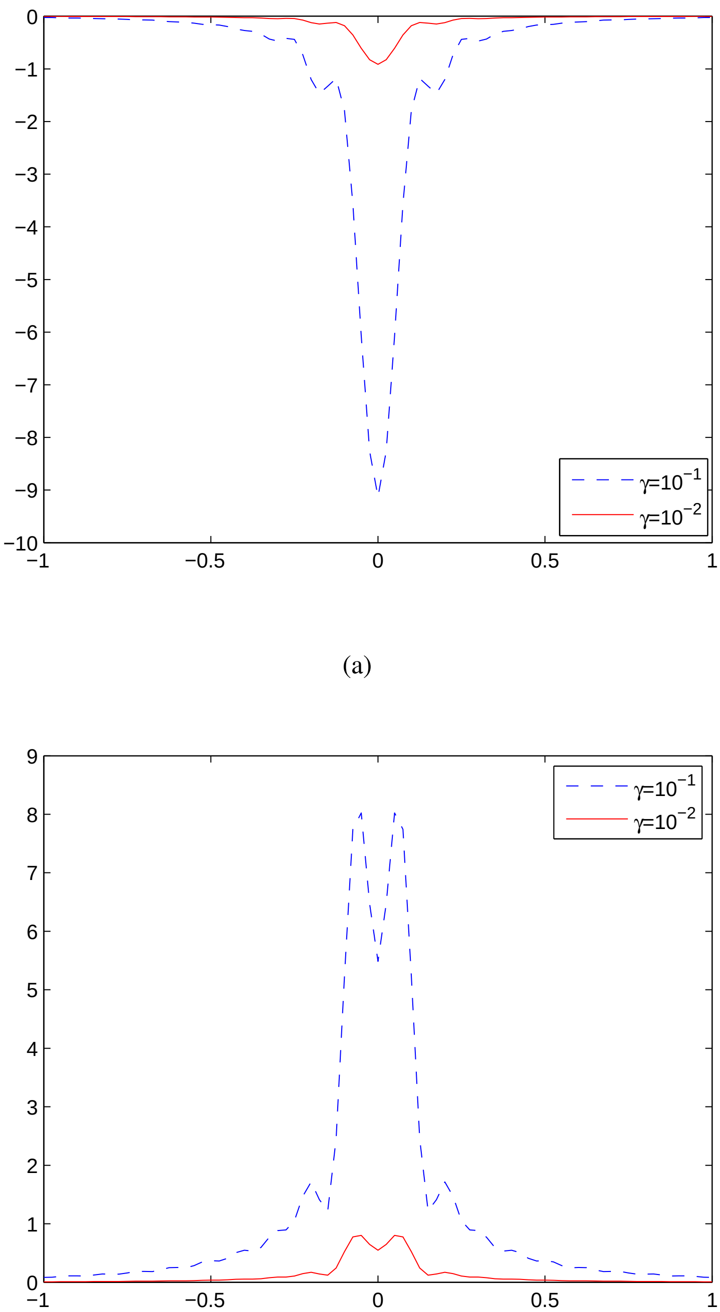

(a)

(b)

Figure 4.1 $\omega = 2c$, (a) $1D$ plot of $Re(E_2^1(z,z,0))$; (b) $1D$ plot of $Re(E_3^1(z,z,0))$ for $\gamma = 10^{-1}, 10^{-2}$

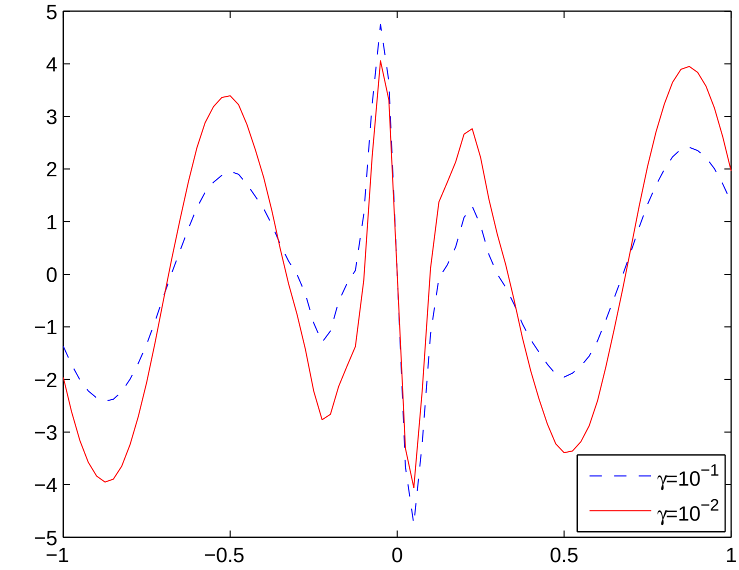

(a)

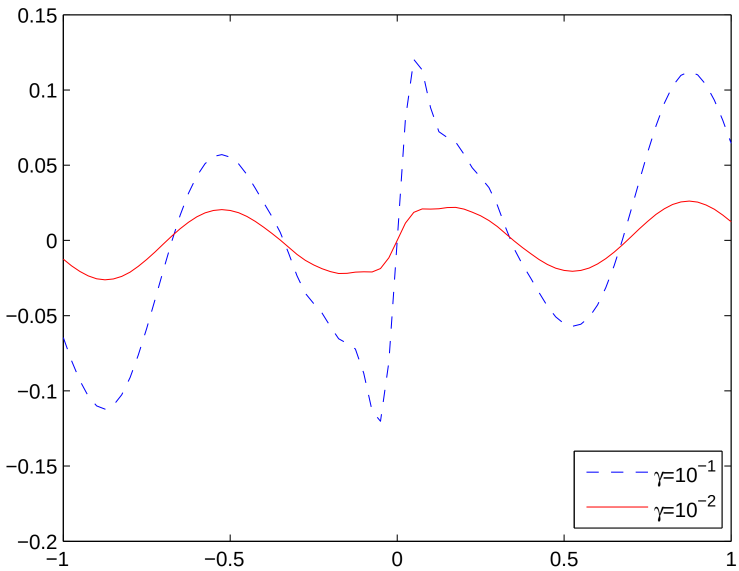

(b)

Figure 4.2 $\omega = 2c$, $\gamma = 10^{-1}, 10^{-2}$, (a) $1D$ plot of $Im(H_3^1(z,z,0))$; (b) $1D$ plot of $Re(H_3^1(z,z,0))$

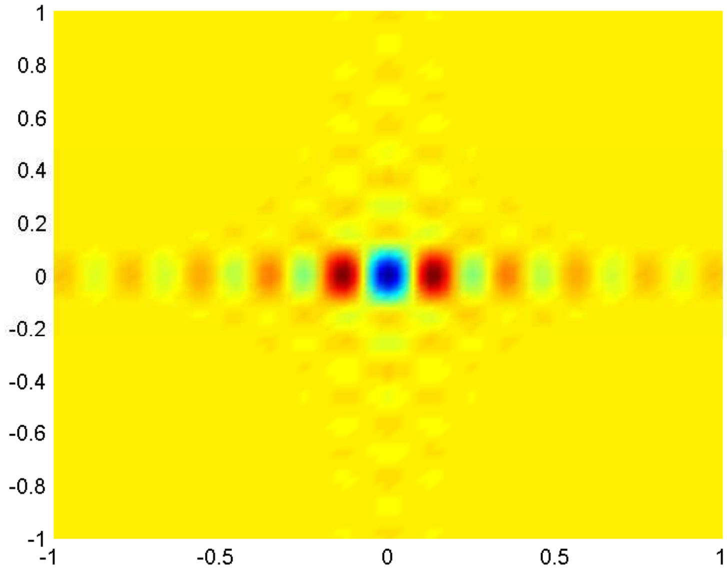

(a)

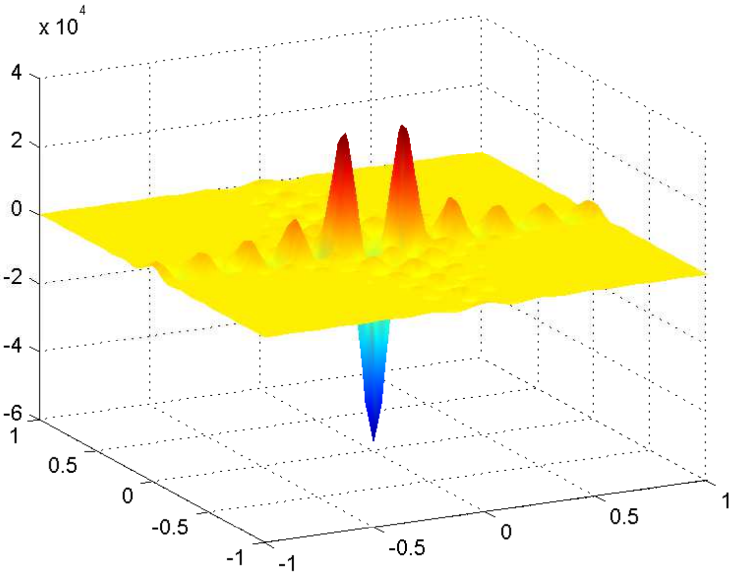

(b)

Figure 4.3 $\omega = 2c$, $\gamma = 10^{-1}$, (a) $2D$ plot of $Im(E_1^1(x_1, x_2, 0))$; (b) $3D$ plot of $Im(E_1^1(x_1, x_2, 0))$

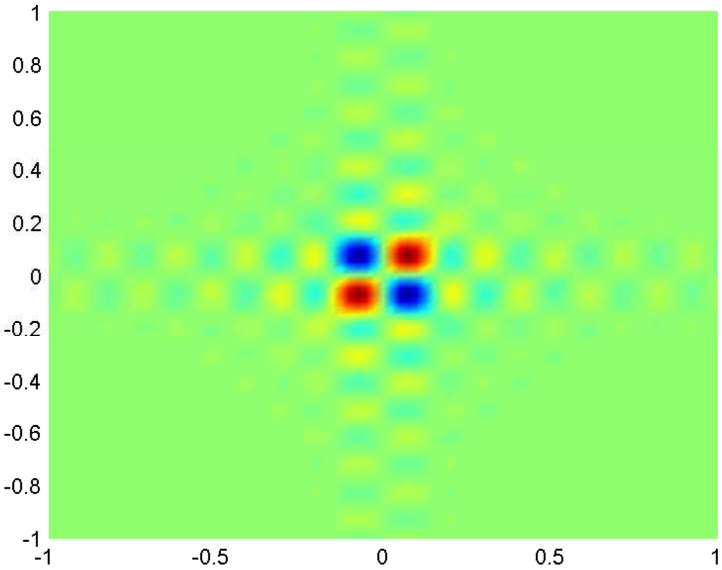

(a)

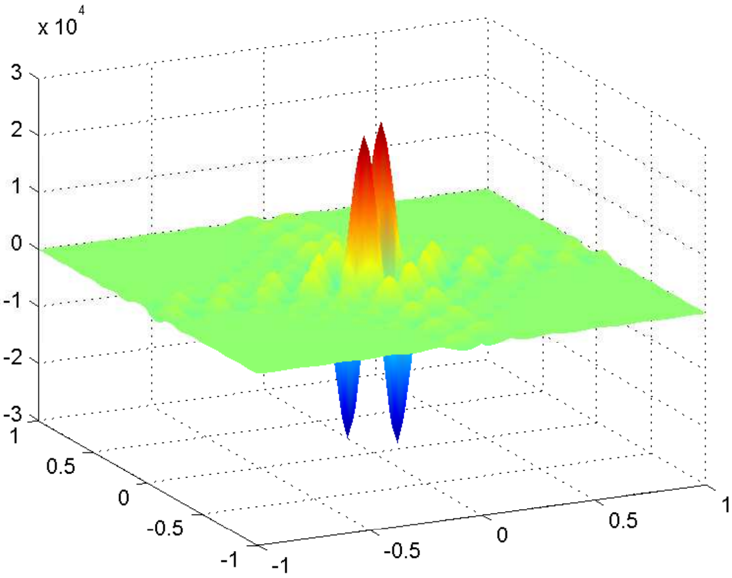

(b)

Figure 4.4 $\omega = 2c$, $\gamma = 10^{-1}$, (a) $2D$ plot of $Im(E_2^1(x_1, x_2, 0))$; (b) $3D$ plot of $Im(E_2^1(x_1, x_2, 0))$

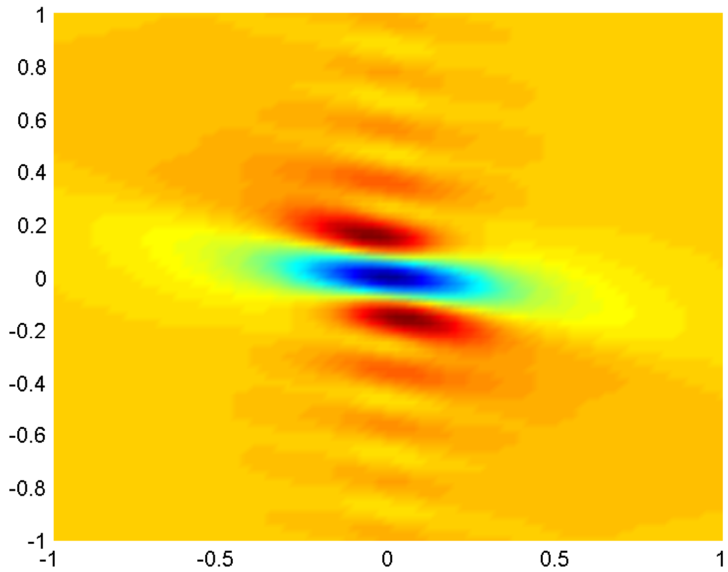

(a)

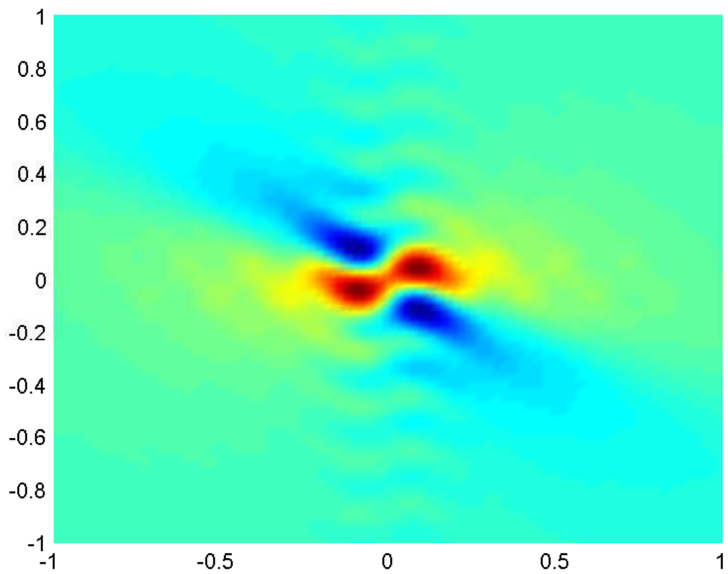

(b)

Figure 4.5 $\omega = 2c$, $\gamma = 10^{-1}$, (a) $2D$ plot of $Im(E_3^1(x_1, x_2, 0))$; (b) $2D$ plot of $Re(E_3^1(x_1, x_2, 0))$

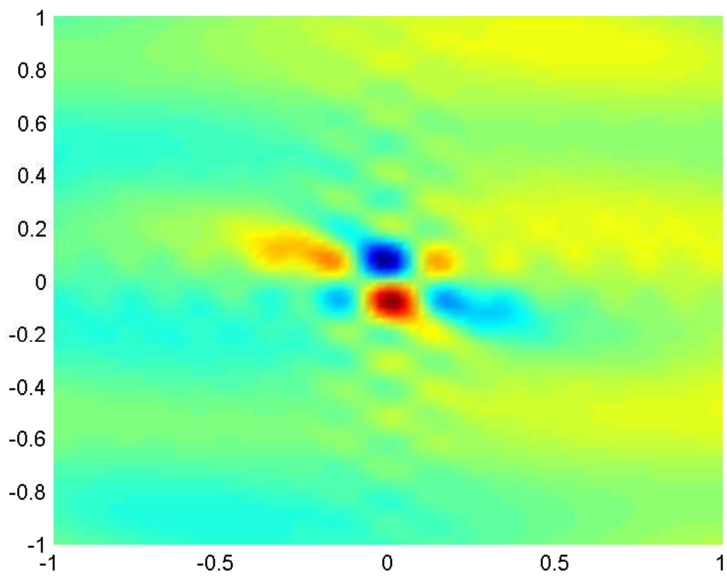

(a)

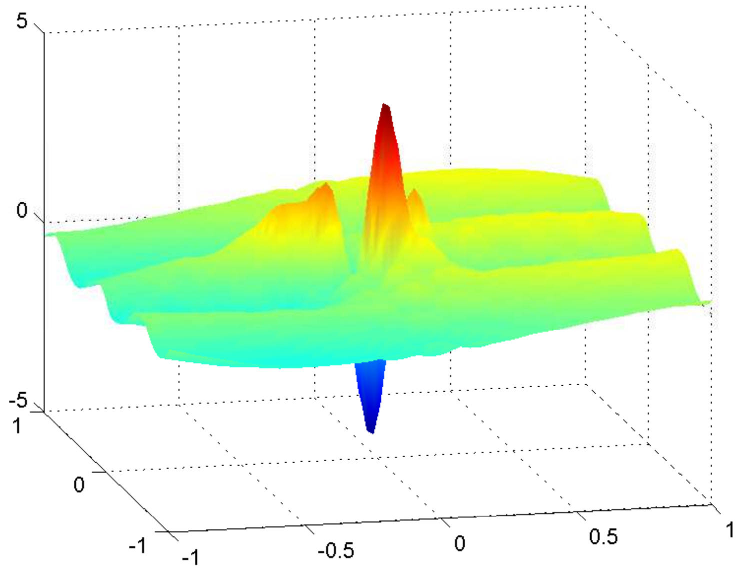

(b)

Figure 4.6 $\omega = 2c$, $\gamma = 10^{-1}$, (a) $2D$ plot of $Im(H_1^1(x_1, x_2, 0))$; (b) $3D$ plot of $Im(H_1^1(x_1, x_2, 0))$

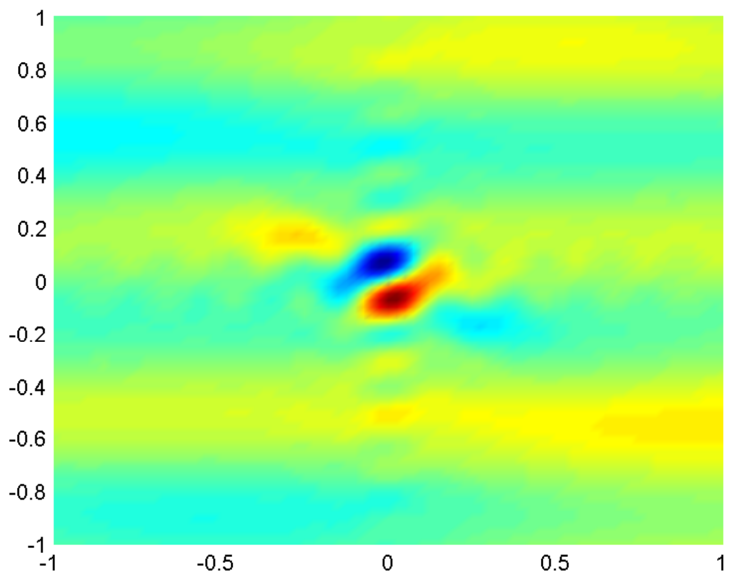

(a)

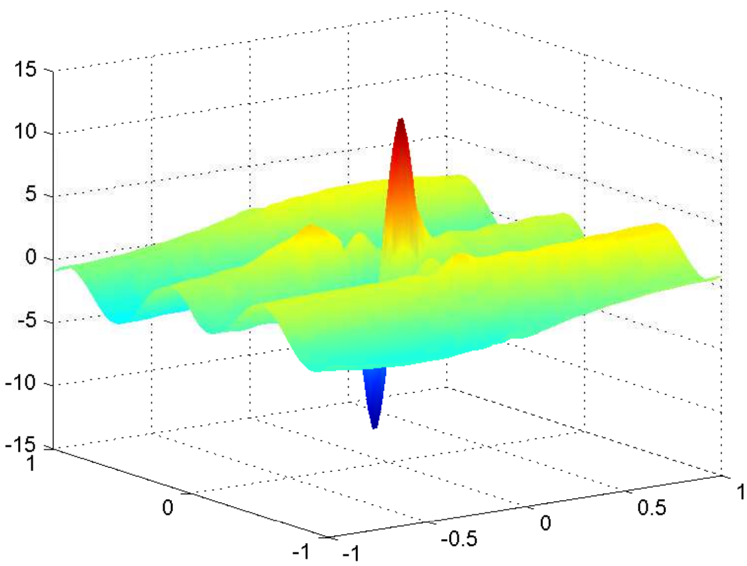

(b)

Figure 4.7 $\omega = 2c$, $\gamma = 10^{-1}$, (a) $2D$ plot of $Im(H_3^1(x_1, x_2, 0))$; (b) $3D$ plot of $Im(H_3^1(x_1, x_2, 0))$

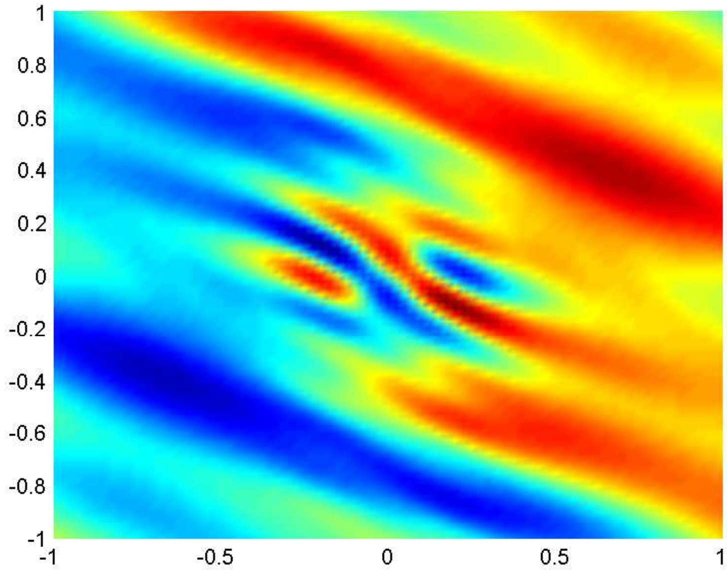

(a)

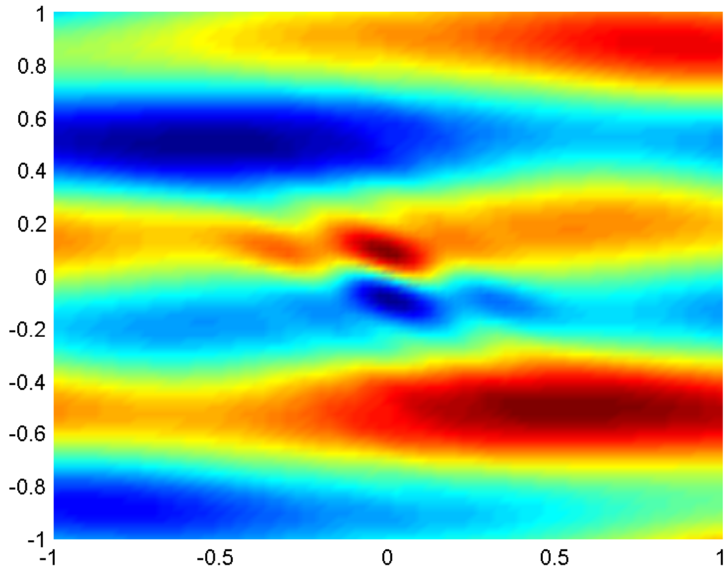

(b)

Figure 4.8 $\omega = 2c$, $\gamma = 10^{-1}$, (a) $2D$ plot of $Re(H_1^1(x_1, x_2, 0))$; (b) $2D$ plot of $Re(H_3^1(x_1, x_2, 0))$

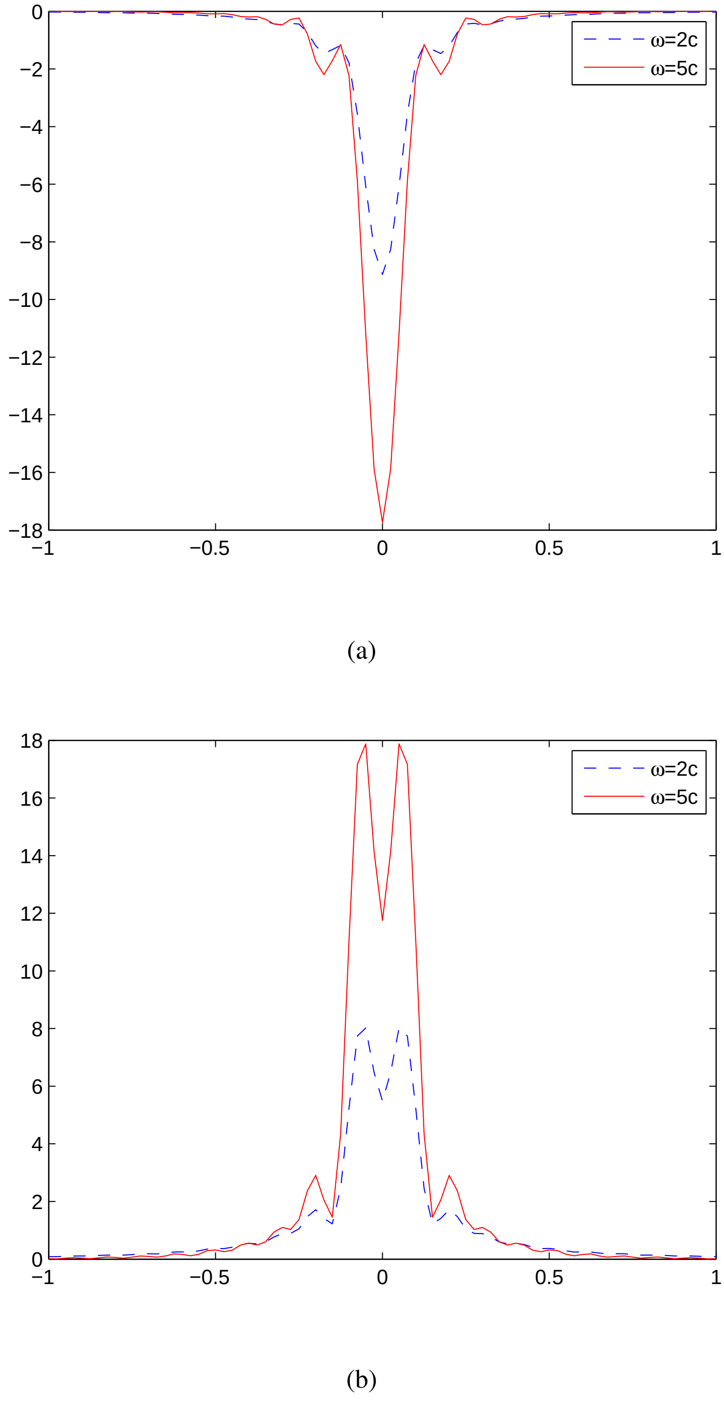

(a)

(b)

Figure 4.9 $\gamma = 10^{-1}$, (a) $1D$ plot of $Re(E_2^1(z,z,0))$; (b) $1D$ plot of $Re(E_3^1(z,z,0))$ for $\omega = 2c, 5c$

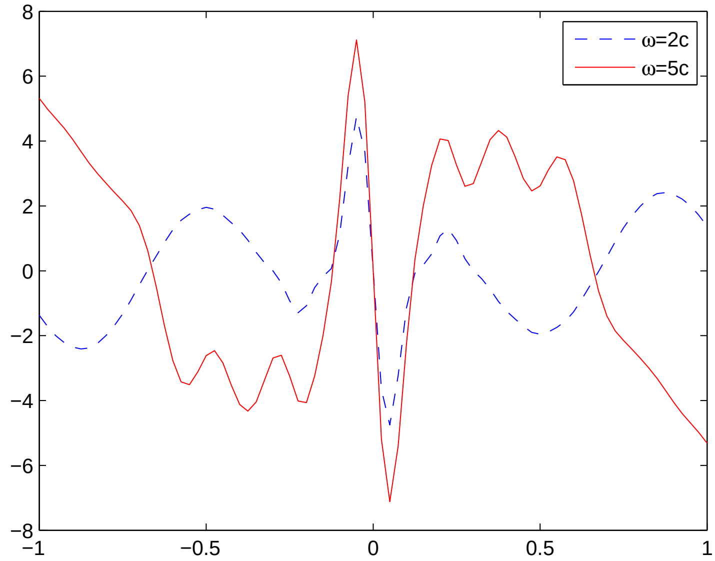

(a)

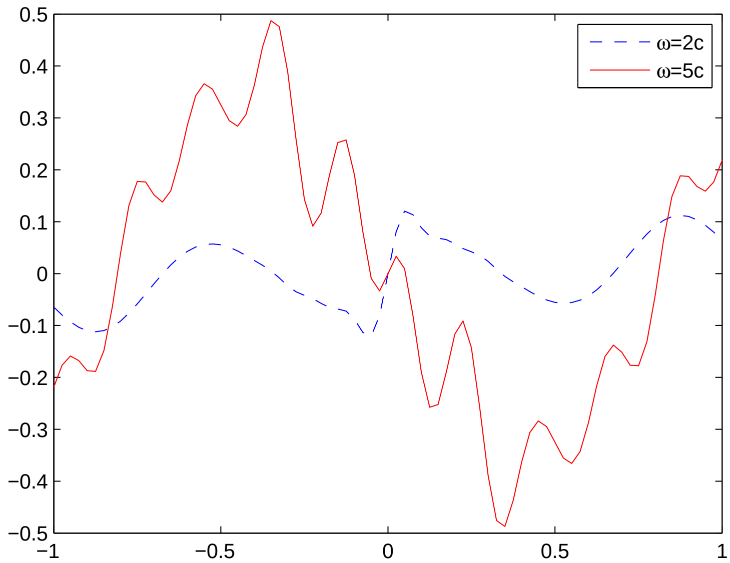

(b)

Figure 4.10 $\gamma = 10^{-1}$, (a) $1D$ plot of $Im(H_3^1(z,z,0))$; (b) $1D$ plot of $Re(H_3^1(z,z,0))$ for $\omega = 2c, 5c$

4.3 Summary of the Chapter Four

The method for the approximate computation of the electric and magnetic Green's functions in general gyro-magnetic materials has been developed. This method consists of the following. Applying the Fourier transform with respect to space variables to the partial differential equations, defining column matrix Green's functions, the linear algebraic systems for Fourier images of these columns were obtained. These images were computed by the matrix transformation in MATLAB. The inverse Fourier transform of these images has been done numerically in the regularized (approximate) form in MATLAB. The parameters of this regularization have been chosen using the explicit formulae of the Green's function and its Fourier image for the Helmholtz equation. Two types of the computational experiments were presented in this chapter. The first one demonstrates the high level of computational accuracy for the Fourier images and the inverse Fourier transform. The second one has been done for computing the electric and magnetic Green's functions in a general gyro-magnetic material. These computational experiments confirm the robustness of the method.

CHAPTER FIVE
THE APPROXIMATE COMPUTATION OF THE FUNDAMENTAL SOLUTION OF TIME-DEPENDENT MAXWELL'S EQUATIONS FOR GENERAL ANISOTROPIC CONDUCTIVE MATERIALS

In this chapter, we suggest a new method of the approximate computation of the fundamental solution of Maxwell's equations for general anisotropic conductive materials. The method consists of the following. The equations for the fundamental solution are written in the form of the Fourier transformation with respect to the space variables. The obtained equations are reduced to a vector integral equation of the Volterra type. The solution of the obtained integral equation is corrected by the successive approximations in the form of the uniformly convergent infinite functional series. Finally, the inverse Fourier transform is applied to constructed series with respect to the Fourier parameters. The computation of the fundamental solutions of electric fields in general anisotropic conductive materials have been made by replacement of infinite series by a sum with finite terms and implemented numerically in MATLAB, the inverse Fourier transform by the integration over a bounded domain. Computational experiments confirm the robustness of our method.

5.1 The Derivation of the Fundamental Solution of the Electric Field

5.1.1 The Fourier Transform of the Equation for the Fundamental Solution

Let $x = (x_1, x_2, x_3) \in \mathbb{R}^3$, $\mathbf{E}^m(x,t) = (E_1^m(x,t), E_2^m(x,t), E_3^m(x,t))^T$ be m^{th} column of the fundamental solution of the electric field, $\widetilde{\mathbf{E}}^m(\nu,t)$ be the Fourier transform of $\mathbf{E}^m(x,t)$ with respect to $x = (x_1, x_2, x_3) \in \mathbb{R}^3$, i.e. field $\widetilde{\mathbf{E}}^m(x,t) = (\widetilde{E}_1^m(x,t), \widetilde{E}_2^m(x,t), \widetilde{E}_3^m(x,t))^T$ are defined by $\widetilde{E}_k^m(\nu,t) = \mathcal{F}_x[E_k^m](\nu,t)$, $k = 1,2,3$, where the Fourier operator $\mathcal{F}_x$ is given by (see, for example, Vladimirov, 1971)

$$\widetilde{E}_k^m(\nu,t) = \mathcal{F}_x[E_k^m](\nu,t) = \int_{-\infty}^{\infty}\int_{-\infty}^{\infty}\int_{-\infty}^{\infty} E_k^m(x,t)\, e^{ix\cdot\nu}\, dx_1 dx_2 dx_3\,, \tag{5.1}$$

where $\nu = (\nu_1, \nu_2, \nu_3) \in \mathbf{R}^3$, $x \cdot \nu = x_1\nu_1 + x_2\nu_2 + x_3\nu_3$, $i^2 = -1$.

Equation (1.22) can be written in the form of their Fourier transform as follows

$$\mathscr{E}\frac{\partial^2}{\partial t^2}\widetilde{E}^m(\nu,t)+c^2A(\nu)\widetilde{E}^m(\nu,t) \quad = \quad -4\pi\frac{\partial}{\partial t}\Big(\sigma\widetilde{E}^m(\nu,t)+\mathbf{e}^m\delta(t)\Big)\,, \tag{5.2}$$

where

$$A(\nu)\widetilde{E}^m(\nu,t)=\mathcal{F}_x[curl_x\Big(\mathscr{M}^{-1}curl_x\,E^m(x,t)\Big)](\nu,t)\,,$$

and $A(\nu) = S(\nu)\,\mathscr{M}^{-1}\,S(\nu)$, where $S(\nu)$ is given in (2.3).

5.1.2 The Reduction of (5.2) to a Vector Integral of the Volterra Type

Since $\mathscr{E}$ is symmetric positive definite and $A(\nu)$ is symmetric positive semi-definite matrices, we can construct a nonsingular matrix $\bar{\bar{T}}(\nu)$ and a diagonal matrix $\bar{\bar{D}}(\nu) = \mathrm{diag}(d_1(\nu),d_2(\nu),d_3(\nu))$ with non-negative elements such that

$$\bar{\bar{T}}^T(\nu)\mathscr{E}\bar{\bar{T}}(\nu)=\bar{\bar{I}},\quad \bar{\bar{T}}^T(\nu)A(\nu)\bar{\bar{T}}(\nu)=\bar{\bar{D}}(\nu)\,,$$

where $\bar{\bar{I}}$ is the identity matrix, $\bar{\bar{T}}^T(\nu)$ is the transposed matrix or $\bar{\bar{T}}(\nu)$. The similar reduction of pair symmetric matrices to diagonal form by congruence has been considered before by (Goldberg, 1992). Moreover computing $\bar{\bar{D}}(\nu)$ and $\bar{\bar{T}}(\nu)$ can be made by the following way; firstly find $\mathscr{E}^{-1/2}$ and then using the matrix $\mathscr{E}^{-1/2}A(\nu)\mathscr{E}^{-1/2}$ we construct $\bar{\bar{D}}(\nu)$ and $\bar{\bar{T}}(\nu)$.

Finding $\mathscr{E}^{-1/2}$. We note that for a given diagonal matrix $\mathscr{E} = diag(\varepsilon_{11},\varepsilon_{22},\varepsilon_{33})$ with positive elements on the diagonal matrix $\mathscr{E}^{-1/2}$ is given by $\mathscr{E}^{-1/2} = diag(\frac{1}{\sqrt{\varepsilon_{11}}},\frac{1}{\sqrt{\varepsilon_{22}}},\frac{1}{\sqrt{\varepsilon_{33}}})$. For the given positive definite non-diagonal matrix $\mathscr{E}$ we construct an orthogonal matrix $\bar{\bar{R}}$ by the eigenfunctions of $\mathscr{E}$ such that $\bar{\bar{R}}^T\mathscr{E}\bar{\bar{R}} = \bar{\bar{L}} = diag(\lambda_1,\lambda_2,\lambda_3)$, where $\bar{\bar{R}}^T$ is the transpose matrix of $\bar{\bar{R}}$ and $\lambda_k > 0$, $k = 1,2,3$ are eigenvalues of $\mathscr{E}$. The $\mathscr{E}^{-1/2}$ is defined by $\mathscr{E}^{-1/2} = \bar{\bar{R}}\bar{\bar{L}}^{1/2}\bar{\bar{R}}^T$, where $\bar{\bar{L}}^{1/2} = diag(\sqrt{\lambda_1},\sqrt{\lambda_2},\sqrt{\lambda_3})$. The matrix $\mathscr{E}^{-1/2}$ is the inverse to $\mathscr{E}$.

Finding $\bar{\bar{D}}(\nu)$ and $\bar{\bar{T}}(\nu)$. Let us take the given positive semi-definite matrix $A(\nu)$ and the matrix $\mathscr{E}^{-1/2}$ which assumed to be found. Let us consider the matrix

$\mathscr{E}^{-1/2}A(\nu)\mathscr{E}^{-1/2}$ which symmetric positive semi-definite. The diagonal matrix $\bar{\bar{D}}(\nu)$ is constructed by eigenvalues of $\mathscr{E}^{-1/2}A(\nu)\mathscr{E}^{-1/2}$. The columns of the orthogonal matrix $\bar{\bar{Q}}(\nu)$ are formed by normalized orthogonal eigenfunctions of $\mathscr{E}^{-1/2}A(\nu)\mathscr{E}^{-1/2}$ corresponding to eigenvalues $d_k(\nu)$, $k = 1, 2, 3$. The matrix $\bar{\bar{T}}(\nu)$ is defined by the formula $\bar{\bar{T}}(\nu) = \mathscr{E}^{-1/2}\bar{\bar{Q}}(\nu)$.

Let matrices $\bar{\bar{T}}(\nu)$ and $\bar{\bar{D}}(\nu)$ have been constructed using above mentioned technique. Setting $\widetilde{E}^m(\nu,t) = \bar{\bar{T}}(\nu)\,Y^m(\nu,t)$, equation (5.2) can be written as

$$\mathscr{E}\bar{\bar{T}}(\nu)\frac{\partial^2}{\partial t^2}Y^m(\nu,t) + c^2A(\nu)\bar{\bar{T}}(\nu)Y^m(\nu,t) = -4\pi\frac{\partial}{\partial t}\left(\sigma\bar{\bar{T}}(\nu)Y^m(\nu,t) + \mathbf{e}^m\delta(t)\right). \quad (5.3)$$

Multiplying (5.3) by $\bar{\bar{T}}^T(\nu)$ we have

$$\frac{\partial^2}{\partial t^2}Y^m(\nu,t) + c^2d_m(\nu)Y^m(\nu,t) = -4\pi\frac{\partial}{\partial t}\left(\bar{\bar{T}}^T(\nu)\sigma\bar{\bar{T}}(\nu)Y^m(\nu,t) + \bar{\bar{T}}^T(\nu)\mathbf{e}^m\delta(t)\right). \quad (5.4)$$

Integrating (5.4) and using $Y^m(\nu,t)|_{t<0} = 0$ we find

$$\begin{aligned} Y^m(\nu,t) &= \frac{1}{c\sqrt{d_m}}\int_0^t \sin(c\sqrt{d_m}(t-\tau))\Big[-4\pi\frac{\partial}{\partial\tau}(\bar{\bar{T}}^T(\nu)\sigma\bar{\bar{T}}(\nu)Y^m(\nu,t) \\ &\qquad + \bar{\bar{T}}^T(\nu)\mathbf{e}^m\delta(\tau))\Big]d\tau. \end{aligned} \quad (5.5)$$

Equation (5.5) can be written as follows

$$Y^m(\nu,t) = -4\pi\cos(c\sqrt{d_m}t)\bar{\bar{T}}^T(\nu)\mathbf{e}^m + \int_0^t -4\pi\cos(c\sqrt{d_m}\tau)\bar{\bar{T}}^T(\nu)\sigma\bar{\bar{T}}(\nu)Y^m(\nu,\tau)d\tau. \quad (5.6)$$

Since $\widetilde{E}^m = \bar{\bar{T}}(\nu)\,Y^m(\nu,t)$, multiplying (5.6) by $\bar{\bar{T}}(\nu)$ we get

$$\begin{aligned} \widetilde{E}^m(\nu,t) &= -4\pi\bar{\bar{T}}(\nu)\cos(c\sqrt{d_m}t)\bar{\bar{T}}^T(\nu)\mathbf{e}^m \\ &\qquad + \int_0^t -4\pi\bar{\bar{T}}(\nu)\cos(c\sqrt{d_m}(t-\tau))\bar{\bar{T}}^T(\nu)\sigma\widetilde{E}^m(\nu,\tau)d\tau. \end{aligned} \quad (5.7)$$

The last equation can be written in the form of Volterra type integral equation

$$\widetilde{E}^m(\nu,t) = \int_0^t K(\nu,t-\tau)\widetilde{E}^m(\nu,\tau)d\tau + \widetilde{f}^m(\nu,t), \quad (5.8)$$

where $K(\nu,t)$ (kernel of integral equation) and $\widetilde{f}^m(\nu,t)$ has the following forms

$$K(\nu,t) = -4\pi\bar{\bar{T}}(\nu)\cos(c\sqrt{d_m}t)\bar{\bar{T}}^T(\nu)\sigma, \quad (5.9)$$

$$\widetilde{f}^m(\nu,t) = -4\pi\bar{\bar{T}}(\nu)\cos(c\sqrt{d_m}t)\bar{\bar{T}}^T(\nu)\mathbf{e}^m. \quad (5.10)$$

The following two lemmas demonstrates the continuity and boundedness of the Kernel $K(v,t)$ and the boundedness of inhomogeneous term $\widetilde{f^m}(v,t)$ which will be used in the next section for constructing a solution of equation (5.8).

Lemma 5.1.1. *Let T be a fixed number; v be a fixed point in $\mathbb{R}^3$; $K(v,t) = (k_{ij}(v,t))_{3\times3}$ be a matrix defined by (5.9) for any $t \in [0,T]$. Then components of the vector function*

$$\int_0^t K(v,t-\tau)\widetilde{E}(v,\tau)d\tau,$$

belongs to $C^1[0,T]$ for any $\widetilde{E}(v,t) = (\widetilde{E}_1(v,t), \widetilde{E}_2(v,t), \widetilde{E}_3(v,t))$ whose components are continuous function with respect to $t \in [0,T]$.

Proof. Since elements of matrix $K(v,t)$ are continuously differentiable with respect to $t \in [0,T]$ and $\widetilde{E}_j(v,t)$, $j = 1,2,3$ are continuous then $\int_0^t K(v,t-\tau)\widetilde{E}(v,\tau)d\tau$ form $C^1[0,T]$ for even fixed v in $\mathbb{R}^3$. □

Lemma 5.1.2. *Let v be a fixed point in $\mathbb{R}^3$; $K(v,t) = (k_{ij}(v,t))_{3\times3}$ be a matrix defined by (5.9) for any $t \in [0,T]$. Then*

$$|K(v,t-\tau)\widetilde{E}(v,\tau)| \le M\|\widetilde{E}(v,\tau)\|_\infty,$$

for $\forall t \in [0,T]$, $\tau \in [0,t]$, where

$$M = \frac{4\pi\sqrt{\sigma_{max}(\sigma^T\sigma)}}{\lambda_{min}(\mathscr{E})},$$

here $\sigma_{max}(\sigma^T\sigma)$ is the maximum eigenvalue of 3×3 matrix $\sigma = (\sigma_{ij})_{3\times3}$ and $\lambda_{min}(\mathscr{E})$ is the minimum eigenvalue of non-singular 3×3 matrix $\mathscr{E}$.

Proof. Let $K(v,t-\tau)$ be a matrix defined by (5.9), then

$$|K(v,t-\tau)\widetilde{E}(v,\tau)| = |4\pi\bar{\bar{T}}\cos(c\sqrt{\bar{\bar{D}}}(t-\tau))\bar{\bar{T}}^T(v)\sigma\widetilde{E}(v,\tau)|.$$

Taking maximum norm (see, for example, (Sundarapandian, 2008), pp.125 or Appendix A4) we obtain the following result

$$\begin{aligned}
\|K(v,t-\tau)\widetilde{E}(v,\tau)\|_\infty &= \|4\pi\bar{\bar{T}}(v)\cos(c\sqrt{\bar{\bar{D}}}(t-\tau))\bar{\bar{T}}^T(v)\sigma\widetilde{E}(v,\tau)\|_\infty \\
&\le 4\pi\|\bar{\bar{T}}(v)\|_\infty\|\cos(c\sqrt{\bar{\bar{D}}}(t-\tau))\|_\infty\|\bar{\bar{T}}^T(v)\|_\infty\|\sigma\|_\infty\|\widetilde{E}(v,\tau)\|_\infty \\
&\le 4\pi\|\bar{\bar{T}}(v)\|_\infty\|\bar{\bar{T}}^T(v)\|_\infty\|\sigma\|_\infty\|\widetilde{E}(v,\tau)\|_\infty, \\
&\le \frac{4\pi\sqrt{\sigma_{max}(\sigma^T\sigma)}}{\lambda_{min}(\mathscr{E})}\|\widetilde{E}(v,\tau)\|_\infty,
\end{aligned}$$

here we used

$$\begin{aligned} \|\cos(c\sqrt{\bar{\bar{D}}}(t-\tau))\|_\infty &= \max\left\{\cos(c\sqrt{d_1}(t-\tau)), \cos(c\sqrt{d_2}(t-\tau)), \cos(c\sqrt{d_3}(t-\tau))\right\} \\ &\leq 1 \end{aligned}$$

and

$$\begin{aligned} \|\bar{\bar{T}}(\nu)\|_\infty \|\bar{\bar{T}}^T(\nu)\|_\infty &= \|\mathscr{E}^{-\frac{1}{2}}\,\bar{\bar{Q}}(\nu)\|_\infty \|\bar{\bar{Q}}(\nu)\,\mathscr{E}^{-\frac{1}{2}}\|_\infty \\ &\leq \|\mathscr{E}^{-\frac{1}{2}}\|_2 \|\bar{\bar{Q}}(\nu)\|_2 \|\bar{\bar{Q}}(\nu)\|_2 \|\mathscr{E}^{-\frac{1}{2}}\|_2 \text{ Appendix A4)} \\ &\leq \|\mathscr{E}^{-\frac{1}{2}}\|_2^2 \text{ (lemma A4.7)} \\ &\leq \frac{1}{\lambda_{min}(\mathscr{E})}, \end{aligned}$$

and

$$\|\sigma\|_\infty \leq \|\sigma\|_2 \leq \sqrt{\sigma_{max}(\sigma^T\sigma)}.$$

□

In this place, we can find a bound for $\widetilde{f^m}(\nu,t)$ (using (Sundarapandian, 2008) or Appendix A4) to use in the next section with same notations as

$$\begin{aligned} \|\widetilde{f^m}(\nu,t)\|_\infty &= \|4\pi\bar{\bar{T}}(\nu)\cos(c\sqrt{\bar{\bar{D}}}(t-\tau))\bar{\bar{T}}^T(\nu)e^m\|_\infty \\ &\leq 4\pi\|\bar{\bar{T}}(\nu)\|_\infty \|\cos(c\sqrt{\bar{\bar{D}}}(t-\tau))\|_\infty \|\bar{\bar{T}}^T(\nu)\|_\infty \|\mathbf{e}^m\|_\infty \\ &\leq \frac{4\pi}{\lambda_{min}(\mathscr{E})}, \end{aligned}$$

where $\|\mathbf{e}^m\|_\infty = 1$ for $m = 1,2,3$.

5.1.3 Solution of the Volterra Type Integral Equation (5.8) by Using the Method of Successive Approximations

Theorem 5.1.3. *Suppose that for any fixed $\nu \in \mathbb{R}^3$, $\widetilde{f}(\nu,t) \in C^1[0,T]$ is given function, $K(\nu,t) = (k_{ij}(\nu,t))_{3\times 3}$ be a matrix defined by (5.9) for any $t \in [0,T]$ there exits a unique solution $\widetilde{E}(\nu,t) \in C[0,T]$ of the integral equation (5.8).*

Proof. Let us consider the sequence of functions

$$\widetilde{E}_0(v,t) = \widetilde{f}(v,t),$$

$$\widetilde{E}_1(v,t) = \int_0^t K(v,t-\tau)\widetilde{E}_0(v,\tau)d\tau,$$

inductively we have

$$\widetilde{E}_p(v,t) = \int_0^t K(v,t-\tau)\widetilde{E}_{p-1}(v,\tau)d\tau.$$

□

Lemma 5.1.4. *Let $v \in \mathbb{R}^3$ be fixed; t be a fixed positive number then summation gives*

$$\sum_{k=0}^{p} \widetilde{E}_k(v,t) = \sum_{k=0}^{p-1} \int_0^t K(v,t-\tau)\widetilde{E}_k(v,\tau)d\tau + \widetilde{f}(v,t). \tag{5.11}$$

Lemma 5.1.5. *Let $v \in \mathbb{R}^3$ be fixed; t be a fixed positive number then we have*

$$|\widetilde{E}_k(v,t)| \leq \frac{(Mt)^k}{k!} \|\widetilde{f}(v,t)\|_\infty, \ \forall k = 0,1,...,p.$$

Proof. **for** $k = 0$**:**

$$|\widetilde{E}_0(v,t)| = |\widetilde{f}(v,t)|, \ \forall t \in [0,T],$$

and

$$|\widetilde{f}(v,t)| \leq \max_{\tau\in[0,t]} |\widetilde{f}(v,\tau)| = \|\widetilde{f}(v,t)\|_\infty,$$

implies

$$|\widetilde{E}_0(v,t)| \leq \|\widetilde{f}(v,t)\|_\infty,$$

for $k = 1$**:**

$$\begin{aligned} |\widetilde{E}_1(v,t)| &= \left|\int_0^t K(v,t-\tau)\widetilde{f}(v,\tau)d\tau\right|, \\ &\leq \int_0^t |K(v,t-\tau)||\widetilde{f}(v,\tau)|d\tau, \\ &\leq Mt \max_{\tau\in[0,t]} |\widetilde{f}(v,\tau)| \leq Mt\|\widetilde{f}(v,t)\|_\infty, \end{aligned} \tag{5.12}$$

implies

$$|\widetilde{E}_1(v,t)| \le Mt\|\widetilde{f}(v,t)\|_\infty,$$

for $k = 2$**:**

$$\begin{aligned} |\widetilde{E}_2(v,t)| &= \left|\int_0^t K(v,t-\tau)\widetilde{E}_1(v,\tau)d\tau\right|, \\ &\le M\int_0^t M\tau\|\widetilde{f}(v,\tau)\|_\infty d\tau, \\ &\le \frac{(Mt)^2}{2!}\|\widetilde{f}(v,t)\|_\infty, \end{aligned} \tag{5.13}$$

implies

$$|\widetilde{E}_2(v,t)| \le \frac{(Mt)^2}{2!}\|\widetilde{f}(v,t)\|_\infty,$$

induction completes proof. □

Lemma 5.1.6. *Under above mentioned assumptions,* $v \in \mathbb{R}^3$ *and* $T > 0$ *be fixed,* $\sum_{k=0}^{p}\widetilde{E}_k(v,t)$ *converges uniformly over* $[0,T]$ *to a continuous function* $\widetilde{E}(v,t) \in C[0,T]$ *as* $p \to \infty$.

Proof. Since

$$\begin{aligned} \widetilde{E}_0(v,t) &= \widetilde{f}(v,t) \in C[0,T], \\ \widetilde{E}_1(v,t) &= \int_0^t K(v,t-\tau)\widetilde{E}_0(v,\tau)d\tau \in C[0,T], \end{aligned}$$

then

$$\widetilde{E}_k(v,t) = \int_0^t K(v,t-\tau)\widetilde{E}_{k-1}(v,\tau)d\tau \in C[0,T],$$

and from lemma 5.1.5 we have

$$|\widetilde{E}_k(v,t)| \le \frac{(Mt)^k}{k!}\|\widetilde{f}(v,t)\|_\infty \le \frac{(MT)^k}{k!}\|\widetilde{f}(v,t)\|_\infty,\ \forall t \in [0,T],$$

The expression $\sum_{k=0}^{p}\frac{(Mt)^k}{k!}\|\widetilde{f}(v,t)\|_\infty$ converges uniformly to $e^{MT}\|\widetilde{f}(v,t)\|_\infty$.

From 1^{st} Weierstrass theorem, we have $\sum_{k=0}^{p} \widetilde{E}_k(\nu,t)$ converges uniformly to $\widetilde{E}(\nu,t)$.

□

Lemma 5.1.7. *Under above mentioned assumptions $\widetilde{E}(\nu,t) \in C[0,T]$ is a solution of the integral equation (5.8), satisfying $|\widetilde{E}(\nu,t)| \leq N$ for $\forall t \in [0,T]$, where $N = e^{MT}\frac{4\pi}{\lambda_{min}}$.*

Proof. Taking limit as $p \to \infty$ to (5.11), we have

$$\sum_{k=0}^{\infty} \widetilde{E}_k(\nu,t) = \lim_{p\to\infty} \int_0^t \sum_{k=0}^{p} \widetilde{E}_k(\nu,t) = \lim_{p\to\infty} \int_0^t \sum_{k=0}^{p-1} K(\nu,t-\tau)\widetilde{E}_k(\nu,t) + \widetilde{f}(\nu,t).$$

From 2^{nd} Weierstrass theorem (changing order of limit and integral), we get

$$\widetilde{E}(\nu,t) = \int_0^t \lim_{p\to\infty} \sum_{k=0}^{p-1} K(\nu,t-\tau)\widetilde{E}_k(\nu,t) + \widetilde{f}(\nu,t), \tag{5.14}$$

and lemma 5.1.6 implies

$$\lim_{p\to\infty} \sum_{k=0}^{p-1} K(\nu,t-\tau)\widetilde{E}_k(\nu,t) = K(\nu,t-\tau)\widetilde{E}(\nu,t), \tag{5.15}$$

implies

$$\widetilde{E}(\nu,t) = \int_0^t K(\nu,t-\tau)\widetilde{E}(\nu,\tau)d\tau + \widetilde{f}^m(\nu,t),$$

hence $\widetilde{E}(\nu,t)$ is the solution of (5.8). From lemma 5.1.6 and $\|\widetilde{f}(\nu,t)\| \leq \frac{4\pi}{\lambda_{min}}$ we have $|\widetilde{E}(\nu,t)| \leq N$ where $N = e^{MT}\frac{4\pi}{\lambda_{min}}$ □

Lemma 5.1.8. *Under above mentioned assumptions the solution $\widetilde{E}(\nu,t)$ of the integral equation (5.8) is unique.*

Proof. Let $\widetilde{E}_1(\nu,t)$ and $\widetilde{E}_2(\nu,t)$ be solutions of (5.8) , then we have

$$\begin{aligned} \widetilde{E}_1(\nu,t) &= \int_0^t K(\nu,t-\tau)\widetilde{E}_1(\nu,\tau)d\tau + \widetilde{f}^m(\nu,t), \\ \widetilde{E}_2(\nu,t) &= \int_0^t K(\nu,t-\tau)\widetilde{E}_2(\nu,\tau)d\tau + \widetilde{f}^m(\nu,t), \end{aligned}$$

substraction gives

$$\widetilde{E}_1(\nu,t) - \widetilde{E}_2(\nu,t) = \int_0^t K(\nu,t-\tau)(\widetilde{E}_1(\nu,\tau) - \widetilde{E}_2(\nu,\tau))d\tau,$$

Denoting $\varphi(\nu,t) = \widetilde{E}_1(\nu,t) - \widetilde{E}_2(\nu,t)$, the last equation can be written as

$$\varphi(\nu,t) = \int_0^t K(\nu,t-\tau)\varphi(\nu,\tau)d\tau\,,$$

Taking module gives

$$\begin{aligned} |\varphi(\nu,t)| &= \left|\int_0^t K(\nu,t-\tau)\varphi(\nu,\tau)d\tau\right|, \\ &\leq \int_0^t |K(\nu,t-\tau)\varphi(\nu,\tau)|d\tau \leq M\int_0^t |\varphi(\nu,\tau)|d\tau\,. \end{aligned}$$

Taking maximum implies

$$\begin{aligned} ||\varphi(\nu,t)||_\infty &\leq M\int_0^t ||\varphi(\nu,\tau)||_\infty d\tau\,, \\ \frac{d}{dt}||\varphi(\nu,t)||_\infty &\leq M||\varphi(\nu,t)||_\infty\,, \\ e^{Mt}\frac{d}{dt}||\varphi(\nu,t)||_\infty &\leq e^{Mt}M||\varphi(\nu,t)||_\infty\,, \\ \frac{d}{dt}\left[e^{Mt}||\varphi(\nu,t)||_\infty\right] &\leq 0\,, \end{aligned}$$

which implies that $e^{Mt}||\varphi(\nu,t)||_\infty \leq 0$. Since $e^{Mt} \geq 0$ we have $||\varphi(\nu,t)||_\infty = 0$ which proves uniqueness of the problem. □

Theorem 5.1.9. *Under above mentioned assumptions, the solution of the integral equation (5.8) has the solution of the Neumann series form*

$$\widetilde{E}(\nu,t) = \sum_{k=0}^{\infty} K^k(\nu,t)\widetilde{f}(\nu,t)\,. \tag{5.16}$$

After finding our solution as in the form of Neumann series, we should prove that the inverse Fourier transform exists for generalized functions space $\mathcal{S}'$. Let us consider the following theorem:

Theorem 5.1.10. *(L. Schwartz, p115, Vladimirov, 1971) In order that the linear functional f over $\mathcal{S}$ should belong to $\mathcal{S}'$, (that is, be continuous over $\mathcal{S}$), it is necessary and sufficient that there be numbers $C > 0$ and $p \geq 0$, p being an integer, such that for any $\varphi \in \mathcal{S}$ the inequality*

$$|(f,\varphi)| \leq C\,||\varphi||_p\,,$$

is valid, where

$$\|\varphi\|_p = \sup_{|\alpha|\leq p,\, x\in\mathbb{R}^n} (1+|x|)^p \, |D^\alpha \varphi(x)| \, .$$

From theorem, we have

$$|(\widetilde{E},\varphi)| = |\int_{\mathbb{R}^3} \widetilde{E}(\nu,t)\,\varphi(\nu) d\nu| \leq N \int_{\mathbb{R}^3} |\varphi(\nu)| d\nu \, ,$$

and we can find a restriction for p in $\mathbb{R}^3$ such that

$$|\varphi(\nu)| \leq \frac{1}{(1+|\nu|)^p} \leq \frac{1}{|\nu|^p} = \frac{1}{|r|^p} r^2 \sin(\theta) dr d\theta d\phi = \frac{1}{|r|^{p-2}} \, ,$$

implies

$$\int_1^\infty \frac{1}{|r|^{p-2}} dr = \left. \frac{r^{-p+3}}{-3+p} \right|_1^\infty ,$$

converges for $p > 3$.

Then for $p = 4$, we have

$$\begin{aligned} |\varphi(\nu)| &= \frac{1}{(1+|\nu|)^4} (1+|\nu|)^4 |\varphi(\nu)| \\ &\leq \frac{1}{(1+|\nu|)^4} \sup_{\nu\in\mathbb{R}^n} (1+|\nu|)^4 \, |\varphi(\nu)| \\ &\leq \frac{1}{(1+|\nu|)^4} \sup_{|\alpha|\leq 4, \nu\in\mathbb{R}^n} (1+|\nu|)^4 \, |D^\alpha \varphi(\nu)| \\ &= \frac{1}{(1+|\nu|)^4} \|\varphi(\nu)\|_4 \, , \end{aligned}$$

then the functional $(\widetilde{E},\varphi)$ have

$$|(\widetilde{E},\varphi)| \leq N \, \|\varphi(\nu)\|_4 \int_{\mathbb{R}^3} \frac{1}{(1+|\nu|)^4} d\nu \, ,$$

and we get C as

$$C = N \int_{\mathbb{R}^3} \frac{1}{(1+|\nu|)^4} d\nu \, . \tag{5.17}$$

This means that, $\exists C > 0$, $\exists p \geq 0$ such that

$$|(\widetilde{E},\varphi)| \leq C \|\varphi(\nu)\|_p \text{ for } p = 4 \, ,$$

where C is given in equation (5.17).

From (Vladimirov, 1971), page 125, the Fourier transform $\mathcal{F}$ and $\mathcal{F}^{-1}$ map $\mathcal{S}'(\mathbb{R}^3)$ onto $\mathcal{S}'(\mathbb{R}^3)$ mutually one-to-one. Finally, we can find the solution by applying inverse Fourier transformation to equation (5.16) as in the form

$$E(x,t) = \mathcal{F}_\nu^{-1}[\widetilde{E}(\nu,t)](x,t) = \frac{1}{(2\pi)^3}\int_{-\infty}^{\infty}\int_{-\infty}^{\infty}\int_{-\infty}^{\infty}\widetilde{E}(\nu,t)\,e^{-i\nu\cdot x}\,d\nu_1 d\nu_2 d\nu_3\,, \quad (5.18)$$

where $E(x,t) = (E^1(x,t), E^2(x,t), E^3(x,t))$.

5.2 Computational Experiments

In this section, in the first part, we obtained an explicit formula for isotropic materials to check the robustness of our method because of the difficulties to obtain explicit formula for anisotropic materials, it is not possible to compare for anisotropic materials. This comparison is done for Fourier images of electric field vectors and the obtained tables proves the robustness of our method for suitable parameters. The second part of this section is related with the determining parameters for the approximate computation of inverse Fourier transformation. For the best approximation we fixed our parameters and for these fixed parameters we simulated our results for monoclinic and triclinic anisotropic conductive materials.

5.2.1 Explicit Formulae of the Problem for Isotropic Conductive Media

In this section we will obtain an explicit formula for isotropic materials with conductivity, let us assume that $\mathscr{E} = (\mathscr{E}_{ij})_{3\times 3}$ and $\mathscr{M} = (\mathscr{M}_{ij})_{3\times 3}$ are symmetric positive definite matrices with constant elements. Moreover we suppose that

$$\mathscr{E} = \varepsilon I, \quad \mathscr{M} = \mu I, \quad \sigma = \sigma I$$

where and ε, μ and σ are scalars and for $t \le 0$

$$E(x,t) = 0\,, \quad H(x,t) = 0\,, \quad \rho = 0\,, \quad j(x,t) = 0\,. \quad (5.19)$$

After substitutions, we get the following system

$$
\begin{aligned}
curl_x H^m(x,t) &= \frac{1}{c}\varepsilon\frac{\partial E^m}{\partial t}(x,t) + \frac{4\pi}{c}\sigma E^m(x,t) + \frac{4\pi}{c} j^m(x,t), &(5.20)\\
curl_x E^m(x,t) &= -\frac{1}{c}\mu\frac{\partial H^m}{\partial t}(x,t), &(5.21)\\
div_x(\varepsilon E^m(x,t)) &= \rho, &(5.22)\\
div_x(\mu H^m(x,t)) &= 0, &(5.23)
\end{aligned}
$$

Differentiating (5.20) with respect to t and using (5.21), we get the following initial value problems

Problem 1:

$$\varepsilon\mu\frac{\partial^2 E^m}{\partial t^2}(x,t) + c^2 curl_x curl_x E^m(x,t) = -4\pi\mu\sigma\frac{\partial E^m}{\partial t}(x,t) - 4\pi\mu\frac{\partial j^m}{\partial t}(x,t), \quad (5.24)$$

$$E^m(x,t)|_{t\leq 0} = 0. \quad (5.25)$$

Therefore for the solution of the main problem first of all we have to find $E^m(x,t)$ satisfying (5.24) and (5.25) and after that we can find $H^m(x,t)$ satisfying (5.21) in the following form

Problem 2:

$$\frac{\partial H^m}{\partial t}(x,t) = -c\mu^{-1} curl_x E^m(x,t), \quad (5.26)$$

$$H^m(x,t)|_{t\leq 0} = 0, \quad (5.27)$$

if $E(x,t)$ is given.

In this chapter, we find a solution of problem 1.

5.2.1.1 *Solution of the System (5.24)-(5.25):*

Applying Fourier transform to (5.24) with respect to $x = (x_1, x_2, x_3) \in \mathbb{R}^3$ we have the following system

$$
\begin{aligned}
\varepsilon\mu\frac{\partial^2 \widetilde{E}^m}{\partial t^2}(\nu,t) + c^2 A(\nu)\widetilde{E}^m(\nu,t) &= -4\pi\mu\sigma\frac{\partial \widetilde{E}^m}{\partial t}(\nu,t) - 4\pi\mu\frac{\partial \widetilde{j}^m}{\partial t}(\nu,t), &(5.28)\\
\widetilde{E}^m(\nu,t)|_{t\leq 0} = 0 \quad &, \quad \frac{\partial \widetilde{E}^m}{\partial t}(\nu,t)|_{t\leq 0} = 0, &(5.29)
\end{aligned}
$$

where

$$A(\nu)\widetilde{E^m}(\nu,t) = \mathcal{F}_x[curl_x curl_x E^m(x,t)](\nu,t)\,.$$

where $A(\nu)$ is given in equation (3.4).

Dividing (5.28) by $\varepsilon\mu$, we have

$$\begin{aligned} \frac{\partial^2 \widetilde{E^m}}{\partial t^2}(\nu,t) + \frac{c^2}{\varepsilon\mu}A(\nu)\widetilde{E^m}(\nu,t) &= -4\pi\frac{\sigma}{\varepsilon}\frac{\partial \widetilde{E^m}}{\partial t}(\nu,t) - 4\pi\frac{1}{\varepsilon}\frac{\partial \widetilde{j^m}}{\partial t}(\nu,t)\,, \qquad (5.30)\\ \widetilde{E^m}(\nu,t)|_{t\le 0} = 0 \quad &, \qquad \frac{\partial \widetilde{E^m}}{\partial t}(\nu,t)|_{t\le 0} = 0\,. \qquad (5.31) \end{aligned}$$

For finding the solution of the system (5.30)-(5.31), we have three cases

Case 1 $\nu_1 = \nu_2 = \nu_3 \neq 0$

Case 2 $\nu_1 = \nu_3 = 0, \nu_2 \neq 0$

Case 3 $\nu_1 = \nu_2 = \nu_3 = 0$

CASE 1: Solution for $\nu_1 = \nu_2 = \nu_3 \neq 0$ **:**

Setting $\widetilde{E^m}(\nu,t) = T(\nu)\,Y^m(\nu,t)$, substitution gives

$$T(\nu)\frac{\partial^2 Y^m}{\partial t^2}(\nu,t) + \frac{c^2}{\varepsilon\mu}A(\nu)T(\nu)Y^m(\nu,t) = -\frac{4\pi\sigma}{\varepsilon}T(\nu)\frac{\partial Y^m}{\partial t}(\nu,t) - \frac{4\pi}{\varepsilon}\frac{\partial \widetilde{j^m}}{\partial t}(\nu,t)\,, \quad (5.32)$$

after multiplying (5.2.1.1) and using the following identities

$$\begin{aligned} T^{-1}(\nu)T(\nu) &= I\,,\\ T^{-1}(\nu)A(\nu)T(\nu) &= D(\nu) = \mathrm{diag}(d_m(\nu)\,, m = 1,2,3)\,, \end{aligned}$$

where the matrix $T(\nu)$ has the following form:

$$T(\nu) = \begin{pmatrix} \frac{\nu_1}{|\nu|} & \frac{-\nu_3}{\sqrt{\nu_1^2+\nu_3^2}} & \frac{-\nu_1\nu_2}{|\nu|\sqrt{\nu_1^2+\nu_3^2}} \\ \frac{\nu_2}{|\nu|} & 0 & \frac{\sqrt{\nu_1^2+\nu_3^2}}{|\nu|} \\ \frac{\nu_3}{|\nu|} & \frac{\nu_1}{\sqrt{\nu_1^2+\nu_3^2}} & \frac{-\nu_2\nu_3}{|\nu|\sqrt{\nu_1^2+\nu_3^2}} \end{pmatrix}, \quad |\nu| = \sqrt{\nu_1^2+\nu_2^2+\nu_3^2}\,,$$

then we get the following system

$$\begin{aligned}\frac{\partial^2 Y^m}{\partial t^2}(\nu,t)+\frac{4\pi\sigma}{\varepsilon}\frac{\partial Y^m}{\partial t}(\nu,t)+\frac{c^2 d_m}{\varepsilon\mu}Y^m(\nu,t) &= -\frac{4\pi}{\varepsilon}[T^{-1}(\nu)\vec{e}]^m\delta'(t), &(5.33)\\ Y^m(\nu,t)|_{t\le 0} &= 0, \quad \frac{\partial Y^m}{\partial t}(\nu,t)|_{t\le 0}=0. &(5.34)\end{aligned}$$

Solution of (5.33)-(5.34):

Let $Y^m(\nu,t)=\Theta(t)Z^m(\nu,t)$ be the solution of the following initial value problem

$$\begin{aligned}\frac{\partial^2 Y^m}{\partial t^2}(\nu,t)+\frac{4\pi\sigma}{\varepsilon}\frac{\partial Y^m}{\partial t}(\nu,t)+\frac{c^2 d_m}{\varepsilon\mu}Y^m(\nu,t) &= -\frac{4\pi}{\varepsilon}T^{-1}_{m1}(\nu)\delta(t), &(5.35)\\ Y^m(\nu,t)|_{t<0}&=0, &(5.36)\end{aligned}$$

for $m=1,2,3$, where $Z^m(\nu,t)$ is the solution of the following problem

$$\frac{d^2 Z^m}{dt^2}(\nu,t)+\frac{4\pi\sigma}{\varepsilon}\frac{dZ^m}{dt}(\nu,t)+\frac{c^2 d_m}{\varepsilon\mu}Z^m(\nu,t)=0, \tag{5.37}$$

$$Z^m(\nu,t)|_{t=0}=0, \quad \frac{dZ^m}{dt}(\nu,t)|_{t=0}=-\frac{4\pi}{\varepsilon}T^{-1}_{m1}. \tag{5.38}$$

Solution of (5.37)-(5.38): Since $d_1=0,\ d_2=d_3=|\nu|^2=(\nu_1^2+\nu_2^2+\nu_3^2)$ then the discriminant of the equation (5.37) has the form

$$\Delta(\nu)=(\frac{4\pi\sigma}{\varepsilon})^2-4\frac{c^2|\nu|^2}{(\sqrt{\varepsilon\mu})^2},$$

by setting

$$\frac{4\pi\sigma}{\varepsilon}=2c\frac{2\pi\sigma}{\varepsilon c}=2c\xi,$$

where $\xi=\frac{2\pi\sigma}{\varepsilon c}$, and setting $\omega=\frac{1}{\sqrt{\varepsilon\mu}}$ we have (5.37) as in the following form:

$$\frac{d^2 Z^m}{dt^2}(\nu,t)+2c\xi\frac{dZ^m}{dt}(\nu,t)+c^2\omega^2|\nu|^2 Z^m(\nu,t)=0, \tag{5.39}$$

and

$$\Delta(\nu)=4c^2\xi^2-4c^2\omega^2|\nu|^2,$$

and the roots of (5.39) are

$$m_{1,2}(\nu)=\frac{-2c\xi\mp\sqrt{4c^2\xi^2-4c^2\omega^2|\nu|^2}}{2},$$

or equivalently

$$m_{1,2}(\nu) = c\,(-\xi \mp \sqrt{\xi^2 - \omega^2|\nu|^2})\,. \tag{5.40}$$

Now we have three cases and since $d_1 = 0$, we can find a special solution for $k = 1$ as following

For $m = 1$**,** $d_1(\nu) = 0$**:** The solution has the form

$$Z^1(\nu,t) = \frac{-[T^{-1}(\nu)]_{11}}{\sigma}[1 - e^{-\frac{4\pi\sigma}{\varepsilon}t}]\,.$$

And since $Y^m(\nu,t) = \Theta(t)Z^m(\nu,t)$, we have

$$S^1(\nu,t) = -\Theta(t)\frac{[T^{-1}(\nu)]_{11}}{\sigma}[1 - e^{-\frac{4\pi\sigma}{\varepsilon}t}]\,.$$

and then, we can find $Y^1(\nu,t)$ by using

$$Y^m(\nu,t) = \frac{d}{dt}(Y^m(\nu,t-\tau) * \delta(\tau))\,. \tag{5.41}$$

we get

$$Y^1(\nu,t) = -\frac{4\pi}{\varepsilon}[T^{-1}(\nu)]_{11}e^{-\frac{4\pi\sigma}{\varepsilon}t}\,. \tag{5.42}$$

For $m = 2,3,\ d_2(\nu) = d_3(\nu) = |\nu|^2$:

If $\Delta(\nu) = 0 \ \Rightarrow\ m = m_1 = m_2 = -c\xi$ then the solution has the form

$$Z^m(\nu,t) = -\frac{4\pi}{\varepsilon}[T^{-1}(\nu)]_{m1}te^{-c\xi t}\,,$$

and using (5.41) we have

$$Y^m(\nu,t) = -\frac{4\pi}{\varepsilon}[T^{-1}(\nu)]_{m1}e^{-c\xi t}[1 - c\xi t]\,. \tag{5.43}$$

If $\Delta(\nu) < 0$ setting $\beta(\nu) = \omega^2|\nu|^2 - \xi^2$ we have the solution in the following form

$$Z^m(\nu,t) = e^{-c\xi t}\left(-\frac{4\pi}{\varepsilon}\frac{1}{c\beta(\nu)}T^{-1}_{m1}(\nu)\right)\sin(c\beta(\nu)t)\,,$$

and using (5.41) we have

$$Y^m(\nu,t) = (-\frac{4\pi}{\varepsilon})\frac{1}{\beta(\nu)}[T^{-1}(\nu)]_{m1}e^{-c\xi t}[-\xi\sin(c\beta(\nu)t)+\beta(\nu)\cos(c\beta(\nu)t)]. \qquad (5.44)$$

If $\Delta(\nu) > 0$ since

$$\begin{aligned} m_1(\nu) &= -c\xi + c\sqrt{\xi^2-\omega^2|\nu|^2}, \\ m_2(\nu) &= -c\xi - c\sqrt{\xi^2-\omega^2|\nu|^2}, \end{aligned}$$

we have the solution in the following form

$$Z^m(\nu,t) = -\frac{4\pi}{\varepsilon}[T^{-1}(\nu)]_{m1}\frac{1}{m_{12}(\nu)}(e^{m_1(\nu)t}-e^{m_2(\nu)t}),$$

where $m_{12}(\nu) = m_1(\nu)-m_2(\nu) = 2c\sqrt{\xi^2-\omega^2|\nu|^2}$and using (5.41) we have

$$Y^m(\nu,t) = (-\frac{4\pi}{\varepsilon})[T^{-1}(\nu)]_{m1}\frac{1}{m_{12}(\nu)}(m_1(\nu)e^{m_1(\nu)t}-m_2(\nu)e^{m_2(\nu)t}). \qquad (5.45)$$

CASE 2: Solution for $\nu_1 = \nu_3 = 0,\ \nu_2 \neq 0$ **:** By our assumption we have $A(\nu)$ matrix as in the following form:

$$A(\nu) = \begin{pmatrix} \nu_2^2 & 0 & 0 \\ 0 & 0 & 0 \\ 0 & 0 & \nu_2^2 \end{pmatrix}. \qquad (5.46)$$

After substitution of (5.46) into (5.30), we get the following system

$$\begin{aligned} \frac{\partial^2\widetilde{E}^m}{\partial t^2}(\nu,t)+\frac{4\pi\sigma}{\varepsilon}\frac{\partial\widetilde{E}^m}{\partial t}(\nu,t)+\frac{c^2d_m}{\varepsilon\mu}\widetilde{E}^m(\nu,t) &= -\frac{4\pi}{\varepsilon}\vec{e}^m\delta'(t), && (5.47) \\ \widetilde{E}^m(\nu,t)|_{t\le 0} &= 0, \quad \frac{\partial\widetilde{E}^m}{\partial t}(\nu,t)|_{t\le 0} = 0, && (5.48) \end{aligned}$$

where $d_m(\nu) = diag(\nu_2^2, 0, \nu_2^2)$.

Solution of (5.47)-(5.48): Let $Y^m(\nu,t) = \Theta(t)Z^m(\nu,t)$ be the solution of the following initial value problem

$$\begin{aligned} \frac{\partial^2 Y^m}{\partial t^2}(\nu,t)+\frac{4\pi\sigma}{\varepsilon}\frac{\partial Y^m}{\partial t}(\nu,t)+\frac{c^2d_m}{\varepsilon\mu}Y^m(\nu,t) &= -\frac{4\pi}{\varepsilon}\vec{e}^m\delta(t), && (5.49) \\ Y^m(\nu,t)|_{t<0} &= 0, && (5.50) \end{aligned}$$

for $m = 1,2,3$, where $Z^m(\nu,t)$ is the solution of the following problem

$$\frac{d^2Z^m}{dt^2}(\nu,t) + \frac{4\pi\sigma}{\varepsilon}\frac{dZ^m}{dt}(\nu,t) + \frac{c^2 d_m}{\varepsilon\mu} Z^m(\nu,t) = 0\,, \tag{5.51}$$

$$Z^m(\nu,t)|_{t=0} = 0\,, \quad \frac{dZ^m}{dt}(\nu,t)|_{t=0} = -\frac{4\pi}{\varepsilon}\vec{e}^m\,. \tag{5.52}$$

Solution of (5.51)-(5.52): Since $d_2(\nu) = 0$, $d_1(\nu) = d_3(\nu) = \nu_2^2$ and the discriminant of the equation (5.51) has the form

$$\Delta(\nu) = (\frac{4\pi\sigma}{\varepsilon})^2 - 4\frac{c^2\nu_2^2}{(\sqrt{\varepsilon\mu})^2}\,,$$

by setting

$$\frac{4\pi\sigma}{\varepsilon} = 2c\frac{2\pi\sigma}{\varepsilon c} = 2c\xi\,,$$

where $\xi = \frac{2\pi\sigma}{\varepsilon c}$, and setting $\omega = \frac{1}{\sqrt{\varepsilon\mu}}$ we have (5.51) as in the following form:

$$\frac{d^2Z^m}{dt^2}(\nu,t) + 2c\xi\frac{dZ^m}{dt}(\nu,t) + c^2\omega^2\nu_2^2 Z^m(\nu,t) = 0\,, \tag{5.53}$$

and

$$\Delta(\nu) = 4c^2\xi^2 - 4c^2\omega^2\nu_2^2\,,$$

and the roots of (5.53) are

$$m_{12}(\nu) = \frac{-2c\xi \mp \sqrt{4c^2\xi^2 - 4c^2\omega^2\nu_2^2}}{2}\,,$$

or equivalently

$$m_{12}(\nu) = c\,(-\xi \mp \sqrt{\xi^2 - \omega^2\nu_2^2})\,. \tag{5.54}$$

Now we have three cases and since $d_2(\nu) = 0$, we can find a special solution for $k = 2$ as following

For $m = 2$, $d_2(\nu) = 0$**:** The solution has the form

$$Z^1(\nu,t) = \frac{-1}{\sigma}[1 - e^{-\frac{4\pi\sigma}{\varepsilon}t}]\,.$$

And since $Y^m(\nu,t) = \Theta(t)Z^m(\nu,t)$, we have

$$S^1(\nu,t) = -\Theta(t)\frac{1}{\sigma}[1 - e^{-\frac{4\pi\sigma}{\varepsilon}t}].$$

and then, we can find $\widetilde{E}^2(\nu,t)$ by using (5.41), we get

$$\widetilde{E}^2(\nu,t) = -\frac{4\pi}{\varepsilon}e^{-\frac{4\pi\sigma}{\varepsilon}t}. \tag{5.55}$$

For $m = 1,3,\ d_1 = d_3 = \nu_2^2$**:**

If $\Delta(\nu) = 0 \ \Rightarrow\ m = m_1 = m_2 = -c\xi$ then the solution has the form

$$\widetilde{E}^m(\nu,t) = -\frac{4\pi}{\varepsilon}e^{-c\xi t}[1 - c\xi t]. \tag{5.56}$$

If $\Delta(\nu) < 0$ setting $\beta(\nu) = \omega^2\nu_2^2 - \xi^2$ we have the solution in the following form

$$\widetilde{E}^m(\nu,t) = (-\frac{4\pi}{\varepsilon})\frac{1}{\beta(\nu)}e^{-c\xi t}[-\xi\sin(c\beta(\nu)t) + \beta(\nu)\cos(c\beta(\nu)t)]. \tag{5.57}$$

If $\Delta(\nu) > 0$ since

$$\begin{aligned} m_1(\nu) &= -c\xi + c\sqrt{\xi^2 - \omega^2\nu_2^2}, \\ m_2(\nu) &= -c\xi - c\sqrt{\xi^2 - \omega^2\nu_2^2}, \end{aligned}$$

we have the solution in the following form

$$\widetilde{E}^m(\nu,t) = (-\frac{4\pi}{\varepsilon})\frac{1}{m_{12}(\nu)}(m_1(\nu)e^{m_1(\nu)t} - m_2(\nu)e^{m_2(\nu)t}). \tag{5.58}$$

CASE 3: Solution for $\nu_1 = \nu_2 = \nu_3 = 0$ **:** In this case our matrix $A(\nu)$ is a zero matrix and we get the following system

$$\frac{\partial^2\widetilde{E}^m}{\partial t^2}(\nu,t) + \frac{4\pi\sigma}{\varepsilon}\frac{\partial\widetilde{E}^m}{\partial t}(\nu,t) = -\frac{4\pi}{\varepsilon}\vec{e}^m\delta'(t), \tag{5.59}$$

$$\widetilde{E}^m(\nu,t)|_{t\le 0} = 0, \quad \frac{\partial\widetilde{E}^m}{\partial t}(\nu,t)|_{t\le 0} = 0. \tag{5.60}$$

Solution of (5.59)-(5.60): Let $Y^m(\nu,t) = \Theta(t)Z^m(\nu,t)$ be the solution of the following initial value problem

$$\frac{\partial^2 Y^m}{\partial t^2}(\nu,t) + \frac{4\pi\sigma}{\varepsilon}\frac{\partial Y^m}{\partial t}(\nu,t) = -\frac{4\pi}{\varepsilon}\vec{e}^m\delta(t), \tag{5.61}$$

$$Y^m(\nu,t)|_{t<0} = 0, \tag{5.62}$$

for $m = 1,2,3$, where $Z^m(\nu,t)$ is the solution of the following problem

$$\frac{d^2Z^m}{dt^2}(\nu,t) + \frac{4\pi\sigma}{\varepsilon}\frac{dZ^m}{dt}(\nu,t) = 0\,, \tag{5.63}$$

$$Z^m(\nu,t)|_{t=0} = 0\,, \qquad \frac{dZ^m}{dt}(\nu,t)|_{t=0} = -\frac{4\pi}{\varepsilon}\vec{e}^m\,. \tag{5.64}$$

Solution of (5.63)-(5.64): The solution has the form for $m = 1,2,3$,

$$Z^m(\nu,t) = \frac{-1}{\sigma}[1 - e^{-\frac{4\pi\sigma}{\varepsilon}t}].$$

And since $Y^m(\nu,t) = \Theta(t)Z^m(\nu,t)$, we have

$$Y^m(\nu,t) = -\Theta(t)\frac{1}{\sigma}[1 - e^{-\frac{4\pi\sigma}{\varepsilon}t}].$$

and then, we can find $\widetilde{E}^m(\nu,t)$ by using (5.41), we get

$$\widetilde{E}^m(\nu,t) = -\frac{4\pi}{\varepsilon}e^{-\frac{4\pi\sigma}{\varepsilon}t}. \tag{5.65}$$

And since $\widetilde{E}^m(\nu,t) = T(\nu)\,Y^m(\nu,t)$ we can construct $\widetilde{E}^m(\nu,t)$ and after finding $\widetilde{E}^m(\nu,t)$, by using the inverse Fourier transformation we can construct the general solution as in the following form

$$E^m(x,t) = \frac{1}{(2\pi)^3}\int_{-\infty}^{\infty}\int_{-\infty}^{\infty}\int_{-\infty}^{\infty}\widetilde{E}^m(\nu,t)e^{ix\cdot\nu}d\nu_1 d\nu_2 d\nu_3$$

where $\nu = (\nu_1,\nu_2,\nu_3)$, $\nu\cdot x = \nu_1x_1 + \nu_2x_2 + \nu_3x_3$, $i^2 = -1$.

5.2.1.2 *Comparison of the Values of $\widetilde{E}(x,t)$ for the Isotropic Conductive Materials*

In this subsection we check the robustness of the method by using the exact solution before applying inverse transform method and we find a limit of convergency by changing the σ values. Let us assume t, $\mathcal{E}$, $\mathcal{M}$ and σ are fixed values which has the following forms

$$\mathcal{E} = \begin{pmatrix} 9.4 & 0 & 0 \\ 0 & 9.4 & 0 \\ 0 & 0 & 9.4 \end{pmatrix}, \mathcal{M} = \begin{pmatrix} 1 & 0 & 0 \\ 0 & 1 & 0 \\ 0 & 0 & 1 \end{pmatrix}, \sigma = \sigma_0\begin{pmatrix} 1 & 0 & 0 \\ 0 & 1 & 0 \\ 0 & 0 & 1 \end{pmatrix}.$$

for fixed direction $\vec{\mathbf{e}} = (1,0,0)$, where $\sigma_0 = 0, 1, 10$.

Let us denote r as a parameter which satisfies:

$$\begin{aligned} v_1 &= r\cos(\phi)\sin(\theta), \\ v_2 &= r\sin(\phi)\sin(\theta), \\ v_3 &= r\cos(\theta), \end{aligned}$$

fixing $\phi = \pi/4$ and $\theta = \pi/4$ we obtain

$$v_1 = v_2 = r/2,\ v_3 = r\sqrt{2}/2.$$

For fixed element of electric field vector $\widetilde{\mathbf{E}}^1$, let us denote $\widetilde{\mathbf{E}}^{1(m)}$ as solution obtained from our method and $\widetilde{\mathbf{E}}^{1(e)}$ as exact solution of isotropic Maxwell's equations, for different σ_0 values, we created Table 5.1-Table 5.3 :

We can see that the Fourier images of exact solution $\widetilde{\mathbf{E}}^{1(e)}$ and solution obtained from our method $\widetilde{\mathbf{E}}^{1(m)}$ has closeness which depends on conductivity σ. Here we assumed that $\mathcal{E} = 9.4I$ where I is the identity matrix and it must be dominant to conductivity σ. Because of that reason, for better approximation, we have to choose our σ matrix smaller than $\mathcal{E}$ to protect the convergence. This idea will be applied in this chapter for computational experiments.

5.2.2 Determining Parameters for the Approximate Computation of Inverse Fourier Transform

In this section, we will explain our method for approximate computation of inverse Fourier transformation. Let us consider the following wave equation:

$$\frac{\partial^2}{\partial t^2}u(x,t) - a^2\Delta u(x,t) = \delta(x)\delta(t), \tag{5.66}$$

$$u(x,t)\big|_{t<0} = 0, \tag{5.67}$$

where $x = (x_1, x_2, x_3)$ is the space variable, t is the time. Using generalized functions theory and Green's functions, applying Fourier transform we have the following

Table 5.1 The comparison of $\widetilde{\mathbf{E}}^{1(m)}$ and $\widetilde{\mathbf{E}}^{1(e)}$ for $\sigma_0 = 0$.

r	$\widetilde{E}_1^{1(m)}$	$\lvert\widetilde{E}_1^{1(m)} - \widetilde{E}_1^{1(e)}\rvert$	$\widetilde{E}_2^{1(m)}$	$\lvert\widetilde{E}_2^{1(m)} - \widetilde{E}_2^{1(e)}\rvert$	$\widetilde{E}_3^{1(m)}$	$\lvert\widetilde{E}_3^{1(m)} - \widetilde{E}_3^{1(e)}\rvert$
10^{-6}	-1.3369	0	$-7.1276x10^{-14}$	$0.5551x10^{-16}$	$-1.0064x10^{-13}$	$0.5551x10^{-16}$
10^{-5}	-1.3369	$0.2220x10^{-15}$	$-7.1110x10^{-12}$	$0.1110x10^{-15}$	$-1.0056x10^{-11}$	0
10^{-4}	-1.3369	$0.2220x10^{-15}$	$-7.1109x10^{-12}$	0	$-1.0056x10^{-9}$	$0.1665x10^{-15}$
10^{-3}	-1.3369	$0.2220x10^{-15}$	$-7.1109x10^{-8}$	0	$-1.0056x10^{-7}$	$0.5551x10^{-14}$
10^{-2}	-1.3368	0	$-7.1108x10^{-6}$	0	$-1.0056x10^{-5}$	0
10^{-1}	-1.3347	0	$-7.1084x10^{-4}$	0	$-0.1005x10^{-2}$	$0.5551x10^{-16}$
1	-1.1310	$0.2220x10^{-15}$	-0.0686	0	-0.09701	$0.1110x10^{-15}$
10^{1}	-1.3081	0	-0.0096	$0.5551x10^{-16}$	-0.0136	0
10^{2}	-0.4058	0	-0.5809	$0.1110x10^{-15}$	-0.8215	$0.1110x10^{-15}$
10^{3}	-0.7682	0	-0.1896	$0.2776x10^{-16}$	-0.2681	0
10^{4}	-0.5691	0	-0.2559	0	-0.3619	$0.5551x10^{-16}$
10^{5}	-1.0488	$0.2220x10^{-15}$	-0.0960	0	-0.1358	0
10^{6}	-0.4139	0	-0.3076	0	-0.4351	0

Table 5.2 The comparison of $\widetilde{\mathbf{E}}^{1(m)}$ and $\widetilde{\mathbf{E}}^{1(e)}$ for $\sigma_0 = 1$.

r	$\widetilde{E}_1^{1(m)}$	$\lvert\widetilde{E}_1^{1(m)} - \widetilde{E}_1^{1(e)}\rvert$	$\widetilde{E}_2^{1(m)}$	$\lvert\widetilde{E}_2^{1(m)} - \widetilde{E}_2^{1(e)}\rvert$	$\widetilde{E}_3^{1(m)}$	$\lvert\widetilde{E}_3^{1(m)} - \widetilde{E}_3^{1(e)}\rvert$
10^{-6}	-1.3369	$0.1489x10^{-8}$	$-7.1276x10^{-14}$	$0.1489x10^{-8}$	$-1.0064x10^{-13}$	$0.2106x10^{-8}$
10^{-5}	-1.3369	$0.1489x10^{-8}$	$-7.1110x10^{-12}$	$0.1489x10^{-8}$	$-1.0056x10^{-11}$	$0.2106x10^{-8}$
10^{-4}	-1.3369	$0.1489x10^{-8}$	$-7.1109x10^{-10}$	$0.1489x10^{-8}$	$-1.0056x10^{-9}$	$0.2106x10^{-8}$
10^{-3}	-1.3369	$0.1489x10^{-8}$	$-7.1109x10^{-8}$	$0.1489x10^{-8}$	$-1.0056x10^{-7}$	$0.2106x10^{-8}$
10^{-2}	-1.3368	$0.1489x10^{-8}$	$-7.1109x10^{-6}$	$0.1489x10^{-8}$	$-1.0056x10^{-5}$	$0.2106x10^{-8}$
10^{-1}	-1.3347	$0.1448x10^{-8}$	$-7.1084x10^{-4}$	$0.1503x10^{-8}$	$-0.1005x10^{-2}$	$0.2126x10^{-8}$
1	-1.1310	$0.1912x10^{-8}$	-0.0686	$0.2623x10^{-8}$	-0.0971	$0.3710x10^{-8}$
10^{1}	-1.3081	$0.9470x10^{-8}$	-0.0096	$0.1171x10^{-8}$	-0.0136	$0.1656x10^{-8}$
10^{2}	-0.4058	$0.1200x10^{-7}$	-0.5809	$0.0201x10^{-7}$	-0.8215	$0.0285x10^{-7}$
10^{3}	-0.7682	$0.2079x10^{-8}$	-0.1896	$0.1293x10^{-8}$	-0.2681	$0.1829x10^{-8}$
10^{4}	-0.5691	$0.1177x10^{-8}$	-0.2559	$0.1594x10^{-8}$	-0.3620	$0.2254x10^{-8}$
10^{5}	-1.0488	$0.5113x10^{-8}$	-0.0960	$0.0281x10^{-8}$	-0.1358	$0.0398x10^{-8}$
10^{6}	-0.4139	$0.1219x10^{-8}$	-0.3077	$0.1579x10^{-8}$	-0.4351	$0.2234x10^{-8}$

Table 5.3 The comparison of $\widetilde{\mathbf{E}}^{1(m)}$ and $\widetilde{\mathbf{E}}^{1(e)}$ for $\sigma_0 = 10$.

r	$\widetilde{E}_1^{1(m)}$	$\lvert\widetilde{E}_1^{1(m)} - \widetilde{E}_1^{1(e)}\rvert$	$\widetilde{E}_2^{1(m)}$	$\lvert\widetilde{E}_2^{1(m)} - \widetilde{E}_2^{1(e)}\rvert$	$\widetilde{E}_3^{1(m)}$	$\lvert\widetilde{E}_3^{1(m)} - \widetilde{E}_3^{1(e)}\rvert$
10^{-6}	-1.3369	$0.1489x10^{-7}$	$-7.1276x10^{-14}$	$0.1489x10^{-7}$	$-1.0064x10^{-13}$	$0.2106x10^{-7}$
10^{-5}	-1.3369	$0.1489x10^{-7}$	$-7.1110x10^{-12}$	$0.1489x10^{-7}$	$-1.0056x10^{-11}$	$0.2106x10^{-7}$
10^{-4}	-1.3369	$0.1489x10^{-7}$	$-7.1109x10^{-10}$	$0.1489x10^{-7}$	$-1.0056x10^{-9}$	$0.2106x10^{-7}$
10^{-3}	-1.3369	$0.1489x10^{-7}$	$-7.1109x10^{-8}$	$0.1489x10^{-7}$	$-1.0056x10^{-7}$	$0.2106x10^{-7}$
10^{-2}	-1.3368	$0.1489x10^{-7}$	$-7.1109x10^{-6}$	$0.1489x10^{-7}$	$-1.0056x10^{-5}$	$0.2106x10^{-7}$
10^{-1}	-1.3347	$0.1448x10^{-7}$	$-7.1084x10^{-4}$	$0.1503x10^{-7}$	$-0.1005x10^{-2}$	$0.2126x10^{-7}$
1	-1.1310	$0.1912x10^{-7}$	-0.0686	$0.2623x10^{-7}$	-0.0971	$0.3710x10^{-7}$
10^{1}	-1.3081	$0.9470x10^{-7}$	-0.0096	$0.1171x10^{-7}$	-0.0136	$0.1656x10^{-7}$
10^{2}	-0.4058	$0.1200x10^{-6}$	-0.5809	$0.0201x10^{-6}$	-0.8215	$0.0285x10^{-6}$
10^{3}	-0.7682	$0.2079x10^{-7}$	-0.1896	$0.1293x10^{-7}$	-0.2681	$0.1829x10^{-7}$
10^{4}	-0.5691	$0.1177x10^{-7}$	-0.2559	$0.1594x10^{-7}$	-0.3620	$0.2254x10^{-7}$
10^{5}	-1.0488	$0.5113x10^{-7}$	-0.0960	$0.0282x10^{-7}$	-0.1358	$0.0398x10^{-7}$
10^{6}	-0.4139	$0.1219x10^{-7}$	-0.3077	$0.1580x10^{-7}$	-0.4351	$0.2233x10^{-7}$

system

$$\frac{\partial^2}{\partial t^2}\tilde{u}(\nu,t,\tau)-a^2|\nu|^2\tilde{u}(\nu,t,\tau) = \delta(t-\tau)\,, \tag{5.68}$$

$$\tilde{u}(\nu,t,\tau)\Big|_{t<0} = 0\,, \tag{5.69}$$

where τ and $\nu=(\nu_1,\nu_2,\nu_3)$ are real parameters and $|\nu|^2=\nu_1^2+\nu_2^2+\nu_3^2$. The solution of (5.66)-(5.67) is given in the following form

$$\tilde{u}(\nu,t,\tau)=\Theta(t-\tau)\frac{\sin(a|\nu|(t-\tau))}{a|\nu|}\,. \tag{5.70}$$

Now, we must apply the inverse Fourier Transform to the equation (5.70), with respect to ν,

$$\mathcal{F}_\nu^{-1}[\tilde{u}(\nu,t,\tau)]=u(x,t,\tau)=\frac{1}{(2\pi)^3}\int_{-\infty}^{\infty}\int_{-\infty}^{\infty}\int_{-\infty}^{\infty}\Theta(t-\tau)\frac{\sin(a|\nu|(t-\tau))}{a|\nu|}e^{-i\nu x}d\nu\,, \tag{5.71}$$

where $\nu=(\nu_1,\nu_2,\nu_3)$, $d\nu=d\nu_1 d\nu_2 d\nu_3$ and $\nu x=\nu_1x_1+\nu_2x_2+\nu_3x_3$. After calculating inverse Fourier transform, we get the solution as in the following form:

$$U(x,t,\tau)=\frac{\Theta(t-\tau)}{2a\pi}\delta(a^2(t-\tau)^2-|x|^2)\,, \tag{5.72}$$

where $\delta(a^2(t-\tau)^2-|x|^2)$ is replaced by

$$\delta_\varepsilon(a^2(t-\tau)^2-|x|^2)=\frac{1}{\sqrt{\pi\varepsilon}}\exp-\frac{(a^2(t-\tau)^2-|x|^2)^2}{4\varepsilon}\,,$$

where $\varepsilon=0.0001$.

Now, we will apply inverse Fourier transform to (5.70) numerically by using our method for different A and $\Delta\nu$ values to find better approximation by considering suitable computation time. The following figures show that for better approximation it is enough to choose regularization parameters as $A=80$ and $\Delta\nu=0.025$. Figure 5.1 is simulated for regularized solution (5.72) of wave equation and Figure 5.2 is simulated for approximate computation of inverse Fourier transformation to (5.70) by using our approximation.

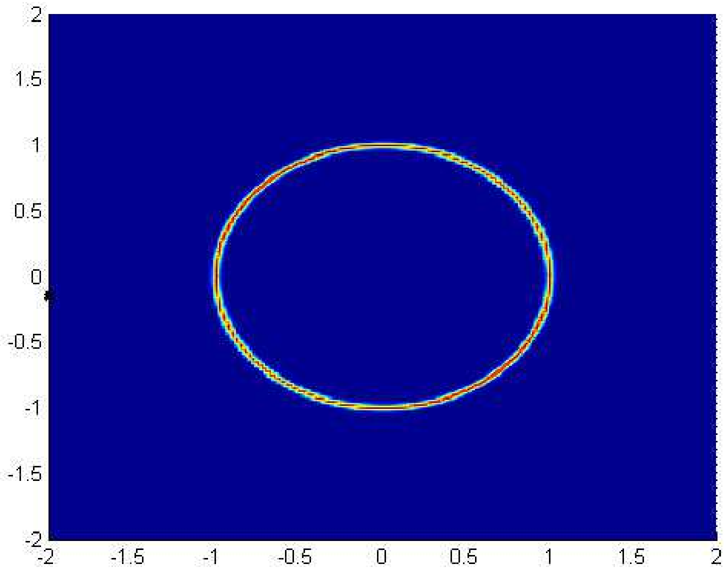

Figure 5.1 Graphic for regularized form of the Dirac delta function for A = 80 and $\Delta\nu$ = 0.025

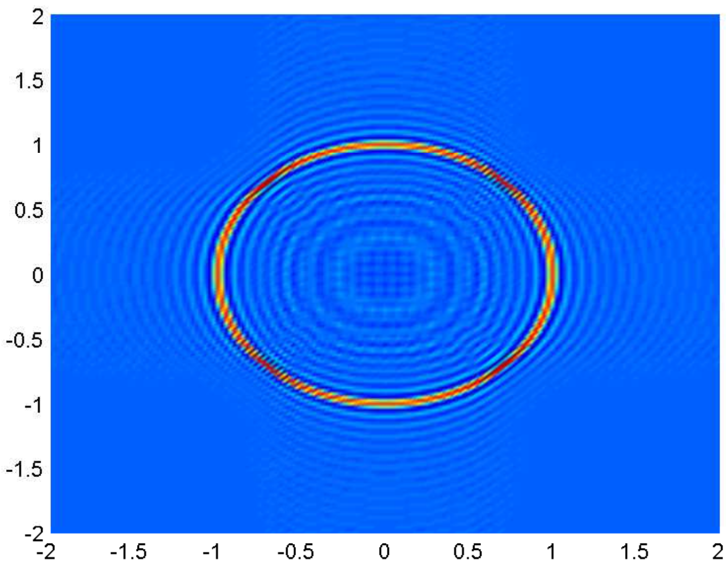

Figure 5.2 Graphic for numerical inverse Fourier transformation for A = 80 and $\Delta\nu$ = 0.025

5.2.3 Computational Experiments for an Anisotropic Monoclinic Structure

In this subsection, we will show some computational experiments for conductive anisotropic monoclinic structures. Here we fixed $\vec{\mathbf{e}} = (1/2, 0, \sqrt{3}/2)$, $N = 20$, $t = 8$ and we choose permittivity $\mathscr{E}$, permeability $\mathscr{M}$ and conductivity σ as in the form:

$$\mathscr{E} = \begin{pmatrix} 17.1598 & 13.0178 & 0 \\ 13.0178 & 23.6688 & 0 \\ 0 & 0 & 44.4444 \end{pmatrix}, \quad \mathscr{M} = \begin{pmatrix} 3 & 1 & 0 \\ 1 & 5 & 0 \\ 0 & 0 & 9 \end{pmatrix},$$

$$\sigma = \sigma_0 \begin{pmatrix} 0.1000 & 0.0667 & 0 \\ 0.0667 & 0.1667 & 0 \\ 0 & 0 & 0.2667 \end{pmatrix},$$

where σ_0 is a fixed parameter.

We obtained the following simulations for $E_1(x_1, x_2, -\sqrt{1/3}x_1, 8)$ for different σ_0. The $2D$ and $3D$ plots of $E_1(x_1, x_2, -\sqrt{1/3}x_1, 8)$ are presented in Figure 5.3 and Figure 5.4, respectively for $\sigma_0 = 0$. The result of the $2D$ simulation of $E_1(x_1, x_2, -\sqrt{1/3}x_1, 8)$ is presented in Figure 5.5 for $\sigma_0 = 1$. The Figure 5.6, Figure 5.7 and Figure 5.8 are the $2D$ simulation of $E_1(x_1, x_2, -\sqrt{1/3}x_1, 8)$ for $\sigma_0 = 3$, $\sigma_0 = 5$ and $\sigma_0 = 8$ respectively and the Figure 5.9 present the $2D$ simulation of $E_1(x_1, x_2, -\sqrt{1/3}x_1, 8)$ for $\sigma_0 = 10$.

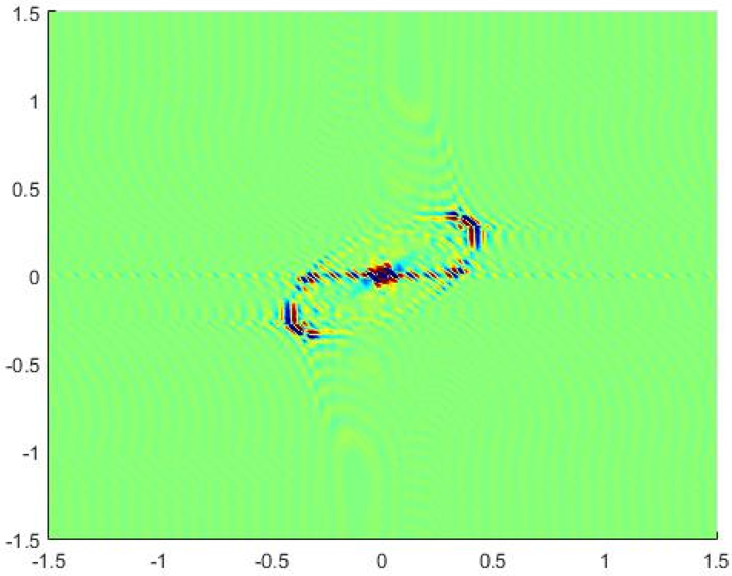

Figure 5.3 $2D$ graph of $E_1(x_1, x_2, -\sqrt{1/3}x_1, 8)$ for $\sigma_0 = 0$.

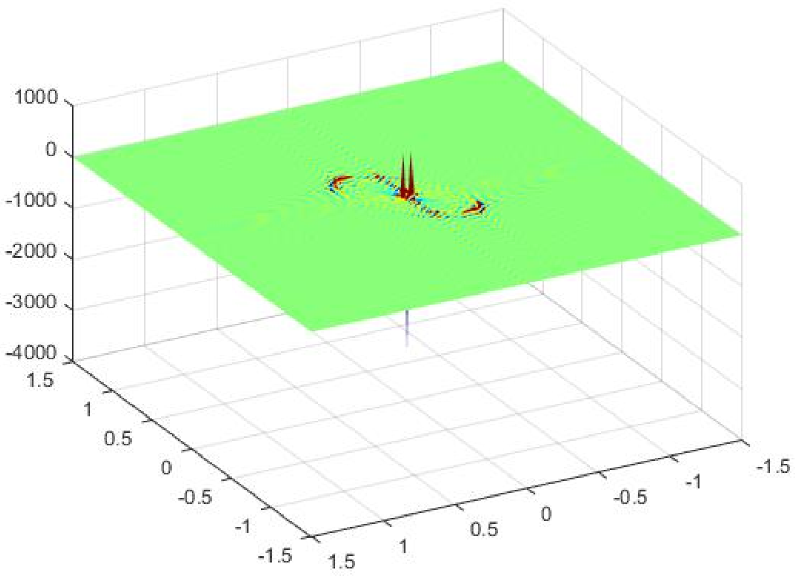

Figure 5.4 $3D$ graph of $E_1(x_1, x_2, -\sqrt{1/3}x_1, 8)$ for $\sigma_0 = 0$.

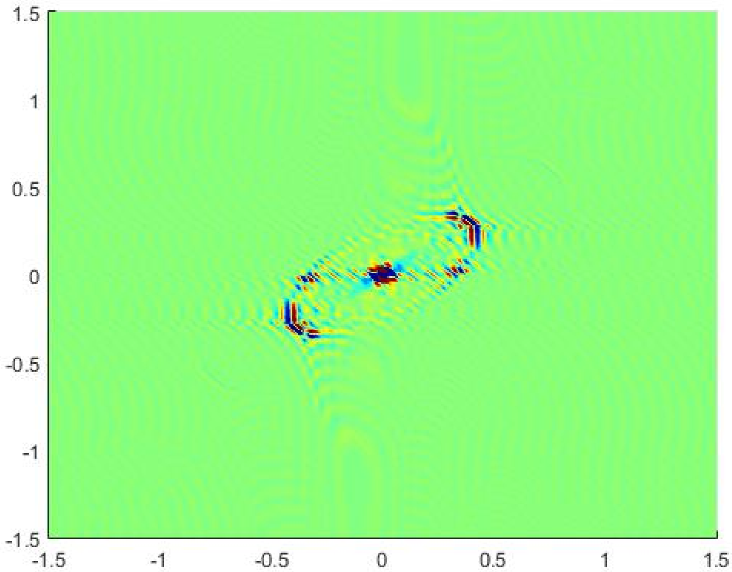

Figure 5.5 $2D$ graph of $E_1(x_1, x_2, -\sqrt{1/3}x_1, 8)$ for $\sigma_0 = 1$.

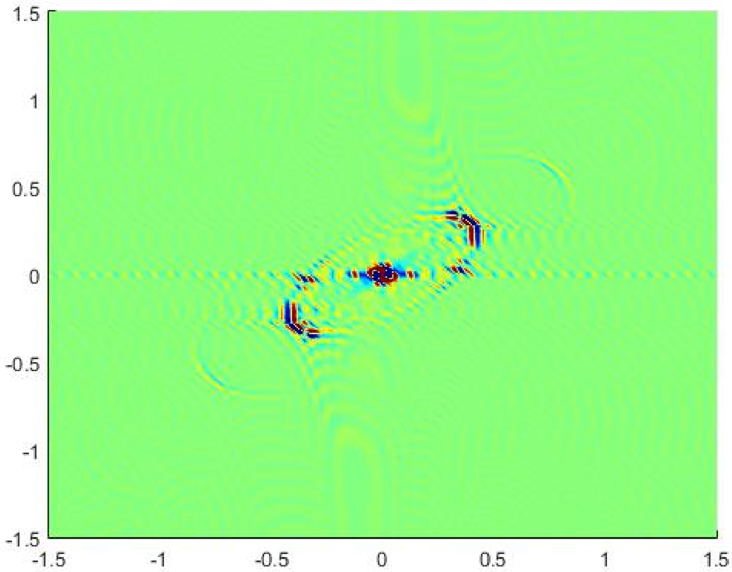

Figure 5.6 $2D$ graph of $E_1(x_1, x_2, -\sqrt{1/3}x_1, 8)$ for $\sigma_0 = 3$.

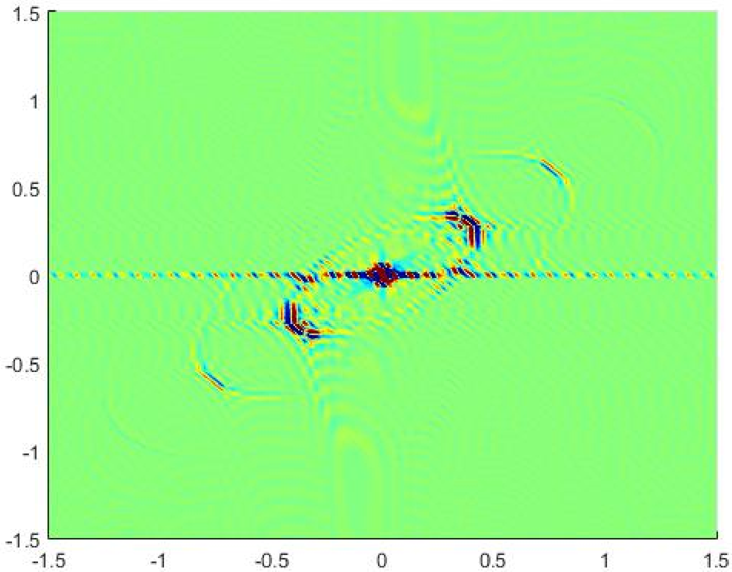

Figure 5.7 $2D$ graph of $E_1(x_1, x_2, -\sqrt{1/3}x_1, 8)$ for $\sigma_0 = 5$.

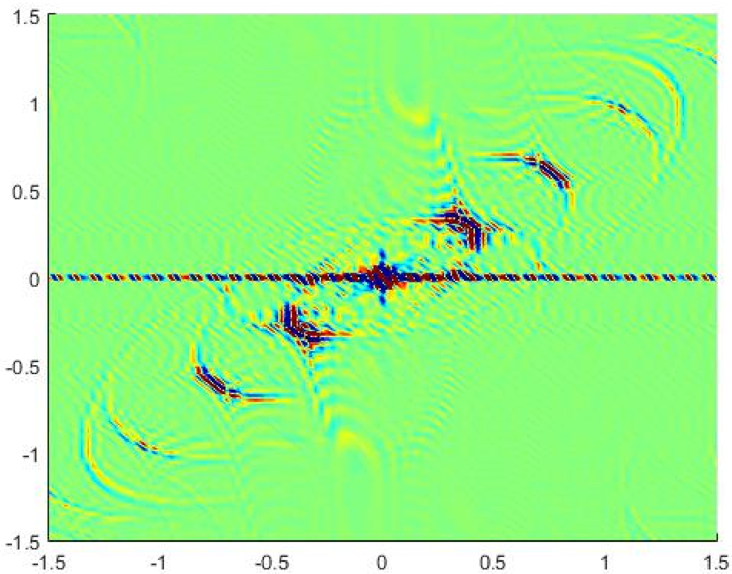

Figure 5.8 $2D$ graph of $E_1(x_1, x_2, -\sqrt{1/3}x_1, 8)$ for $\sigma_0 = 8$.

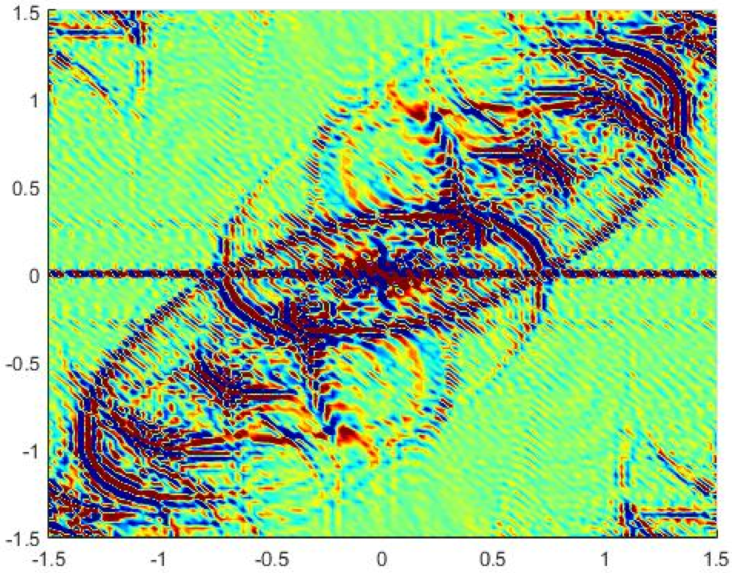

Figure 5.9 $2D$ graph of $E_1(x_1, x_2, -\sqrt{1/3}x_1, 8)$ for $\sigma_0 = 10$.

5.2.4 Computational Experiments for an Anisotropic Triclinic Structure

In this subsection, we will show some computational experiments for conductive anisotropic triclinic structures. Here we fixed $\vec{\mathbf{e}} = (1/2, 0, \sqrt{3}/2)$, $N = 20$, $t = 0.5$ and we choose $\mathscr{E}$, $\mathscr{M}$ and σ as in the form:

$$\varepsilon = \begin{pmatrix} 30.7929 & -12.7337 & -14.3432 \\ -12.7337 & 5.51497 & 5.86982 \\ -14.3432 & 5.86982 & 6.74556 \end{pmatrix}, \quad \mathscr{M} = \begin{pmatrix} 3 & -1 & -2 \\ -1 & 5 & 4 \\ -2 & 4 & 9 \end{pmatrix},$$

$$\sigma = \sigma_0 \begin{pmatrix} 0.0050 & -0.0020 & -0.0023 \\ -0.0020 & 0.0007 & 0.0007 \\ -0.0023 & 0.0007 & 0.0010 \end{pmatrix},$$

and we obtained the following simulations for $E_3(x_1, x_2, -\sqrt{1/3}x_1, t)$ for $\sigma_0 = 0, 1, 5, 8, 10$.

We have two computational experiments on this section. In the first, we assumed permeability $\mathscr{M}$ as identity matrix and we obtained the Figure 5.10-Figure 5.15. Secondly, we assumed permeability $\mathscr{M}$ as triclinic matrix given in previous equation and we obtained the Figure 5.16-Figure 5.21 to see the effect of permittivity $\mathscr{M}$ to the system together with conductivity σ.

The following computations are done for $\mathscr{M} = I$. The $2D$ and $3D$ plots of $E_3(x_1, x_2, -\sqrt{1/3}x_1, 0.5)$ are presented in Figure 5.10 and Figure 5.11, respectively and $\sigma_0 = 0$. The result of the $2D$ simulation of $E_3(x_1, x_2, -\sqrt{1/3}x_1, 0.5)$ is presented in Figure 5.12 for $\sigma_0 = 1$. The Figure 5.13, Figure 5.14 are the $2D$ simulation of $E_3(x_1, x_2, -\sqrt{1/3}x_1, 0.5)$ for $\sigma_0 = 5$ and $\sigma_0 = 8$, respectively and the Figure 5.15 present the $2D$ simulation of $E_3(x_1, x_2, -\sqrt{1/3}x_1, 0.5)$ for $\sigma_0 = 10$.

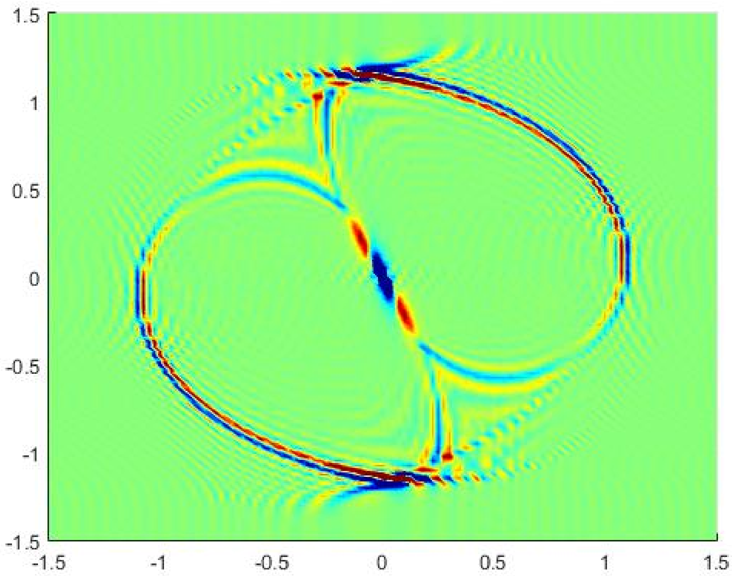

Figure 5.10 $2D$ graph of $E_3(x_1, x_2, -\sqrt{1/3}x_1, 0.5)$ for $\mathscr{M} = I$ and $\sigma_0 = 0$.

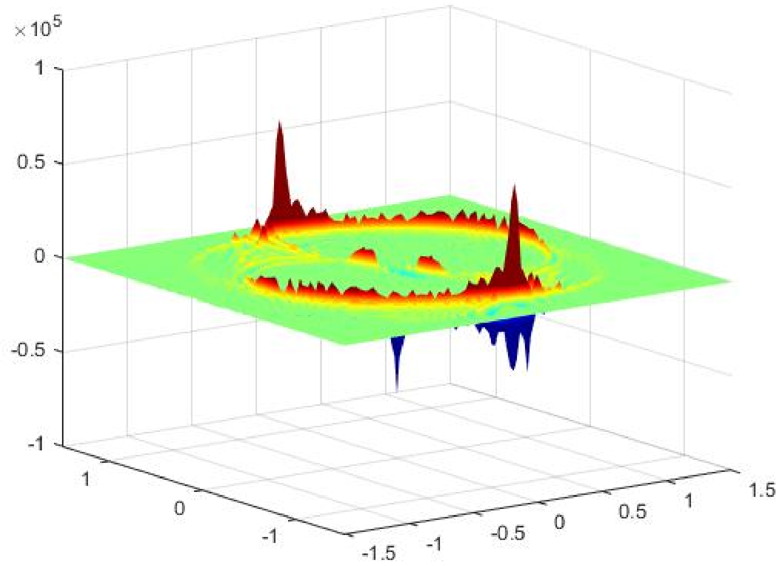

Figure 5.11 $3D$ graph of $E_3(x_1, x_2, -\sqrt{1/3}x_1, 0.5)$ for $\mathscr{M} = I$ and $\sigma_0 = 0$.

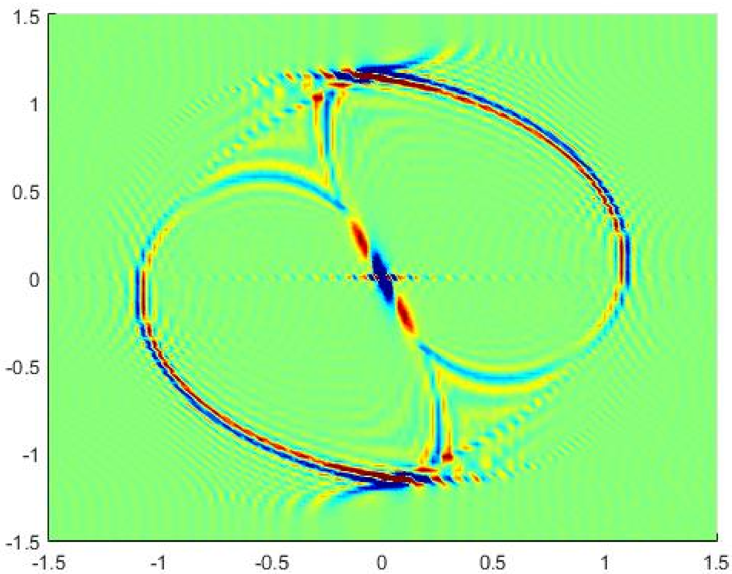

Figure 5.12 $2D$ graph of $E_3(x_1, x_2, -\sqrt{1/3}x_1, 0.5)$ for $\mathscr{M} = I$ and $\mathscr{M} = I$ and $\sigma_0 = 1$.

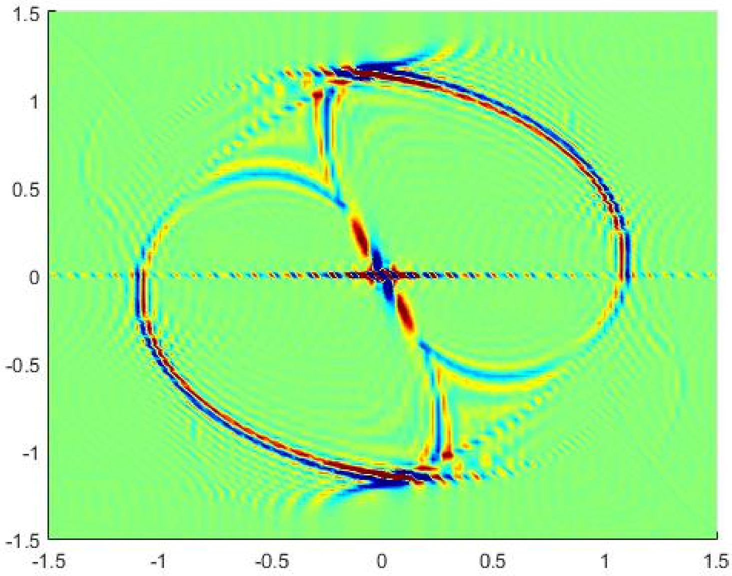

Figure 5.13 $2D$ graph of $E_3(x_1, x_2, -\sqrt{1/3}x_1, 0.5)$ for $\mathscr{M} = I$ and $\sigma_0 = 5$.

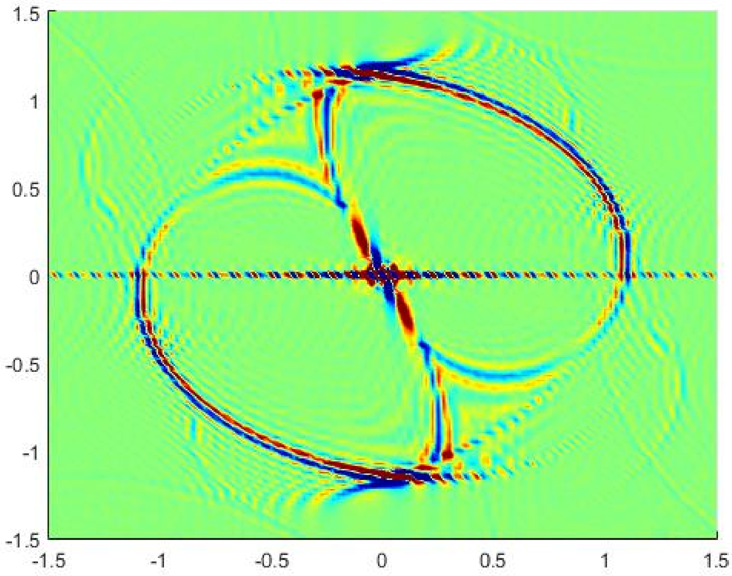

Figure 5.14 $2D$ graph of $E_3(x_1, x_2, -\sqrt{1/3}x_1, 0.5)$ for $\mathscr{M} = I$ and $\sigma_0 = 8$.

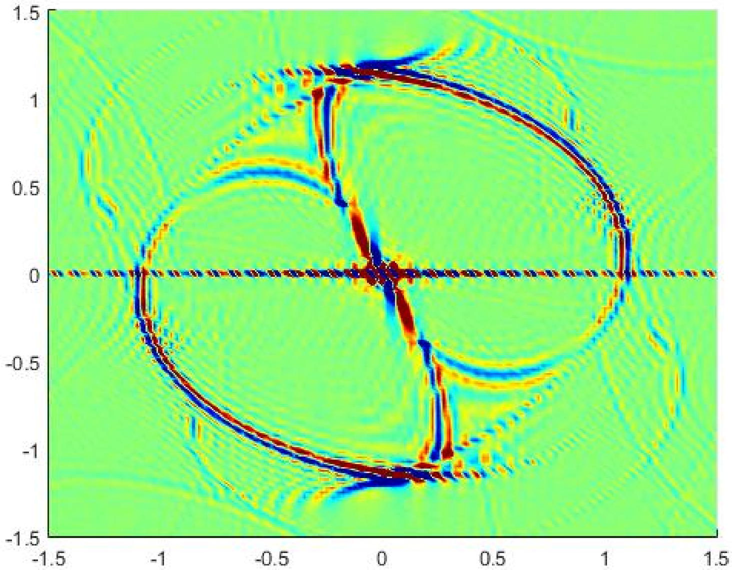

Figure 5.15 $2D$ graph of $E_3(x_1, x_2, -\sqrt{1/3}x_1, 0.5)$ for $\mathscr{M} = I$ and $\sigma_0 = 10$.

The following computations are related to the second part. Figure 5.16 and Figure 5.17 are the the $2D$ and $3D$ plots of $E_3(x_1, x_2, -\sqrt{1/3}x_1, 0.5)$, respectively for $\sigma_0 = 0$. We presented $2D$ simulation of $E_3(x_1, x_2, -\sqrt{1/3}x_1, 0.5)$ in Figure 5.18 for $\sigma_0 = 1$. The Figure 5.19, Figure 5.20 are the $2D$ simulation of $E_3(x_1, x_2, -\sqrt{1/3}x_1, 0.5)$ for $\sigma_0 = 5$ and $\sigma_0 = 8$ respectively and the Figure 5.21 present the $2D$ simulation of $E_3(x_1, x_2, -\sqrt{1/3}x_1, 0.5)$ for $\sigma_0 = 10$.

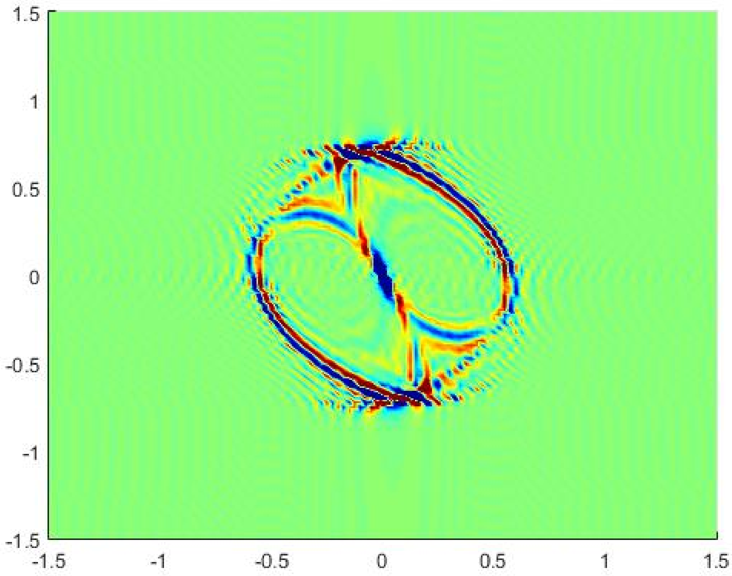

Figure 5.16 $2D$ graph of $E_3(x_1, x_2, -\sqrt{1/3}x_1, 0.5)$ for triclinic $\mathscr{M}$ and $\sigma_0 = 0$.

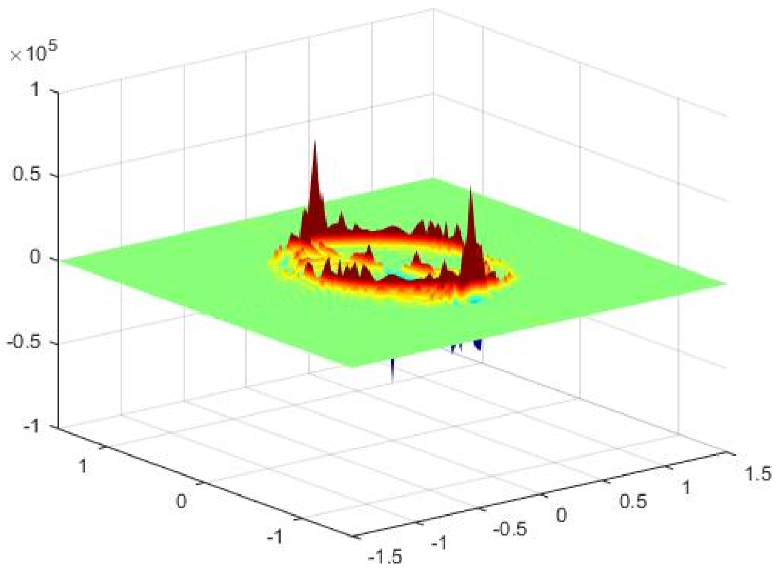

Figure 5.17 $3D$ graph of $E_3(x_1, x_2, -\sqrt{1/3}x_1, 0.5)$ for triclinic $\mathscr{M}$ and $\sigma_0 = 0$.

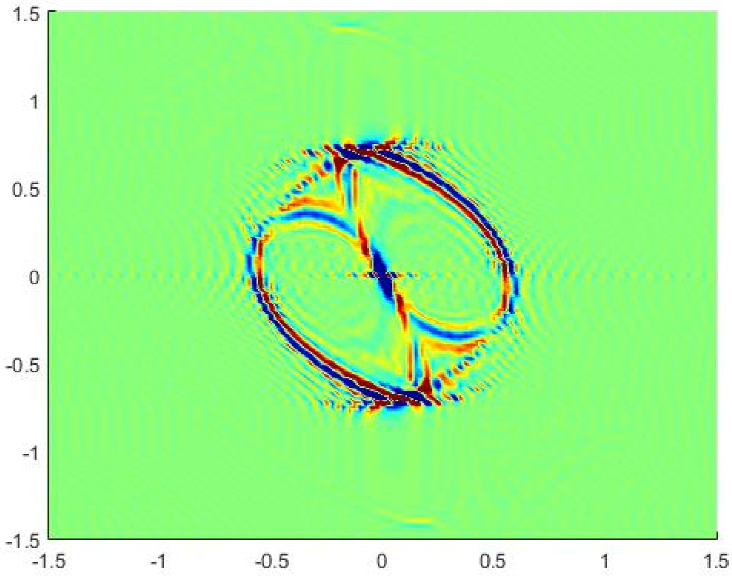

Figure 5.18 $2D$ graph of $E_3(x_1, x_2, -\sqrt{1/3}x_1, 0.5)$ for triclinic $\mathscr{M}$ and $\sigma_0 = 1$.

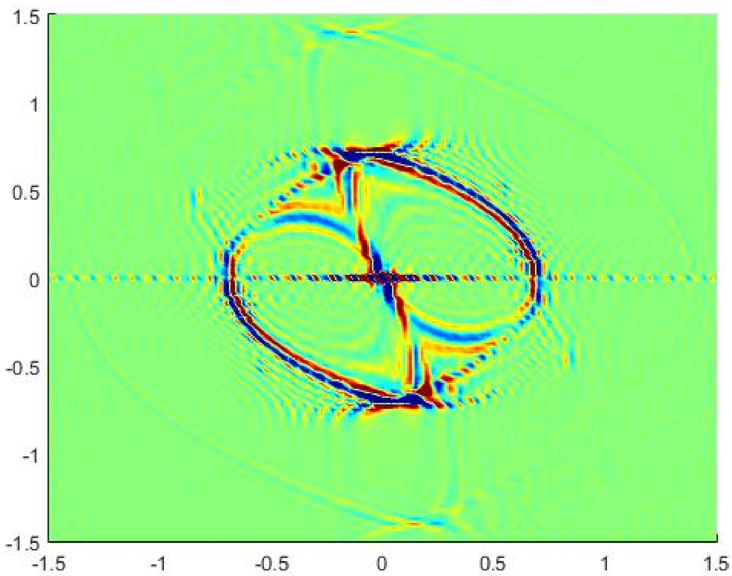

Figure 5.19 $2D$ graph of $E_3(x_1, x_2, -\sqrt{1/3}x_1, 0.5)$ for triclinic $\mathscr{M}$ and $\sigma_0 = 5$.

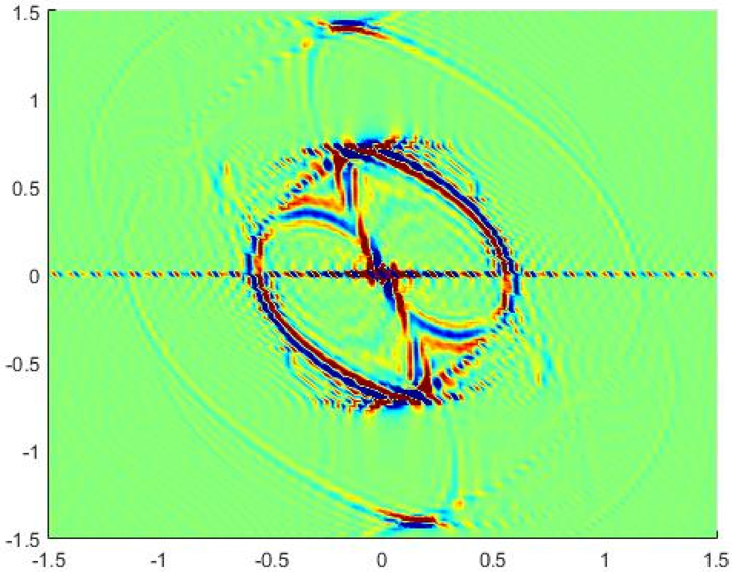

Figure 5.20 $2D$ graph of $E_3(x_1, x_2, -\sqrt{1/3}x_1, 0.5)$ for triclinic $\mathscr{M}$ and $\sigma_0 = 8$.

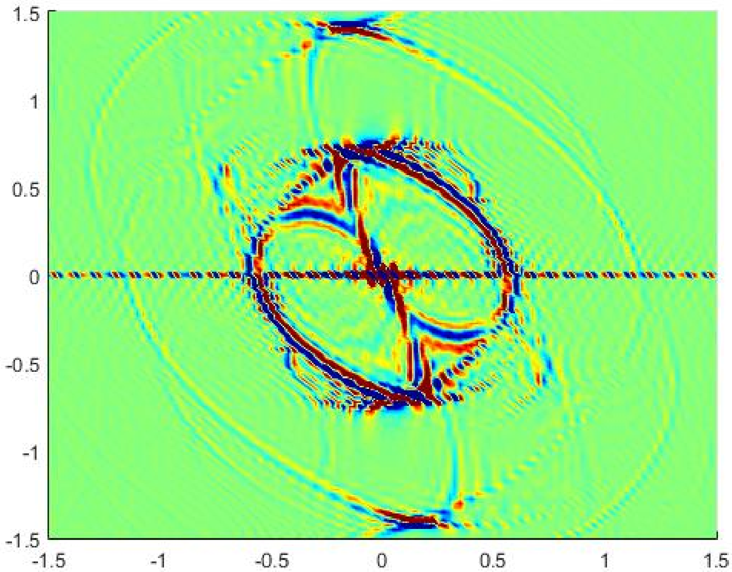

Figure 5.21 $2D$ graph of $E_3(x_1, x_2, -\sqrt{1/3}x_1, 0.5)$ for triclinic $\mathscr{M}$ and $\sigma_0 = 10$.

5.3 Summary of the Chapter Five

In this chapter we suggested the new method of approximate computation of the fundamental solution of Maxwell's equations for general anisotropic conductive materials which is based the following. The equations for the fundamental solution are written in the form of the Fourier transformation with respect to the space variables. The obtained equations have been reduced to the vector integral equation of the Volterra type. The solution of the obtained integral equation were constructed by successive approximations in the form of the uniformly convergent infinite functional series. The variable of the functional series were Fourier parameters and the time variable. Finally, the inverse Fourier transform were applied to constructed series with respect to the Fourier parameters. We had showed that the results of this transformation was generalized function (distribution) from the Schwartz space. The computation of the fundamental solutions of electric fields in general anisotropic conductive materials had been made by replacement of finite series by a sum with finite terms and implemented numerically in MATLAB, the inverse Fourier transform by the integral over a bounded domain.

CHAPTER SIX
CONCLUSION

This thesis deals with the problems of the electromagnetic wave propagation in gyrotropic media and anisotropic conductive media.

The results of the thesis are the following.

- The new method of the approximate computation of the electric and magnetic matrix Green's functions in general gyrotropic media has been developed. The Fourier images of the elements of the electric and magnetic matrix Green's functions with respect to space variables are computed exactly by symbolic transformations in MATLAB. The elements of the Green's functions for the electric and magnetic fields are derived approximately by the regularized numerical computation of the inverse Fourier transform of their images obtained on the previous step. The robustness of the method for the approximate computation of the Green's functions has been tested by the comparison with exact formulae for the Green's functions of magnetic fields in isotropic homogeneous media.
- The new method of approximate computation of the fundamental solution of Maxwell's equations for general anisotropic conductive materials has been found. This method based on the following. Applying the Fourier transformation with respect to the space variables, the initial value problem is reduced to the Volterra integral equation. Method of successive approximations is applied for solving the obtained system of the integral equations. Finally, the inverse Fourier transform is applied numerically to the finite sum of constructed series with respect to the Fourier parameters in MATLAB. The robustness of the method is confirmed by the computational experiments.

The result of Chapter 3 were published in the work:

- V. Yakhno and B. Cicek, "Computing the Electric and Magnetic Green's

Functions in General Electrically Gyrotropic Media", CMC: Computers, Materials & Continua, Vol. 44, No. 3, pp. 141-166, 2014.

Conference Paper is the following:

- B. Cicek and V. Yakhno, Computing the Electric and Magnetic Green's Functions in General Gyrotropic Media. PIERS Proceedings, 335 - 339, July 6-9, Prague, 2015.

REFERENCES

Albuquerque, E. L., Sollero, P., & Aliabadi, M. H. (2002). The boundary element method applied to time dependent problems in anisotropic materialse. *International Journal of Solids Structures*, *39*, 1405–1422.

Barkleshli, S. (1993). Electromagnetic dyadic green's function for multilayered symmetric gyro-electric media. *Radio Science*, *28*, 23–36.

Beskos, D. E. (1987a). Boundary element methods in dynamic analysis. *Applied Mechanics Reviews*, *40*, 1–23.

Beskos, D. E. (1987b). Boundary element methods in mechanics. *Amsterdam: North-Holland*, *3*, 598.

Beskos, D. E. (1989). *Boundary element methods in structural analysis*. New York: ASCE.

Beskos, D. E. (1997). Boundary element methods in dynamic analysis. part ii. *Applied Mechanics Reviews*, *50*, 149–97.

Beskos, D. E., & Manolis, G. D. (1997). *Boundary element methods in elastodynamics*. London: Unwin Hyman.

Burridge, R., & Qian, J. (2006). The fundamental solution of the time-dependent system of crystal optics. *Europen Journal of Applied Mathematics*, *17*, 63–94.

Chen, J., Ke, J., & Liao, H. (2009). Construction of green's function using field integral approach for laplace problems with circular boundaries. *CMC: Computers, Materials and Continua*, *9*, 93–109.

Chew, W. C. (1990). *Waves and fields in inhomogeneous media*. New York: Van Nostrand Reinhold.

Chew, W. C. (1995). *Waves and Fields in Inhomogeneous Media*. New York: IEEE Press.

Commer, M., Newman, G., Carazzone, J., Dickens, T., Green, K., Wahrmund, L., et al. (2008). Massively parallel electrical-conductivity imaging of hydrocarbons using the ibm bluegene/l supercomputer. *IBM Journal of Research and Development*, *52*(1/2), 93–103.

Courant, R., & Hilbert, D. (1962). *Methods of mathematical physics*. New York: Wiley and Sons.

Darvas, F., Pantazis, D., Kucukaltun-Yildirim, E., & Leahy, R. M. (2004). Mapping human brain function with meg and eeg: methods and validation. *Journal of Applied Physics*, *23*, 289–299.

Ehrenpreis, L. (1960). Solution of some problems of division. iv. *Invertible and elliptic operators. American Journal of Mathematics*, *82*, 522–588.

Eroglu, A. (2010). *Wave Propagation and Radiation in Gyrotropic and Anisotropic Media*. New York: Springer.

Eroglu, A., & Lee, J. (2006a). Wave propagation and dispersion characteristics for a nonreciprocal electrically gyrotropic medium. *Progress In Electromagnetics Research*, *62*, 237–260.

Eroglu, A., & Lee, J. K. (2003). Dyadic green's function for a gyro-electric medium. *IEEE International*, *2*, 1100– 1103.

Eroglu, A., & Lee, J. K. (2005). Application of duality principle on dyadic green's functions for gyrotropic media. *Antennas and Propagation Society International Symposium, 2005 IEEE*, *4B*, 406–409 vol. 4B.

Eroglu, A., & Lee, J. K. (2006b). Dyadic green's function for an electrically gyrotropic medium. *Progres in Electromagnetic Research*, *58*, 223–241.

Faraday, M. (1933). *Faraday's Diary*, vol. 4. London: George Bell and Sons Ltd.

Freiser, M. J. (1968). A survey of magneto-optic effects. *IEEE Transactions on Magnetics*, *4*, 152–161.

Goldberg, J. L. (1992). *Matrix Theory with Applications*. London: McGrawHill International Editions.

Gowri, B., & Shajan, X. S. (2006). Electrical conductivity studies on pure and copper added strontium tartrate trihydrate crystals. *Materials Letters*, *60*, 1338–1340.

Greena, J., Shajan, S., & Devadoss, A. H. (2010). Electrical conductivity studies on pure and barium added strontium tartrate trihydrate crystals. *Indian Journal of Science and Technology*, *3*(3), 250–252.

Gu, M. H., Young, D. L., & Fan, C. M. (2009). The method of fundamental solutions for one-dimensional wave eqautions. *CMC: Computers, Materials and Continua*, *11*, 185–208.

Hirose, S., & Achenbach, J. D. (1989). Time-domain boundary element analysis of elastic wave interaction with a crack. *International Journal for Numerical Methods in Engineering*, *28*, 629–644.

Hirose, S., & Kitahara, M. (1989). Elastic wave scattering by inhomogenous and anisotropic bodies in a half space. *Earthquake Engineering and Structural Dynamics Journal*, *18*, 285–297.

Hirose, S., & Kitahara, M. (1991). Scattering of elastic waves by a crack with spring-mass contact. *International Journal for Numerical Methods in Engineering*, *31*, 789–801.

Hormander, L. (1963). *Linear Partial Differential Operators*. Berlin: Springer.

Kong, J. A. (1984). *Electromagnetic Wave Theory*. New York: John Wiley and Sons.

Lakhtakia, A., & Mackay, T. G. (2006). Dyadic green function for an electromagnetic medium inspired by general relativity. *Chinese Physics Letters*, *23*, 832–833.

Lakhtakia, A., & Weiglhofer, W. S. (1997). Green function for radiation and propagation in helicoidal bi-anisotropic medium. *IEE Proceedings - Microwaves Antennas and Propagation*, *144*, 57–59.

Lee, J. K., & Rhee, S. Y. (2005). Reflection and transmission of plane waves at the planar interface of a magnetically gyrotropic medium. *IEEE, Geoscience and Remote Sensing Symposiumn*.

Lindell, I. V., Sihvola, A. H., Tretyakov, S. A., & Viitanen, A. J. (1994). *Electromagnetic waves in chiral and biisotropic media*. New York: Artech House.

Lindell, I. V., & Weiglhofer, W. S. (1994). Green dyadic for a uniaxial bi-anisotropic medium. *IEEE Transactions on Antennas and Propagation*, *42*, 1013–1016.

Malgrange, B. (1955-56). Existence et approximation des solutions des equations aux derivees partielles et des equations de convolution. *Annales de I'Institut Fourier*, *6*, 271–355.

Meyer, C. D. (2001). *Matrix Analysis and Applied Linear Algebra*. SIAM: Society for Industrial and Applied Mathematics.

Moses, H. E., & Prosser, R. T. (1990). The general solution of the time-dependent maxwell's equations in an infinite medium with constant conductivity. *Mathematical and Physical sciences*, *431*(1883), 493–507.

Newman, G. A., & Alumbaugh, D. L. (2002). Three dimensional induction logging problems, part 2: A finite difference solution for 3-d induction logging problems. *Geophysics*, *67*(2), 484–491.

Okamoto, A. (2006). The invention of ferrites and their contribution to the miniaturization of radios. *GLOBECOM Workshops, 2009 IEEE*, pp. 1–6.

Olyslager, F. (1997). Time harmonic two- and three- dimensional closed form green's dyadic for gyrotropic, bianisotropic, and anisotropic media. *Electromagnetics, Taylor and Fracis*, *17*(4), 369–386.

Ortner, N., & Wagner, P. (2004). Fundamental matrices of homogeneous hyperbolic systems. Applications to crystal optics, elastodynamics, and piezoelectromagnetism. *ZAMM - Journal of Applied Mathematics and Mechanics / Zeitschrift für Angewandte Mathematik und Mechanik*, *84*(5), 314–346.

Ortner, N., & Wagner, P. (2008). The fundamental matrix of the system of linear elastodynamics in hexagonal media. Solution to the problem of conical refraction ima. *Journal of Applied Mathematics*, *73*, 412–447.

Oster, A., & Turbe, N. (1993). On the maxwell's system in composite media. *Mathematical Modelling and Numerical Analysis*, *27*, 481–496.

Pershan, P. S. (1967). Magneto-optical effects. *Journal of Applied Physics*, *38*, 1482.

Prati, E. (2003). Propagation in gyroelectromagnetic guiding system. *Journal of Electromagnetic Waves and Applications*, *17*, 1177–1196.

Rashed, Y. F. (2004). Green's first identity method for boundary-only solution of self-weight in bem formulation for thick slabs. *CMC: Computers, Materials and Continua*, *1*, 319–326.

Schwartz, L. (1966). *Theorie des distributions*. Paris.

Sekino, M., Yamaguchi, K., Iriguchi, N., & Ueno, S. (2003). Conductivity tensor imaging of the brain using diffusion-weighted magnetic resonance imaging. *Journal of Applied Physics*, *93*, 6730–6732.

Simon, B., & Reed, M. (1997). The scattering of classical waves from inhomogeneous media. *Mathematische Zeitschrift*, *155*, 163–168.

Sundarapandian, V. (2008). *Numerical Linear Algebra*. Prentice-Hall.

Tai, C. T. (1994). *Dyadic Green's functions in electromagnetic theory*. New Jersey: IEEE Press.

Takahashi, T., Nishimura, N., & Kobayashi, S. (2004). A fast bem for three-dimensional elastodynamics in time domain. *Engineering Analysis with Boundary Elements*, *28*, 165–180.

Tan, A., Hirose, S., Zhang, C. H., & Wang, C. Y. (2005). A 2d time-domain bem for transient wave scattering analysis by a crack in anisotropic solids. *Engineering Analysis with Boundary Elements*, *29*, 610–623.

Tan, E. L. (2002). Electrostatic green's functions for planar multilayered anisotropic media. *IEE Proceedings - Microwaves Antennas and Propagation*, *149*, 78–83.

Tewary, V., Bartolo, L., & Powell, A. (2002). Green's functions experts meeting 274 and the green digital library. *NIST Workshop Report*.

Tewary, V. K. (1995). Computationally efficient representation for elastodynamic and elastostatic green's functions for anisotropic solids. *Physical Review B*, *51*, 15695–15702.

Tewary, V. K. (2004). Elastostatic green's function for advanced materials subject to surface loading. *Journal of Engineering Mathematics*, *49*, 289–304.

Tsutaoka, T. (2003). Frequency dispersion of complex permeability in mn-zn and ni-zn spinel ferrites and their composite materials. *Journal Of Applied Physics*, *93*(5), 2789–2796.

V. Yakhno, V. G., & T. Yakhno, T. M. (2007). Modeling and simulation of electric and magnetic fields in homogeneous non-dispersive anisotropic materials. *Computers and Structures*, *85*, 1623 – 1634.

V. Yakhno, V. G., & T. Yakhno, T. M. (2012). Computation of the time-dependent green's functions for non-dispersive magnetoelectric materials. *International Journal of Engineering Science*, *54*, 1–14.

Vladimirov, V. S. (1971). *Equations of Mathematical Physics*. New York: Marcel Dekker.

Vladimirov, V. S. (1979). *Generalized Functions in Mathematical Physics*. Moscow: Mir.

Wagner, P. (1999). Electrical conductivity studies on pure and barium added strontium tartrate trihydrate crystals. *Acta Mathematica*, *182*, 283–300.

Wagner, P. (2004). On the explicit calculation of fundamental solutions. *Journal of Mathematical Analysis and Applications*, *297*, 404–418.

Wagner, P. (2005). On the fundamental solutions of a class of hyperbolic quartic operators in dimension 3. *Annali di Matematica Pura ed Applicata*, *184*, 139–159.

Wagner, P. (2006). The herglotz formula and fundamental solutions of hyperbolic cubic operators in r4. *Integral Transforms and Special Functions*, *17*, 307–314.

Wagner, P. (2011a). The singular terms in the fundamental matrix of crystal optics. *Proceedings of Royal Society of London*, *467*, 2663–2689.

Wagner, P. (2011b). The singular terms in the fundamental matrix of crystal optics. *Proceedings of the Royal Society A*, *467*, 2663–2689.

Wang, C. Y., Achenbach, J. D., & Hirose, S. (1996). Two-dimensional time domain bem for scattering of elastic waves in solids of general anisotropy. *International Journal of Solids and Structures*, *3*, 3843–3864.

Wang, T., & Fang, S. (2001). 3-d electromagnetic anisotropy modeling using finite differences. *Geophysics*, *66*, 1386–1398.

Weiglhofer, W. S. (1993). Analytic methods and free space dyadic greens functions. *Padio Science*, *28*, 847–857.

Weiglhofer, W. S. (1995). One-dimensional dyadic green functions for general linear bi-anisotropic media. *Journal of Electromagnetic Waves and Applications*, *9*, 1421–1432.

Weiss, J., & Newman, A. (2002). Electromagnetic induction in a fully 3-d anisotropic earth. *Geophysics*, *67*, 1104–1114.

Weiss, J., & Newman, A. (2003). Electromagnetic induction in a generalized 3d anisotropic earth, part 2: The lin preconditionert. *Geophysics*, *68*, 922–930.

Yakhno, V., Yakhno, T. M., & Kasap, M. (2006). A novel approach for modelig and simulation of electromagnetic waves in anisotropic dielectrics. *Solids and Structures*, *43*, 6261–6276.

Yakhno, V. G. (2005). Constructing green's function for the time-dependent maxwell system in anisotropic dielectrics. *Journal of Physics A: Mathematical and General*, *38*, 2277–2287.

Yakhno, V. G. (2008). Computing and simulation of time-dependent electromagnetic fields in homogeneous anisotropic materials. *International Journal of Engineering Science*, *46*, 411–426.

Yakhno, V. G. (2010). Deriving the time-dependent dyadic green's functions in conductive anisotropic media. *International Journal of Engineering Science*, *48*, 332–342.

Yakhno, V. G. (2011). Computation of dyadic green's functions for electrodynamics in quasi-static approximation with tensor conductivity. *CMC: Computers, Materials and Continua*, *21*(1), 1–15.

Yakhno, V. G., & Altunkaynak, M. (2010). A new method for computing a solution of the cauchy problem with polynomial data for the system of crystal optics. *International Journal of Computer Mathematics*, *87*, 1469–1484.

Yakhno, V. G., & Çerdik Yaslan, H. (2012). Approximate fundamental solutions and wave fronts for general anisotropic materials. *International Journal of Solids and Structures*, *49*, 853–864.

Yakhno, V. G., & Çiçek, B. (2014). Computing the electric and magnetic green's functions in general electrically gyrotropic media. *CMC: Computers, Materials and Continua*, *44*, 141–166.

Yakhno, V. G., & Çerdik Yaslan, H. (2011). Computation of the time-dependent green's function of three dimensional elastodynamics in 3d quasicrystals. *CMES: Computer Modeling in Engineering and Sciences*, *81*(4), 295–310.

Yakhno, V. G., Çerdik Yaslan, H., & Yakhno, T. M. (2012). Computation of the fundamental solution of electrodynamics for anisotropic materials. *Central European Journal of Mathematics*, *10*, 188–203.

Yakhno, V. G., & Ersoy, S. (2014). Computing the electric and magnetic matrix green's functions in a rectangular parallelepiped with a perfect conducting boundary. *Abstract and Applied Analysis*, *1*, 1–13.

Yakhno, V. G., & Ersoy, S. (2015). The computation of the time-dependent magnetic and electric matrix green's functions in a parallelepiped. *Applied Mathematical Modelling*.

Yakhno, V. G., & Ozdek, D. (2012). Computation of the time-dependent green's function for the longitudinal vibration of multi-step rod. *CMES: Computer Modeling in Engineering and Sciences*, *85*(2), 157–176.

Yakhno, V. G., & Ozdek, D. (2013). The time-dependent green's function of the transverse vibration of a composite multi stepped membrane. *CMC: Computers, Materials and Continua*, *33*(2), 155–173.

Yang, B., & Tewary, V. K. (2008). Green's function for multilayered with interfacial membrane and flexural rigidities. *CMC: Computers, Materials and Continua*, *8*, 23–31.

Young, D. L., Chen, C. S., & Wong, T. K. (2005). Solution of maxwell's equations using the mq method. *CMC: Computers, Materials and Continua*, *2*, 267–276.

APPENDICES

A1 MATLAB Code of General Gyrotropic Media

The following subsections are the MATLAB codes for the Chapter 2:

A1.1 MATLAB Code of Symbolic Computation of Matrix $\widetilde{E}(\nu)$

```
Input: c (speed of light), w (frequency)
Input: N, BB, ndelta, xdelta
Input: kappae, kappam, epsi, epsr
Input: mui, mur

Epss=epsr+1i*epsi
Mu=mur+i*mui
InvMu=inv(Mu);
InvMuR=real(InvMu);
InvMuI=imag(InvMu);

Eps=[epsr -epsi; epsi epsr]
[EigVecEps, EigValEps] = eig(Eps);
P = EigVecEps;
PT = P.';
M = EigValEps
Mh = sqrt(M);
SqrEps = P*Mh*PT;
InvSrtEps = inv(SqrEps);

SC=[0 -v3 v2; v3 0 -v1; -v2 v1 0];
Sr=SC*InvMuR*SC;
```

```
Si=SC*InvMuI*SC;
SS=[Sr -Si; Si Sr];
A=InvSrtEps*SS*InvSrtEps;
[EigVecA,EigValA]=eig(A);
De=EigValA;
Q=EigVecA;
for k=1:6;
Q(:,k) = Q(:,k) ./ sqrt(sum (Q(:,k).^2));
end
T=InvSrtEps*Q;
D=diag(De);

transT=(TT).';
ek=[1 0 0]';
FK=[0;0;0;w*mu0*ek];
YK=transT*FK;
for k=1:6
    YKN(k)=YK(k)/((DD(k))-tau^2);
end
Etilda=TT*YKN.';
Output: Etilda
```

A1.2 MATLAB Code of Symbolic Computation of Matrix $\widetilde{H}(\nu)$

```
Input: c (speed of light), w (frequency)
Input: N, BB, ndelta, xdelta
Input: kappae, kappam, epsi, epsr
Input: mui, mur

Epss=epsr+1i*epsi
Mu=mur+i*mui
```

```
InvEps=inv(Eps);
InvEpsR=real(InvEps);
InvEpsI=imag(InvEps);

Mu=[mur -mui; mui mur]
[EigVecMu, EigValMu] = eig(Mu);
P = EigVecMu;
PT = P.';
M = EigValMu
Mh = sqrt(M);
SqrMu = P*Mh*PT;
InvSrtMu = inv(SqrMu);

SC=[0 -v3 v2; v3 0 -v1; -v2 v1 0];
Sr=SC*InvMuR*SC;
Si=SC*InvMuI*SC;
SS=[Sr -Si; Si Sr];
A=InvSrtMu*SS*InvSrtMu;
[EigVecA,EigValA]=eig(A);
De=EigValA;
Q=EigVecA;
for k=1:6;
Q(:,k) = Q(:,k) ./ sqrt(sum (Q(:,k).^2));
end
T=InvSrtEps*Q;
D=diag(De);

transT=(TT).';
ek=[1 0 0]';
FK=[[0 -v3 v2; v3 0 -v1; -v2 v1 0]*epsr*ek;...
[0 -v3 v2; v3 0 -v1; -v2 v1 0]*epsi*ek];
```

```
YK=transT*FK;
for k=1:6
    YKN(k)=YK(k)/((DD(k))-tau^2);
end
Htilda=TT*YKN.';
Output: Htilda
```

A2 MATLAB Code of General Gyro-electric Media

The following subsections are the MATLAB codes for the Chapter 3:

A2.1 MATLAB Code of Computation of Matrix $T(v)$ *and* $D(v)$

```
  INPUT:Eps
[EigVecEps, EigValEps] = eig(Eps);
P = EigVecEps;
PT = P.';
M = EigValEps;
Mh = sqrt(M);
SqrEps = P*Mh*PT;
InvSrtEps = inv(SqrEps);
OUTPUT:SqrEps, InvSrtEps

INPUT:InvSrtEps, S0, SS
S0=zeros(3,3);
SS=[(v2*ndelta)^2+(v3*ndelta)^2 -(v1*ndelta)*(v2*ndelta)
-(v1*ndelta)*(v3*ndelta); -(v1*ndelta)*(v2*ndelta)
(v1*ndelta)^2+(v3*ndelta)^2 -(v2*ndelta)*(v3*ndelta);
-(v1*ndelta)*(v3*ndelta) -(v2*ndelta)*(v3*ndelta)
(v1*ndelta)^2+(v2*ndelta)^2];
```

```
S=[SS S0;S0 SS];
A=InvSrtEps*S*InvSrtEps;
[EigVecA,EigValA]=eig(A);
De=EigValA;
T=EigVecA;
[m,n]=size(T);
T1=zeros(m,n);
R=zeros(n,n);
for j=1:n
    v=T(:,j);
    for i=1:j-1
        R(i,j)=T1(:,i)'*T(:,j);
        v=v-R(i,j)*T1(:,i);
    end
    R(j,j)=norm(v);
    T1(:,j)=v/R(j,j);
end
T=InvSrtEps*Q1;
D=diag(De);
OUTPUT:T, D
```

A2.2 MATLAB Code of Computation of Matrix $Q(v)$ and $M(v)$

```
  INPUT:Eps
Inveps=inv(Eps);
OUTPUT:Inveps

INPUT: InvEps, SC  SC=[0 -v3 v2; v3 0 -v1; -v2 v1 0];
S=SC*Inveps*SC;
Sr=real(S);
```

```
Si=imag(S);
SS=[Sr -Si; Si Sr];
[EigVecSS,EigValSS]=eig(SS);
De=EigValSS;
Q=EigVecSS;
[m,n]=size(Q);
Q1=zeros(m,n);
R=zeros(n,n);

for j=1:n
    v=Q(:,j);
    for i=1:j-1
        R(i,j)=Q1(:,i)'*Q(:,j);
        v=v-R(i,j)*Q1(:,i);
    end
    R(j,j)=norm(v);
    Q1(:,j)=v/R(j,j);
end
Q=Q1;

M=diag(De);
OUTPUT:Q, M
```

A3 MATLAB Code of General Gyro-magnetic Media

The following subsections are the MATLAB codes for the Chapter 4:

A3.1 MATLAB Code of Symbolic Computation of Matrix $\widetilde{E}(v)$

```
Input: c (speed of light), w (frequency)
Input: N, BB, ndelta, xdelta
Input: kappa, mui, mur

Mu=mur+i*mui
InvMu=inv(Mu);
[EigVecMu, EigValMu] = eig(Mu);
SC=[0 -v3 v2; v3 0 -v1; -v2 v1 0];
S=SC*InvMu*SC;
Sr=real(SS); Si=imag(SS);
SS=[Sr -Si; Si Sr];
[EigVecSS,EigValSS]=eig(SS);
De=EigValA;
Q=EigVecA;
for k=1:6;
Q(:,k) = Q(:,k) ./ sqrt(sum (Q(:,k).^2));
end
T=InvSrtEps*Q;
D=diag(De);

transT=(TT).';
ek=[1 0 0]';
FK=[0;0;0;ek];
YK=invT*w*mu0*FK;
for k=1:6
    YKN(k)=YK(k)/((DD(k))-tau^2);
end
Etilda=TT*YKN.';
Output: Etilda
```

A3.2 MATLAB Code of Symbolic Computation of Matrix $\widetilde{H}(v)$

```
Input: c (speed of light), w (frequency)
Input: N, BB, ndelta, xdelta
Input: kappa, epsi, epsr
Input: mui, mur

Mu=[mur -mui; mui mur]
[EigVecMu, EigValMu] = eig(Mu);
P = EigVecMu;
PT = P.';
M = EigValMu
Mh = sqrt(M);
SqrMu = P*Mh*PT;
InvSrtMu = inv(SqrMu);

S0=zeros(3)
SC=[v2^2+v3+2 -v1v2 v1v3; -v1v2 v1^2+v3^2 -v2v3;...
 -v1v3 -v2v3 v1^2+v2^2];
SS=[SC S0; S0 SC];
A=InvSrtMu*SS*InvSrtMu;
[EigVecA,EigValA]=eig(A);
De=EigValA;
Q=EigVecA;
for k=1:6;
Q(:,k) = Q(:,k) ./ sqrt(sum (Q(:,k).^2));
end
T=InvSrtEps*Q;
D=diag(De);

transT=(TT).';
```

```
ek=[1 0 0]';
FK=[[0 -v3 v2; v3 0 -v1; -v2 v1 0]*ek;...
0;0;0];
YK=transT*FK;
for k=1:6
    YKN(k)=YK(k)/((DD(k))-tau^2);
end
Htilda=TT*YKN.';
Output: Htilda
```

A4 Some Basic Concepts for Chapter 5

Lemma A4.1. *The* ∞ *norm for a vector on* $\mathcal{R}^n$ *is a function from* $\mathcal{R}^n$ *to* $\mathcal{R}$ *defined in Sundarapandian (2008) by*

$$||x||_\infty = \max_{1\leq i\leq n} |x_i|,$$

and the ∞ *norm for a matrix* $A = (a_{ij}) \in M_{mn}$*, the set of all real* $m\times n$ *matrices, is defined by*

$$||A||_\infty = \max_{1\leq i\leq m} \sum_{j=1}^{n} |a_{ij}|,$$

Lemma A4.2. *If* $||\cdot||_v$ *is a subordinate matrix norm, then we have the following inequality*

$$||A\,B||_v \leq ||A||_v\,||B||_v$$

where A *is any* $m\times n$ *real matrix, and* B *is any* $n\times p$ *real matrix and*

$$||A\,x||_v \leq ||A||_v\,||x||_v$$

where A *is any* $m\times n$ *real matrix, and* x *is any* $n\times 1$ *vector. Sundarapandian (2008)*

Lemma A4.3. *The subordinate norms satisfies the following relation*

$$||A||_\infty \leq ||A||_2 \leq \sqrt{n}||A||_\infty,$$

where n is space dimension.

Proposition A4.4. *The matrix Q is orthonormal if their columns are orthogonal, such that for* $Q = (q_1, q_2, q_3)$*,*

$$q_i q_j = \begin{cases} 1, \text{ for } i = j \\ 0, \text{ for } i \neq j \end{cases} .$$

Proposition A4.5. *If Q is an orthonormal matrix then the 2-norm is defined by*

$$||Qx||_2 = ||x||_2 \,,$$

for any vector x.

Proposition A4.6. *The 2-norm of any matrix Q is defined by* $||\cdot||_2$ *has the following property*

$$||Qx||_2 = ||Q||_2 \, ||x||_2 \,, \quad \forall\ x \,,$$

for any vector x.

Lemma A4.7. *From proposition (A4.4-A4.6) for any vector x we have*

$$||Q||_2 \, ||x||_2 = ||x||_2$$

implies $||Q||_2 = 1$.

Lemma A4.8. *For any symmetric matrix A, the 2-norm is defined in (Meyer (2001)) by*

$$||A||_2 \leq \sqrt{\lambda_{max}(A^T A)} \,,$$

where $\lambda_{max}(A^T A)$ *is the maximum eigenvalue of the symmetric matrix A and for inverse matrix* A^{-1} *we have*

$$||A^{-1}||_2 \leq \frac{1}{\sqrt{\lambda_{min}(A^T A)}} \,,$$

and where $\lambda_{min}(A^T A)$ *is the minimum eigenvalue of the symmetric matrix* A^{-1}.